Suppression of Intermodulation distortion in Radio-over-Fibre System

By

Shemsi Shaqiri

Department of Electronics Engineering

Royal Holloway University of London

Supervisor: Dr. Shyqyri Haxha

A Thesis submitted to the Royal Holloway University of London for the Degree of Master of Philosophy

30 Sep 2021

Declaration

I, Shemsi Shaqiri hereby declared that the work carried out in this thesis is mine and has been conducted in line with requirements of the Universities Research Degree Regulations and that it has not been submitted for any other academic award. Unless indicated by specific reference in the text, the presented study is the candidate's own work. Research done in collaboration with, or with the assistance of, others, is indicated as such.

Name of Candidate: Shemsi Shaqiri

Signature: 

Date: 30/09/2021

ABSTRACT

Suppression of Intermodulation distortion in Radio-over-Fibre System

Fibre optics communication is considered one of the most innovative methods of communication, originated about 40 years ago. Radio-over-fibre (RoF) was introduced for the very first time in 1990, and since then it has been widely used due to its high bandwidth, low losses, low power consummation, being cost-effective and other fibre-optic signal propagation properties [1-3].

RoF as an analogue communications system includes RF and optical fibre components such as Photodiode, filters, optical amplifiers, optical fibre, optical modulator, and laser. So far, the optical communication system has resulted to be the best solution to the modern mode of communication due to the above-stated properties. However, optical communication has its limitations as well, including non-linearity as a feature that produces Intermodulation Distortions (IMDs), losses and dispersion of signal. One of the most challenging tasks is the suppressing of nonlinear distortions, which strongly affects the performance of the Microwave Photonic Links (MPL).

In this thesis, a background review of the RoF system is presented, with a focus on Analog Photonic Links (APL) linearization techniques. In chapters 1 and 2 an introduction to optical communications is presented, with a focus on how the optical communication system has emerged and the advantages and disadvantages of the optical communications system in comparison to other communications systems available. Later in this chapter, a background study of APL has been presented - which includes optical fibre and fibre dispersion, techniques to compensate for fibre dispersion, nonlinearization in the APL, modulation techniques, and balance detections. Later, research is done in various linearization techniques to eliminate Intermodulation and Harmonics which happen due to modulations.

In chapters 3, 4 and 5, different linearization methods are presented and demonstrated. A high linear analogue photonic link based on a Dual-drive Dual-parallel Mach-Zehnder Modulator (D-DPMZM) with two separate photodetectors is presented. Third-order Intermodulation Distortion and Second-Order Distortions products have been eliminated by controlling the phase of the input RF signal and driving voltage of D- DPMZM. Mathematical modelling and simulations, for the proposed configuration and the purity of the system, are developed and tested by introducing additional RF signals. In the proposed configuration, a high linear down-converted signal is transmitted by changing only the operating modulator biasing point from quadrature to maximum of free Dynamic Range (SFDR) of 58 dB and linearized signal and 77.84 dB down-converted signal.

A different Microwave Photonic Link (MPL) system configuration based on two D- DPMZMs and two Balanced Photo-Detectors (BPDs) is reported. The Intermodulation Distortions (IMDs), as well as the harmonic distortions, have been eliminated. The proposed linearization of RF signal configuration is double side banded in both D-

DPMZM. A full mathematical model has also been developed and simulations have been performed for the proposed configuration. The proposed MPL system configuration exhibits significant performance, and it will have a great impact on aerospace, radar, and satellite-to-ground downlink communication system applications.

AMPL is proposed and experimentally demonstrated by unique ways of deploying Gallium Arsenide (GaAs), two Electro-optic Mach-Zehnder Modulators (MZMs), and BPD. All even and odd intermodulation distortions products are suppressed under the noise floor. Second-Order Harmonics (SOH) are also significantly suppressed by careful arrangements of microwave shifters and MZMs. We have also developed and implemented a full mathematical model for the proposed configuration, and linearization of the system is tested by introducing an additional RF signal. Our experimental measurements exhibit the suppression under the noise floor of all even and odd IMD and significant suppression of SOH. Spurious Free Dynamic Range (SFDR) of the proposed analogue photonic link for a linearized signal is 119.5 dB.Hz2/3.

Contents

List of Figures

spectrum analyser showing suppression of IMD2, d) Electrical spectrum analyser showing suppression of Third order distortion.

Figure 29: a) Power threshold measurements for proposed configuration, b) System stability analyses.

Figure 30: The gain and noise figure of the proposed system is measured.

Figure 31: SFDR performance of a) IMDD link with quadrature biasing, b) IMDD link with Low biasing and c) Proposed AMPL with Dual Parallel MZMs.

Figure 32: Schematic diagram of the proposed AMPL system configuration using two D-DPMZM with two input frequencies.

Figure 33: Electrical spectrum of the proposed structure; (A) Two single subcarriers from D-DPMZM1 without any intermodulation distortions, (B) Two single subcarriers from D-DPMZM2 without any intermodulation distortions, (C) Two single subcarriers after combining without any SOH, (D) shows the non-existence of IMD2 and SOH

Figure 34: (A) SFDR performance of proposed AMPL with Dual Parallel MZMs, (B) System stability analyses (C). Two single subcarriers after changing RF shifters for 1 degree, (D). Two single subcarriers after changing RF shifters for 1 degree and adding Fibre between BPDs and 3dB power combiner.

Figure 35. (A) Two single subcarriers after including 42 dB losses, (B) Two single subcarriers after including 42 dB losses and changing the input of laser to 15dB.

List of Tables

Abbreviations and Acronyms

- A.U Arbitrary Unit
- APL Analog Photonic Link
- AMPL Analog Microwave Photonic Link
- ASE Amplified Spontaneous Emission
- BNL Background Noise level
- BER Bit Error Rate
- BPD Balanced Photodetector
- CIR Carrier to Interference Ratio
- CW Continuous Wave
- DSF Dispersion Shifted Fibre
- DCF Dispersion Compensation Fibre
- DCM Dispersion Compensation Method
- DC Direct Current
- DEMZM Dual-Electrode Mach Zehnder Modulator
- DDMZM Dual-Drive Mach Zehnder Modulator
- DPMZM Dual-Parallel Mach Zehnder Modulator
- D-DPMZM Double-Dual Parallel Mach Zehnder Modulator
- DSB Double Sideband
- DSBSC Double Sideband Suppressed Carrier
- DSBFC Double Sideband Full Carrier
- DFB Distributed Feedback
- DEMUX De-Multiplexer
- EDFA Erbium Doped Fibre Amplifiers

- ER Extinction Ratio
- EO Electro-Optic
- FBG Fibre Bragg Grating
- FWM Four Wave Mixing
- GVD Group Velocity Division
- IF Intermediate Frequency
- IMD Intermodulation Distortion
- IMD3 Third-order Intermodulation Distortion
- IMD2 Second-order Intermodulation Distortion
- IP3 Third-order Intercept Point
- ISNL Input System Noise Level
- ISI Intersymbol Interference
- LD Laser Diode
- LO Local Oscillator
- LSB Lower Sideband
- MWP Microwave Photonic
- MMF Multimode Fibre
- MZM Mach Zehnder Modulator
- MZI Mach-Zehnder Interferometer
- MDS Minimum Detectable Signal
- MOS Minimum Operational Sensitivity
- MUX Multiplexer
- MPM Microwave Photonic Mixer
- NRZ Non-Return to Zero
- NZDSF Non-zero Dispersion Shifter Fibre
- NF Noise Figure/Factor
- NLCFBG Nonlinearity group-delay Chirped Fibre Bragg Grating
- OIP3 Third-order Output Intercept Point
- OSNL Output System Noise Level
- OC Optical Coupler
- OCS Optical Carrier Suppression
- OEO Opto-Electric Oscillator
- OPC Optical Phase Conjugator
- RF Radio Frequency
- RoF Radio Over Fibre

- PON Passive Optical Network
- PMF Polarisation Maintaining Fibre
- SMF Single-Mode Fibre
- SPM Self-Phase Modulation
- SDMZM Single-Drive Mach Zehnder Modulator
- SSB Single Sideband
- SSBSC Single Sideband Suppressed Carrier
- SFDR Spurious-Free Dynamic Range
- SNR Signal to Noise Ratio
- SHD Second-order Harmonic Distortion
- S/I Signal to Interference Ratio
- PMD Polarisation Mode Dispersion
- XPM Cross-phase Modulation
- XMD Cross-Modulation Distortion
- WDM Wavelength-Division Multiplexing
- USB Upper Sideband
- QF Quality Factor
- RIN Relative Intensity Noise
- RZ Return to Zer

Chapter 1

Introduction

Introduction to Optic Communication System

Fibre Optic Communication is one of the most sophisticated modes of communication originating 40 to 50years ago. In search of a wide-band medium for communication, those in the field of science explored the optical window, which then gave birth to what today is called fibre optic communication. If we take a look at the history of communication, starting from Graham Bell's time, the first revolution took place back when the audio signal was converted to electrical form, which was transmitted to electrical cables and then converted back to audio form. The main goal of communication at that time was to carry voice from one point to the other. As time went by, there was seen more demand for communication henceforth larger bandwidth was required. If we look at the Electromagnetic Spectrum Fig.1 [1], we can see all frequencies going from 10m wave to 0.1 μ m, corresponding to frequencies 30 Mhz to 300T.

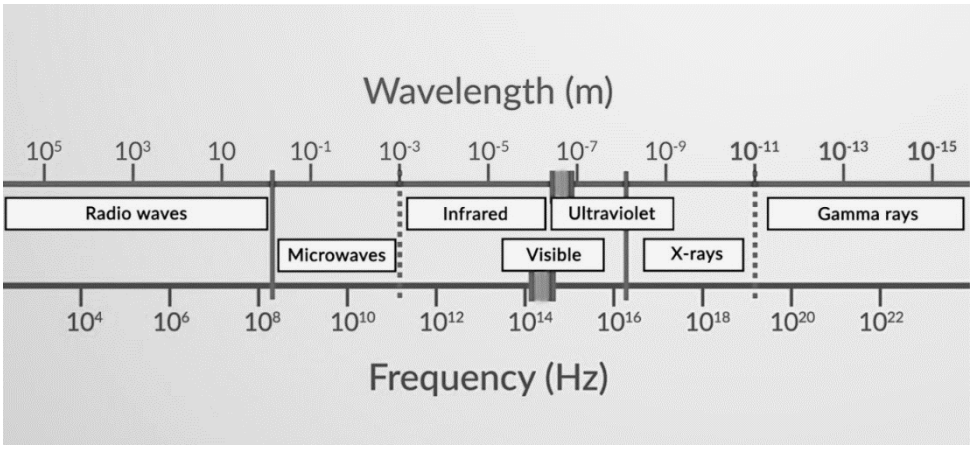

Fig 1: Electromagnetic Spectrum [1]

Formerly communication began in low frequencies, few Megahertz and in the last 100 years the frequencies of operation for communication constantly increased towards the higher end.

While understanding fundamentals required for reliable communication, there are two of them that have been discovered, which share great significance whenever it is required high-quality reliable communication.

1) Signal to noise ratio (ratio of the power of the signal to the power of noise).

2) Bandwidth (proportional to users).

To have reliable communication where many people can send information from one point to the other, we must have a medium with the lowest loss possible and the largest bandwidth possible. The quality factor and bandwidth are related through this relationship [1]

$$BW = \frac{f_0}{Q} \qquad (1)$$

For a given bandwidth (BW) quality factor (Q) is proportional to frequency ($ff0$) or for a given quality factor (Q), the bandwidth (BW) is proportional to frequency ($ff0$) and since the quality factor is independent of the given frequency, what we find is that the bandwidth required is proportional to the operating frequency. This is a very interesting phenomenon, depending on the amount of information we want to send, we require a larger bandwidth. This is the reason why communication started in low frequency and when the demand increased, the frequency increased – which in turn required a larger bandwidth. As we can see from Fig. 1.1, the bandwidth can increase by a factor of 10, which would not be enough to cope with the demand required. We must develop new technology to meet our current demands. If this low bandwidth (BW) is proportional to the operating frequency (f_o), it still stands.

This was in use around the 1960s by a physicist. To use the optical frequency as the medium for transporting information from one point to the other, we need to know if we have a medium to transport light with low loss and have enough sources of light that can carry information. Looking at whether we have a medium that can carry light, we can say yes - as light comes from the Sun to Earth. However, for instance a light bulb can be seen from a short distance but will not be visible from a long distance. Therefore, if we want a medium that can carry the light for long distances, then the air would not be as good as a medium.

Exploring the medium which can transport the light for very long distances and with this idea in mind, the next medium to look at was glass, since it is very transparent. Physicists have been using glass for guiding light and focusing light on the form of prisms and lenses, therefore glass seemed to be a very promising medium for transporting light. However, the use of glass at the time was for very small distances, and the question was: will glass be a medium that can carry light in long distances with low loss? Experiments conducted at the time showed that the losses were thousand dB per kilometer, so it was not a good enough medium.

Scientists believed that the loss of light in the glass was not intrinsic but due to the impurity of the glass itself. Scientists then tried to purify the glass as much as possible at the time, and in the first purity of the glass they managed to reduce the losses from 1000 dB per kilometer to 20 dB per kilometer, which was comparable to other communication options. However, they needed to consider whether they had the light that could carry information from one point to another. For instance, could the light bulb carry information? Light bulbs can carry information if they have some variation in their characteristics, either in frequency or in time. Meaning that,

if we consider a light source whose either amplitude or frequency does not change as a function of time, then this source does not carry any information.

Using a light bulb as a source to send information by switching it on and off would not be a suitable method, as the light bulb would not be able to send a lot of information at a very high rate. The rate in which signal can be sent through a switch turning on and off depends on the spectral width of the light. Having a light which has a spectral width (like white light) as a source cannot be switched on and off at a very high rate. We, therefore, need a different kind of light, which is a very narrow laser kind of source. Luckily, around the time where fibre sources were being explored, the laser was invented. We have sources that can be switched on and off or can be modulated at very high rates and we have a medium that can carry light in long distances, so this combination made fibre communication possible.

The typical optical link consists of three components:

- Transmitter
- Medium (optical Fibre)
- Receiver (optical detector)

Cooperative statement between optical Fibre communication and other technologies which are available [2].

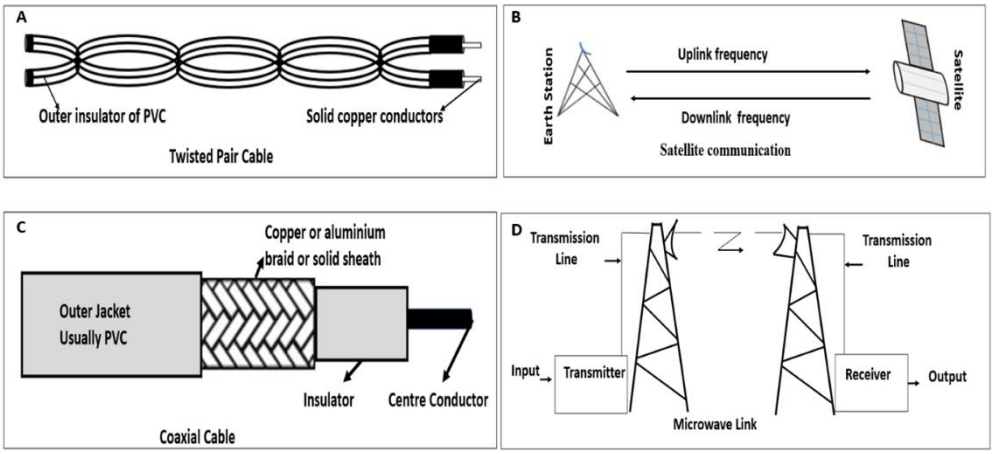

Figure 2: A Twisted cable, B Satellite Communications, C Coaxial Cable, D Microwave Link

Twister Pair Fig. 2 shows point-to-point communication. This medium has high electromagnetic interference (EMI) and it has a very high loss. With the rise of frequency, a twister pair is a good medium for carrying signals which are at low frequencies and are mainly used for telephone lines. Moreover, with the rise of frequency, a more suitable medium is Co-axial Cable (Fig. 2.C), as point-to-point communication. Such structure does not have an exposed electromagnetic field, consequently having low EMI. This cable is used for local area network (LAN), whereas the data rates are higher than the twisted pair structure; this cable is capable of supporting the data rates of a few megabits per second. However, if we want to go to the higher frequency side, we have Microwave Link (*Fig. 2.D*). It is still point to point communication, but it is a wireless communication and is different from the other two medium communication, which are categorised as wired communication. In this case, the signal is transmitted by using a highly directed antenna whereas the signal is received by the other side from another antenna – without having any cables. This mode can be used for long distances since now the frequency is in the

microwave range. In such medium, bandwidths are much larger than co-axial, which typically are capable of supporting bandwidth with fewer than a hundred megabits per second. The only problem with this type of communication is that this is a straight-line communication because of its antennas' direction, and it has a high transmission losses rate because of the free-space propagation.

The next option, if we want to communicate in high frequency and wireless, is Satellite Communication (*Fig. 2. B*). It is point to multi-point communication, which can be used not only in point-to-point communication but also for broadcasting applications. This medium of communication has a station on Earth that transmits signals to satellites, then satellites reflect the signal in different frequencies and are received on different Earth antennas. The signal is in microwave frequencies and as a result, it has a large BW. Such signal scatters from the satellites with Data-monitoring properties has not been available in other communications. However, it has large delays due to the travelling signal. Satellite Communication has advantages in its Mobile Environment and moderate lifetime.

Looking at the media and broadband, which is now available to us, it is fair to say that we probably have two technologies which may compete with each other: one is a satellite technology which has a bandwidth of the order of about 3.7 to 4.2 downlink and 5.9 to 6.4 uplink gigahertz, and the other technology is Fibre optic technology When comparing these two technologies we find that medium of transmission is essentially complementary to one another.

Here we have a comparison table between satellite transmission and fibre optic transmission:

SATELLITE	FIBRE OPTICS
Point to Multi point	Point to point
Bandwidth in GHz	Bandwidth in THz
Maintenance free	Need maintenance
Short life (7-8 years)	Long life
No upgradeability	Upgradeable
Mobile, air, sea	On ground only

Table 1: Comparison table between satellite transmission and Fibre optic transmission

Optic Fibre

Optical fibre is a solid glass rod with a core through which light propagates. This solid glass rod is surrounded by a shell made of glass, called "cladding". This glass rod is made from core and cladding (Fig. 3A), and light propagates through this by what is called total internal reflection.

Fibre is made with silica and plastic, which is a perfect medium for light waves to propagate from one point to the other because of its properties, and it is the basis for optical communications systems [2]. In today's world, fibre has replaced coaxial cable mainly due to its properties, and because as a medium it is more reliable, it is safer, it has a larger capacity and has low loss rates compared to coaxial cable. Transmission loss in fibre depends mainly on the material of fibre its purifications, and its measures in dB per kilometer (dB/km).

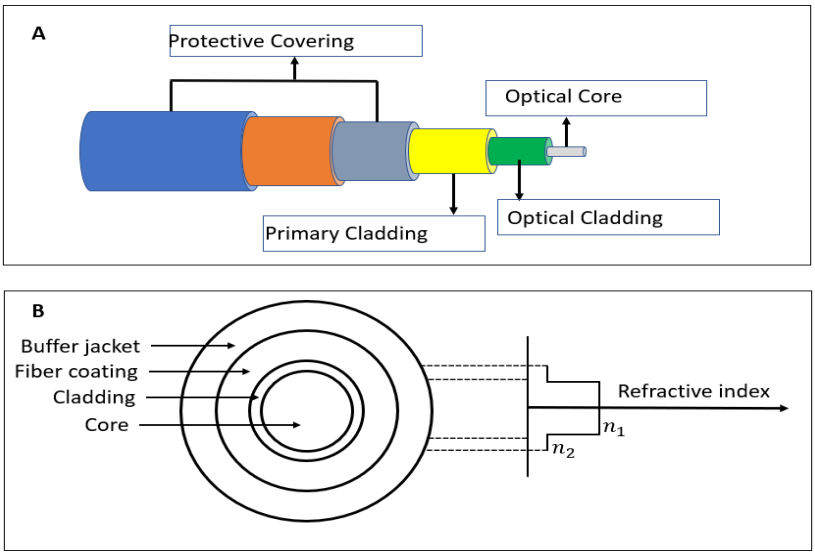

Figure 3: A Fibre Optic, B Typical structure for a glass multimode step index Fibre

The tip of the fibre (cross-section) is of great significance as it is the only way to launch light inside the fibre. Non-linearity depends mainly in the intensity of the light and the power distribution in the cross section of fibre. Therefore, it is very important to take into consideration the cross-sectional area (A_{eff}) when implementing an optical communication system A_{eff} . (Cross-sectional area) is given as follows (3) where R and θ are polar coordinates.

$$\mathrm{A_{eff}} = \frac{\int_r^0 \int_\theta^0 \mathrm{rdrd\theta I(r,\theta)}}{\int_r^0 \int_\theta^0 \mathrm{rdrd\theta I^2(r,\theta)}} \qquad (2)$$

Fibre's are available in 2 types

- Step index
- Gradient index

Step index fibre has a refractive index constant throughout the fibre, therefore when light propagates through, Step Index and Gradient Index travel at different speeds. Light rays (which travel through the middle of the core) travel with higher speed than light which travels near the axis of the fibre. Step index fibre is used in both single and multi-mode fibre.

Gradient index fibre has a different refractive index. The Refractive index near the core is much higher than the one near clouding, which makes it possible for light rays to travel with the same speed throughout the fibre medium Fig.4 B. This is only possible because the light that travels a longer distance has a greater refractive index, therefore, it travels with a speed higher than the light rays, which travel in a shorter distance. Gradient index fibre is only used in multi-mode fibre. Losses in fibre are called attenuation, which reduces the power of signal travelling in the fibre medium. This loss is given by.

$$Loss = \frac{Pout}{Pin} \tag{3}$$

Where Pin is power input and *Pout* is power output in fibre.

$$Loss_{dB} = 10\log\frac{Pout}{Pin} \tag{4}$$

Fibre Dispersions

When light rays travel in fibre, they travel at different speeds. As a result of this, the signal will broaden. This creates a phenomenon which is called dispersion. Signal broadening also happens because of non-linearity. This dispersion can be composited by using dispersion composited fibre (DCF), dispersion-shifted fibre and fibre Bragg grating (FBG).

Lightwaves in fibre will travel at different velocities even when launched at the same time. This phenomenon in an optic is called Intermodal dispersion. Intermodal dispersion is given by [4];

$$\tau = \sqrt{\tau_i^2 + \tau_m^2} \tag{5}$$

Where $\tau_i \wedge \tau_m$are due to intermodal and martial dispersion. Intermodal dispersion is managed by using Bragg grating (FBG). Fibre is made from silica and plastic. During purification of material, there can be small dots with a different refractive index which causes

light scattering. This results in non-linearity of signal and errors in bits. Signal broadening due to material non-linearity is called "*chromatic dispersion*".

When lightwaves propagate in fibre medium at a different speed, it means that they have two orthogonal polarizations modes. That is called Polarization Mode Dispersion (PMD). Polarization modes travel at different speeds due to non-linearity and the purification of material. As a result, these modes arrive on the other side of fibre at different times Fig.4 [5]. This time difference is called Differential Group Delay. PMD is also caused by bi-reference which is natural in fibre, bend in fibre, mechanical stress, and temperature change.

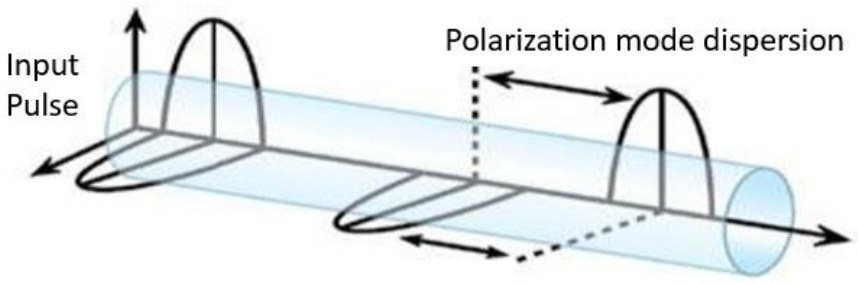

Figure 4: Polarization mode Dispersion in optical Fibre

Dispersion Power Penalty

To maintain a Bit Error Rate (BER) for optical fibre, power is calculated to be of order 10^(-9). Signal loss of power is due to dispersion. To maintain this power throughout, signal propagation over optical fibre power needs to be increased. This extra power is called power communication system penalty. Power penalty is the ratio between BER, and power received.

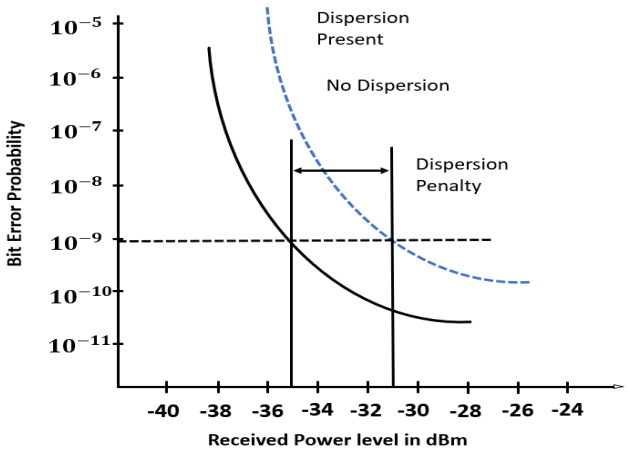

Figure 5: Dispersion power penalty graph

Therefore, it is important to have the required BE. Plotting BER for Fibre with no dispersion and BER for Fibre with dispersion two of the same curves can be achieved Fig.5 [3], difference between these two curves is dispersion power penalty. This is given by the equation.

$$BER = \frac{E(t)}{N(t)} \qquad (6)$$

Where E(t) is the number of bits received in error and N(t) is the total number of bits transmitted.

Dispersion Compensation Fibres

Non-linearity and all dispersion that have been discussed above will affect the quality of signal and limit signal transition lengths. By using single-mode fibre and improving fibre quality, only a few dispersions can be improved: for instance, waveguide and modal dispersion. There is still a need for new and improved techniques to better fibres' quality which improves the overall dispersion in fibre. Some of these techniques are discussed in this paper [6,7].

Dispersion-Shifted Fibre

In earlier years, the communication over fibre took place in an 800 nm window, later the communication shifted to 1310 and 1550 nm windows because of low loss. Today most fibre communications take place around the 1550 nm window. Fibre communication is shifted to a 1550nm window because of very low loss compared to 800nm and large bandwidth.

Fibre communication in the 1310 nm window has very low dispersion and supports very high data rate. That look like the perfect medium to transport data from one point to another, but in 1310nm window only one mode can propagate which makes perfect medium to transport data in long range because of the low dispersion and high data rate. In today's world, the demand for data is exceptionally increasing, which is why 1550nm window is widely used since it supports a large bandwidth. For example, 1550nm is currently being used in laser devices.

In the 1550nm window, a large number of modes can propagate where dispersion starts playing a role, but this dispersion can be compensated using dispersion-shifting fibre (DSF) [8]. Dispersion-shifting fibre worked better in a single-channel compared to WDM, but this limitation has been overcome by using a combination of zero dispersion-shifted fibre and standard single-mode fibre in the same link [6].

Dispersion Compensation Fibre (DCF)

Dispersion-compensated fibre is a technique that is used in recent years to compensate dispersion. This fibre has a negative dispersion which cancels the chromatic dispersion. Dispersion-compensating fibre is more suitable for single-channel transmission as supposed to multi-channels because the channel, which is further away from the center, receives less dispersion compensation effect [6]. DCF depends on the diameter of the fibre, a smaller diameter will mean higher negative dispersion. Because of a small effective OR affected area, it is difficult for dispersion-compensated fibre to handle the high optic power.

In a system where DCF is used, it is very important to calculate the CVD-limited transmission distance for a given bit rate (B). This length is calculated using equations 7 and 8. [3]

$$L = \frac{1}{4\mathrm{B}\left|D\right|\sigma_{\lambda}} \qquad (7)$$

$$L = \frac{2\Pi C}{16\lambda^{2}\left|D\right|B^{2}} \qquad (8)$$

Where B represent bit rate, $\lambda\lambda$ wavelength, D is dispersion parameter.

Standard dispersion parameter in standard Fibre is 16ps/nm/km for single wavelength in 1550nm as in DCF dispersion parameter is -80ps/nm/km or -100ps/nm/km depending on system configuration.

Fibre Bragg Grating

Fibre brag or Bragg grating is another important fibre for dispersion compensation in fibre. Fibre Bragg Grating fibre is a fibre were, inside, some section refractive changes periodically. The idea of having a grating region in fibre is changing the refractive index for beams with selected wavelengths, as result, all waves add up in phase [6]. Changes in the refractive index in fibre brag OR Bragg grating is represented as;

$$\lambda B = 2n_{eff} \wedge_G \qquad (9)$$

Where n_{eff} is refractive index, $\wedge_G$ is period of refractive index modulation.

The graded region in fibre Bragg grading fibre is made by photo-imprinting a hologram, the material used for photo-imprinting is Germanium. Germanium is a material that is highly sensitive to high intensity of light, which increases refractive index as result refractive index is changing Fig. 6 [9].

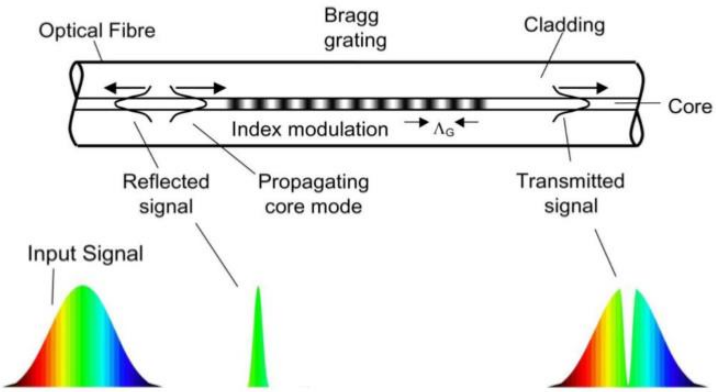

Figure 6: illustration of Fibre Bragg Grating

From figure 6 we can see that the input signal travels through FBG fibre. Some of the spectrum will be reflected with different wavelengths and the signal received on the other side of the fibre is less dispersive.

Dispersion Compensation Schemes

In this section, some compensation techniques for dispersion will be discussed. Chromatic dispersion is one of the main problems in optical communication systems. So far there have been many developed techniques to compensate chromatic dispersion like pre-post-pay, symmetrical pay plans utilizing Dispersion Compensating Fibres (DCF).

In [10] some new techniques to deal with chromatic dispersion have been proposed based on Distributed Feedback laser. Chromatic dispersion is compensated using newly designed non-linear group delay chirp fibre with single-mode fibre and tunable laser. This way group delay is composited in the upper and lower side of RF signal by reducing the wavelength of the optical carrier. Other techniques used in this paper are single-sideband modulation where ratio optical to sideband is controlled using DFB (ultra-strong optical injection-locked distributed feedback) laser. This ratio of DFB Laser is controlled to reach wanted locked mode. When this signal is combined with base signal only locked-mode, signal will be modulated, and the rest of signal will be unchanged. OPS (Optical Phase Conjugator) technique is a successful technique for composition of dispersion in Fibre.

Three common dispersion composition techniques presented in this report have been compared with each other for NRZ (Non-return-to-zero) format. From this, the analysis can be observed that the symmetrical compensation method works better than the pre and post compensation method at 10 Gbit/s. Dispersion compensation techniques vary for different bit rates; therefore, the performance of these compensation techniques is limited to the fixed data rates.

In [11, 12] it can be observed that symmetrical compensation and post-compensation techniques have minimum penalties compared to pre-compensation. This compensation techniques are used Dispersion Compensation Fibre (DCF) which have negative dispersion. This helps fibre to compensate for positive dispersion in single-mode fibre. The main disadvantages of this compensation technique are the large attenuation of signal power which results in using more optical amplifiers, hence the system is more complicated and expensive [13].

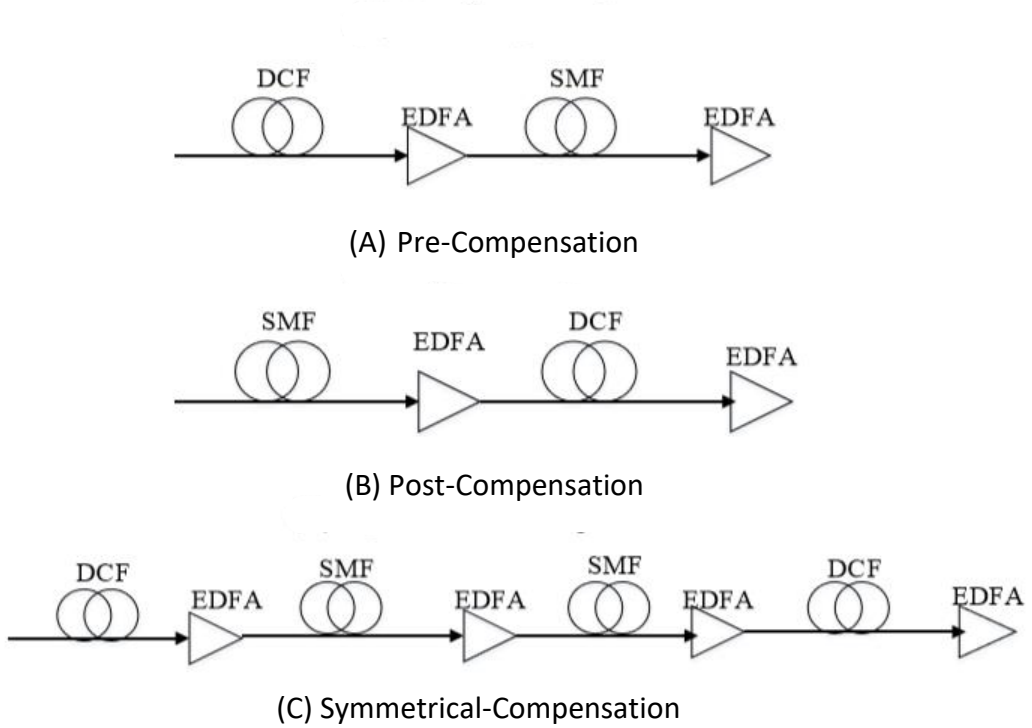

Figure 7: (A) Pre-Compensation, (B) Post Compensation, (C) Symmetrical Compensation

Pre-compensation is achieved by using DCF before the single-mode fibre span Fig 7 A, whereas post-compensation is achieved by using DCF after SMF Fig 7 B, and symmetrical

compensation is achieved by using a mixture of both Pre-compensation and Post-compensation techniques Fig 7 C.

Fibre Non-linearities

In this section, we are discussing non-linear fibre optics – when the light intensity increases, the higher-order vulnerability terms in the induced polarization of dielectric material must be taken into consideration. In a material like glass, the second-order susceptibility contribution is negligible, so the non-linearity primarily is because of the third-order weakness, which leads to what is called the Kerr non-linearity.

The refractive index of the material has a term that is proportional to the square of the electric field or the power density in the material so essentially, we are considering the pulse propagation inside an optical fibre in the presence of this non-linearity.

In optical Fibre the nonlinear effect is enhanced by almost a factor of billions compared to the non-linear effect in a bulk material for the simple reason that once the power is confined to the core of the optical Fibre, the non-linear interaction keeps taking place over the effective length inside the optical Fibre. Due to very low loss on the Fibre, this length turns out to be few kilometers and therefore the overall effect of non-linearity observed inside the optical Fibre is much stronger compared to what you see inside a bulk material.
Power levels which are normally dealt in the optical communication are small, even for those power levels which are a few milli-watts of power the nonlinear effects become significant in the optical Fibre.

From non-linear Schrodinger after certain estimation and certain linearization we can consider different cases depending upon what is the pulse width and what power is in the pulse. Different

effects may dominate at different situations. Therefore, these two different lengths on the optical Fibre, one is dispersion length (L_D) the other one is non-linearity length (L_NL). Depending on the physical length of the optical Fibre, sometimes the non-linearity length may be smaller than the physical length, so the non-linear effects dominate. Sometimes the dispersion length would be less than the physical length of the optical Fibre, so the dispersion effects would dominate, and when both the lengths are smaller than the effective lengths of the optical Fibre, then both effects would start contributing and that would give the evolution of the pulse.

Based on these two different lengths we can consider three different situations.

$$L \ll L_D \ll L_D \qquad (10)$$

$$L \gg L_D \ll L_D \qquad (11)$$

$$L \gg L_D \gg L_D \qquad (12)$$

If the length of fibre is much greater than the dispersion length and the length of fibre is much less than the non-linearity length (11), then the dispersion effects are not dominant but the non-linearity effects are dominant. What will happen if you have large power inside the optical pulse, then we get a phenomenon which is called self-phase modulation. If the length of fibre is much greater than the dispersion length and the length of fibre is much greater than non-linearity length (12), both the effects are present, then we get a pulse that is called a soliton.

Stimulated Raman Scattering and Stimulated Brillion Scattering

The effect of the SRS can be achieved by transferring the power from lower wavelength channels to the higher wavelength channels, Fig. 5, [22][40]. Stimulated Brillion Scattering (SBS) is the conversion of the signal power into a backward frequency-shifted wave [23][41].

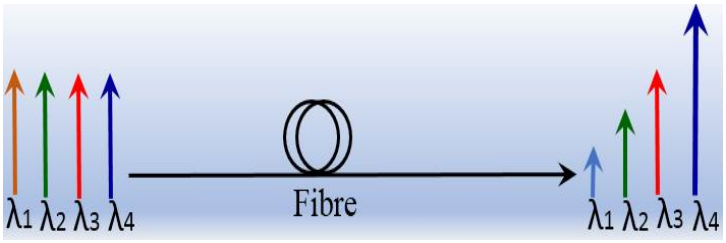

Figure 8: Transferring the power from lower to the higher wavelength channels

In a short pulse experiment, the SBS reflectivity levels were found to be high, while a go under SI-relevant intensifies. Due to the non-linearity and sensitivity conditions, the laser plasma instability deepens. Exploring the parameters of space and understanding plasma instabilities are very important. Instability is very important. SBS and SRS can be convective in low density of the corona, their level of saturation depends on convective gain and seed levels.

Kerr Effect

Kerr effect – happens when varying DC electric field is functional to the non-linear optic fibre, follow-on in the changing of the refractive index of the material. As a result, the material acts as a waveplate that polarizes light in a desired direction. Kerr effects happen because of change

in refractive index as a result of a self-induced effect, this phenomenon is very common in optical fibre. This can be represented as [2].

$$\Delta_n = \lambda K E^2 \qquad (13)$$

Where λ is wavelength of the light, K is the Kerr constant and E is the strength of electrical field.

Group velocity dispersion

Non-linear fibre optics is when the pulse has high intensity then refractive index of the material gets modified because of the pulse and that leads to the modification in the pulse propagation.

In this section, we are looking at the phenomena which are called 'group velocity dispersion' and assume that the non-linearity is not playing a role, but the dispersion is there. Solving the non-linear Schrodinger equation only for dispersion expecting something interesting will happen. If we have a Gaussian pulse then the shape of the pulse remains Gaussian as it travels on the optical fibre, but it goes on broadening also internally, the pulse gets frequency modulated and the chirp has a different nature depending upon whether we are in the normal dispersion regime or the anomalous dispersion regime.

In the normal dispersion regime, frequency chirp is positive as a function of time, whereas, in an anomalous dispersion regime for a wavelength greater than 1300 nanometer then we have the negative chirp which means the frequency decreases as time inside the pulse.

Chapter 2

Background review and methodologies

Radio-Over-Fibre System (RooF) background review

This section gives a basic understanding of the radio-over-fibre system and explains the basic theories behind the design of the system. Considering this research fundamental investigation on optical fibre, fibre desperation, non-linearities, modulation techniques, noise and the IMD, are discussed and clarified in this part.

Radio-Over-Fibre System (RooF)

Transmission of radiofrequency signal over fibre is a technique that is widely used these days. This technique is an analogue communication scheme, as an analogue optical link laser modulation depth should always be small. In digital optical links, modulation depth is nearly 100% or the laser is switched on and off depending on the modulation technique [7].

Radio-over-Fibre communications system includes RF and optical fibre components such as Photodiode, filters, optical amplifiers, optical fibre, optical modulator, and laser.
Radio-Over-Fibre System structure is displayed in Fig.9.

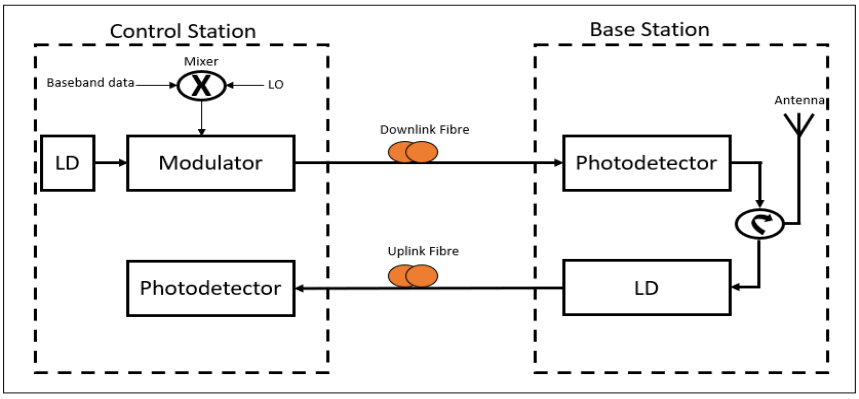

Figure 9: RooF architecture shows downlink and uplink between control and base section

In the transmitter, the RF signal is modulated with light coming from Laser (LD) transmitted over fibre and converted back to RF at the receiver side. RoF has a range of applications such as mobile radio transmutation which includes 3G, 4G, 5G and WIFI, RF L-Band transmission in earth stations for satellite communication and cable television signal transmission.
The advantage of the RoF system is attenuation of the signal transmitted is much less than any other metal cable or WIFI and can hold long distances in transmission reducing the need of using too many amplifiers and repeaters.

Modulation Concept

Modulation is a concept that involves transferring data from the electrical to the optical domain. There are two main modulation concepts: Direct modulation and External modulation. Direct modulation is when light from light sources is directly modulated with an RF signal whereas external modulation uses a continuous wave (CW) and uses an Optical modulator to modulate continuous light from a light source with an RF signal.

The advantage of using direct modulation is a simple system and is easy to implement with low cost but it has limited frequency and response time. External modulation due to having an external device called optical modulator to modulate light source with RF signal allow using high frequency and have high performance. External modulation due to these advantages is highly used today in the RoF system. Mach-Zehnder Modulator (MZM) is mostly used as an optical modulator in external modulation in the RoF systems.

External modulation uses two types of optical modulators:

- Electro-Absorption Modulator (EAM)
- Electro-Optic Modulator (EOM)

EAM is a modulator that modulates the absorbed photons in the optical waveguide semiconductor by applying different electrical power throughout the waveguide. Electro-Optic Modulator (EOM) is mostly used as an optical modulator in an external modulation. The modulation performed by applying different voltages in each arm of MZM is called Phase Modulation. This modulation procedure in this process is performed by applying the voltage in each arm of the MZ by modifying the phase of the electrical field. Modulating the signal in both arms of MZM by applying different voltage and combining the signal from both arms; the signal is then converted into intensity modulations.

Applying the same voltage to both arms of MZM means both arms have the same electrical fields which imply the same phase modulation but different signals. This method is known as the push-pull method [14]. MZM comes as a single drive or dual drive. Dual-drive MZM is used to generate intensity modulation by using inverse data and data on both branches of MZM. For a high-speed communication system, it is essential to use external modulation as it is very difficult to directly modulate the signals at high speed.

Single-drive modulator

The signal-drive modulators can be x, y and z cut whereas dual-drive modulators can only be z-cut [15]. The material used to build an electro-optic modulator should be chosen carefully to consider the environment and for a given wavelength as some materials are unsuitable for peak in the frequency and response. When designing this modulator half-wave voltage is the most important to be achieved for the required degree of modulation, VPI should be low for good quality modulation and Vpi L half-wavelength product is a very important factor. L is the modulator electrode length which is defined as product voltage of phase-difference of two arms of the optic modulator at 180 degrees and the length [16] which can be expressed as:

$$VL\pi = \pi V_0 \tag{14}$$

$$\Delta\beta = \beta_1 - \beta_0 \tag{15}$$

Where $\beta 1$ and $\beta 0$ are propagation constant of MZM branches and V0 is applied voltage [15].

Dual-Electrode Mach-Zehnder Modulator (DEMZM)

The most common external modulator used in microwave photonics is Dual-Electrode Mach-Zehnder Modulator (DEMZM) due to the properties it holds. DEMZM delivers different efficient optical signals it is also used in different ways such as stable and unstable dual-drive and single drive. Dual-drive system uses signal with opposed phase to create an intensity modulation. Also chirp cam be removed by applying same voltage in both arms of the modulator. The dual-drive modulator is formed from upper and lower electrodes where the optical signal passes through which is strengthened by DC voltage and RF signal Fig.9.

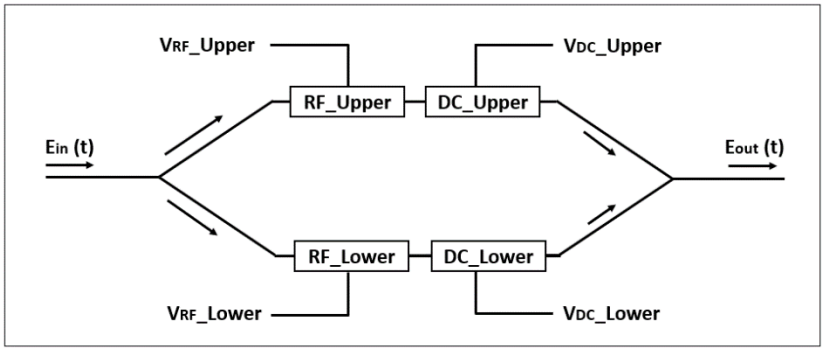

Figure 10: Dual Electrode Mach-Zehnder modulator

Optical signal in dual-drive modulator is modulated in the waveguide by the electrical field generated from these electrodes according to baseband signal required. By controlling DC voltage in the upper and lower arm we can change the phase of the signal to achieve different modulation, for example sideband modulation or to reduce nonlinearity in the system. RF and DC can be applied to upper and lower electrodes in this modulator.

Operation points of modulators

MZM operating point can be changed by changing the bias voltage. By applying voltage in electrodes of modulation the electric field changes the optical path length meaning signal has been phase modulated in each branch of the modulator. The performance of the modulator can be seen by changing the bias voltage. Based on half-wave voltage and bias voltage we can identify the operating point of the modulator fig () illustrates the transfer function used in this regard. A pick point of the transfer function is achieved when the phase difference is a multiplication of 2π or 360 degrees, otherwise known as constructive interference.

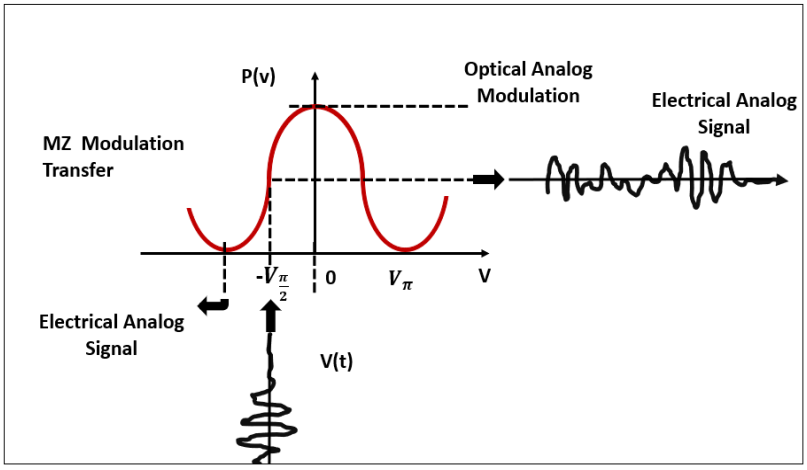

Figure 11: MZM Transfer Function

As it can be seen from Fig.10 pick point or maximum is achieved at 0V. A null point or minimum of the transfer function is achieved when the phase difference is an odd multiplication of π or 180 degrees in other words this state is achieved when applying voltage is Vpi or -Vpi. The transfer function can be mathematically expressed as:

$$E_0(t) = bE_0 \cos 2(\frac{V(t)\pi}{2V\pi}) \qquad (16)$$

Where $E_0(t)$ is transmitted intensity; b is insertion loss; E_0 is laser input power; V(t) is applied voltage and V_π is driving voltage.

A normalised γ bias voltage, normalised amplitude η and operating point are used to configure modulators in different ways. Normalized γ bias voltage is presented as $\gamma = Vdc/V\pi$ where Vdc is DC biased voltage whereas normalised amplitude η is represented as $\eta = Vm/V\pi$ where Vm is the voltage of modulator and $V\pi$ is modulator switching voltage. A product of normalised bias voltage and normalised amplitude represent RF signal modulation index which mathematically can be written as $m = \pi\eta$ or:

$$m = \pi \frac{V_m}{V_\pi} \qquad (17)$$

Dual-drive MZM electrodes for upper and lower arms can be modulated separately, the output of electrical field for DD-MZM mathematically can be expressed as [18]:

$$E_{out}(t) = b\frac{E_0}{2} e^{j2\pi f_0} \left\{ \exp(j[\gamma\pi + \eta\pi\cos(2\pi f_m t)]) + \exp(j[\eta\pi\cos(2\pi f_m t + \phi)] \right\} \qquad (18)$$

Where $\exp(j[\gamma\pi + \eta\pi\cos(2\pi f_m t)]) + \exp(j[\eta\pi\cos(2\pi f_m t + \phi)]$ express the field of electrodes for upper and lower arms of DD-MZM.

Sideband Modulation Process

During the process of modulation expect carrier in the spectrum, we have frequencies in the upper and lower side of the carrier these frequencies are called sideband frequencies which contains all Fourier components of the modulation signal. Similar to AM signal it contains sidebands frequencies and carrier which have data transporting to the end receiver. Carrier in this modulation technically only transport data and don't carry any information, however, carrier uses about 50% of the power hence most of the systems suppress the carrier during transmission and recover back the receiver to recover data information. Two techniques are

used to do sideband modulation: Double Sideband (DSB) modulation and Single Sideband (SSB) modulation. Sideband modulation is demonstrated in Fig.11 including DSB and SSB.

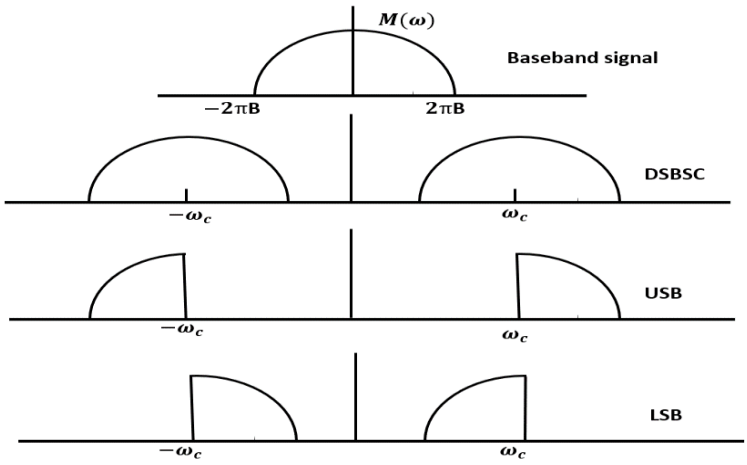

Figure 12: Illustration of DSB and SSB

From Fig.11 can be seen that the baseband modulation signal is modulated with the carrier as a result of two sidebands being created known as DSB, by adjusting the bias voltage we can eliminate one sideband to achieve SSB.

Double SideBand modulation process

Double sideband modulation is when one signal is modulated in the optical modulator as result two sidebands are generated on the upper and lower sides of the carrier this process is called double sideband modulation. During this process, we can suppress the carrier, or we can leave as it is the carrier during propagation hence there are two ways of using DSB, one with carrier suppressed during propagation one without suppressing carrier, this process is called DSB-SC and DSB-FC respectively. Modulation process using DSB can be represented using mathematical model, suppose waveform of carrier is mc(t) and baseband signal is m(t) then mathematically it can be written as [19]:

$$mc(t) = Ac\cos\omega ct \qquad (19)$$

Modulating baseband signal with carrier than modulation signal s(t) will be:

$$s(t) = A_c m(t)\cos\omega_c t \qquad (20)$$

Using Fourier series on baseband signal M(ω) than signal modulation mathematically can be represented [19, 20]:

$$S(\omega) = 0.5A_c M(\omega - \omega_c) + 0.5A_c M(\omega + \omega_c) \qquad (21)$$

Modulation system using double sideband modulation is shown in Fig.12.

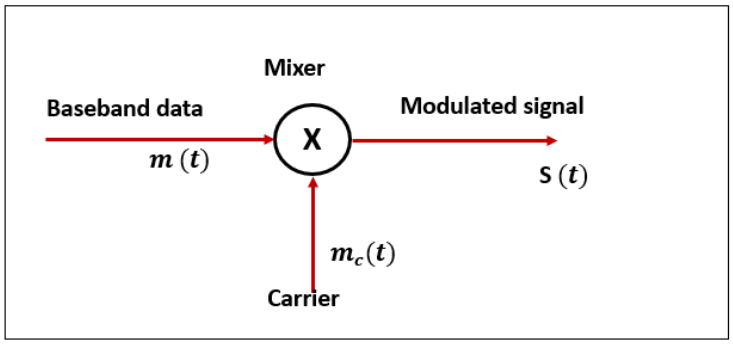

Figure 13: Modulation structure of DSB

From this can be observed that the product of signal and carrier produce DSB spectrum. Frequency range is spectrum range filled with signal message known as baseband signal. Baseband signal ''ω'' in communication system have limited range most of the time however carrier has high frequency '' ωc ''. Upper SideBand (USB) signal in DSB is known as positive sideband and is written as $\omega c + \omega$ where Lower SideBand (LSB) is known as negative sideband and can be written as $\omega c - \omega$ hence bandwidth required for transmission using DSB is two times baseband frequency [45] therefore bandwidth required can mathematically written as:

$$BT = 2\omega \qquad (22)$$

Where, ω is baseband frequency and BT is the bandwidth transmission required.

Amplitude in DSB has periodic flux during transmission for whole length of Fibre in RoF system therefore using SSB modulation will end the periodic fluctuations.

Single SideBand (SSB) Modulation process

When the signal is modulated with the carrier it does produce two sidebands as explained above upper sideband and lower sideband, the process of eliminating one of the other sidebands upper or lower sideband is called single-sideband modulation. The benefit of using SSB is that stops the periodic fluctuation created during modulation and reduces the bandwidth required for signal propagation hence less energy is required as is shown in Fig.13 [21]. Same as in DSB we can suppress carrier during SSB knowing that carrier uses 50% of the energy required for propagation of signal and retrieve carrier with information at receiver or we can have carrier during this process. Therefore, suppressing carrier uses 50% less energy required for signal propagation and reducing bandwidth during SSB will result in improvement in the Signal-to-noise ratio. SSB with carrier suppressed is called SSBSC and with a carrier not suppressed is called SSBFC. Another benefit of using SSB is reduction of fibre dispersion. Few methods are used to achieve SSB, the most common method is the phase-shifting or discrimination method. The process of using a bandpass filter to eliminate the sidebands is called the discrimination method is easy to implement but is more expensive than using the phase-shifting method. The discrimination method uses high pass to eliminate LSB and lowpass USB as shown in Fig. 13.

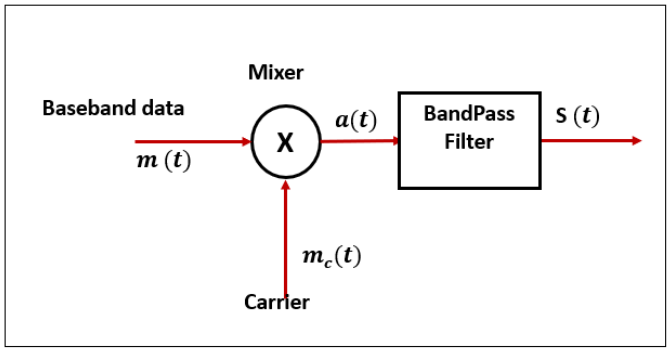

Figure 14: SSB modulation structure with Filter

Mathematical representation of SSB is like DSB, the baseband signal is modulated with the carrier as result signal a(t) is obtained which can be written as [21]:

$$a(t) = A_c m(t) \cos \omega_c t \qquad (23)$$

Fourier transformation of eq. (23) is the same as Fourier transformation of eq. (20) when DSB has gone through LSB or USB filter where both filters have zero-valued spectrum for $|\omega| > \omega c$ and $|\omega| < \omega c$ respectively. SSB can be obtained by using formula [46]:

$$\tilde{s}(t) = 0.5A_c \left[m(t) \pm j\hat{m}(t) \right] \qquad (24)$$

$$\tilde{s}(t) = 0.5A_c \left[m(t) \cos \omega_c t \pm \hat{m}(t) \sin \omega_c t \right] \qquad (25)$$

Where $\hat{m}(t)$ is Hilbert Transformation of the sideband signal m(t). For LSB is used positive sing as for USB is used negative sing in eq. (25).

Phase shifting method for SSB is shown in Fig.14 explain how this method is implemented [21].

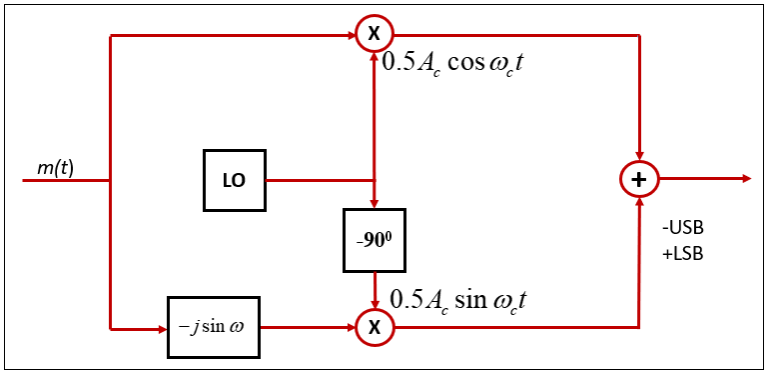

Figure 15: Phase shifting modulation method of SSB [46]

RF Splitter

This Module is commonly used to connect a single output port to more than one input port. When using the graphical interface, it will be automatically inserted when more than one input is connected to the same output, this is also done when the "node-connect" command is used in the interpreter. On the other hand, there are occasions when the automatic insertion of the Fork module is not desirable. For example, when there is a delay on one of the arcs, to avoid ambiguity about the locations of the delay, the Fork module must be inserted by the user. Furthermore, auto forking can cause problems when multiport holes are used. In this case, one may get two outputs and several inputs on the same net. At the moment, there is no way to automatically decipher what the user intends. Thus, why the Fork module should be inserted explicitly.

Balance photodetector in APL (Analog Photonic Link)

Domination of high order distortion product is not as dominant in multi-octave bandwidth APL compared to sub-octave APL. By changing the operating point of the modulator, it can be controlled, or linearization techniques can be used to deal with distorting products as a result of nonlinearity behaviour. Quadrature operating point has an advantage over second-order intermodulation (IMD2) product and enhances SFDR2 whereas biasing modulator at high operating point result in high system noise hence in some system using low biasing is preferable [22]. It's true biasing at low voltage reduces noise to the system however produces IMD2 which limits the bandwidth of the APL system. Balance photodetector can be used to remove noise from EDFA produced by laser RIN and Amplified Spontaneous Emission (ASE) [23]. Balance photodetector is formed by two paired photodiodes to form the differential structure shown in Fig.15. Photodiode one is written as $\Re 1$ and photodiode two is written as $\Re 2$.

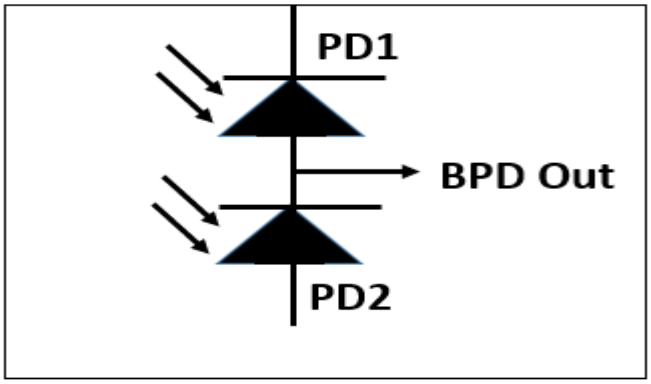

Figure 16: Balanced Photodetector structure [24]

In ideal conditions both photodiodes $\Re 1$ and $\Re 2$ have same responsivity and have opposite bias charge, therefore, common-mode signal will be eliminated this is called Common-Mode Rejection Ratio (CMRR). Mathematical representation of Balance photodetector is [24]:

$$I_{BPD}=I_{PD1}+I_{PD2}$$

Where I_{PD1} is photocurrent in first photodiode and I_{PD2} is photocurrent receiver in second photodiode.

Nonlinearities in APL

The modulation process in APL incurs limitations due to the Intermodulation distortion product and cross-modulation when using more than one signal as a result of nonlinearities in the system produced by the Electro-optic Modulator [26, 27]. Limitations of the APL system is mainly due to intensity modulators. Spurious-Free Dynamic Range (SFDR) is mostly limited by intermodulation products close to signal which are Second-order Intermodulation distortion and Third-order Intermodulation distortion (IMD2 and IMD3) also by Second-order harmonics and Third-order Harmonics (SHD and THD).

For the linearity of APL Intermodulation distortions (IMDs) are important frequencies that measure the linearity of the system [28, 29]. Modulation of two or more frequencies produces

amplitude modulation as a result of e nonlinearity this modulation frequency is called IMD whereas harmonics are sum and difference of fundamental frequencies they also can be multiple addition and subtraction of that sum and difference of frequencies as shown in Table (2) [30].

Second order Distortion	**Third Order Distortion**
$2f_1$	$3f_1$
$2f_2$	$3f_2$
$f_1 - f_2$	$2f_1 - f_2$, $2f_2 - f_1$
$f_1 + f_2$	$2f_1 + f_2$, $2f_2 + f_1$

Table 2: List of 2nd and 3rd distortion products

From the table can be seen that second-order harmonics are twice frequency one 2f1 and twice frequency two 2f2 similarly third-order harmonics are three-time frequency one 3f1 and tree times frequency two 3f2. When two signals interact with each other drives second-order products which are the sum or difference of each other as shown in Fig. 16.

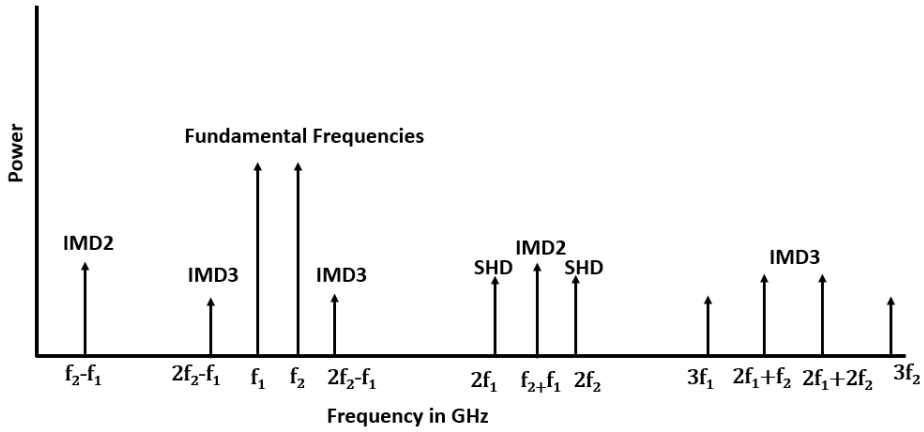

Figure 17: Second-order and third-order Intermodulation Distortion products

IMD3 and Second-Order Distortions (SOD) are the main distortion product cousin nonlinearity of APL system due to being too close to fundamental frequencies and limiting SFDR hence why my main focus was eliminating IMD3 and Second-Order Disortations as explained in chapter (). As explained above nonlinearity in APL is caused also by cross-modulation when two or more frequencies are modulated, in Fig.17. is shown a mixer frequency spectrum with cross-modulation distortion and intermodulation distortion. The signal can be down-converted or up-converted to Intermediate Frequencies (IFs) using these mixer frequencies. When frequencies interact with each other and local oscillator (flo) frequency therefore distortion products are generated as shown in Fig.17 in green colour. When self-beating two-tone RF frequencies produce distortion product in green colour Fig.17.

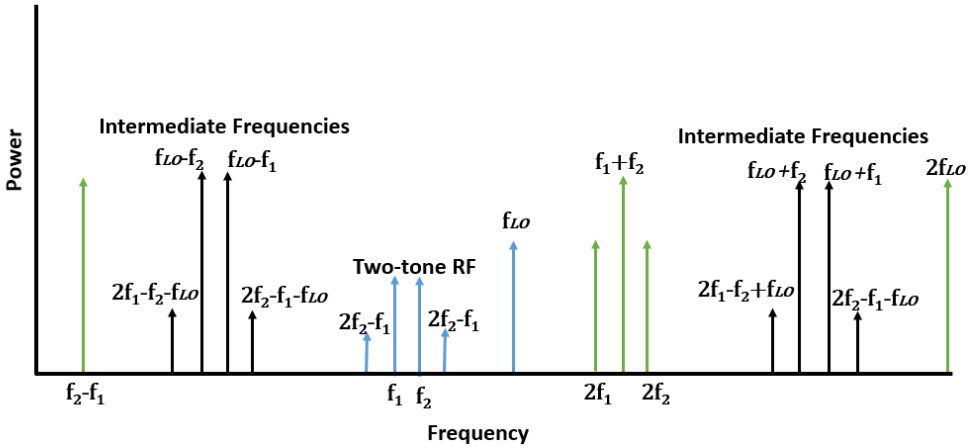

Figure 18: Intermodulation and Cross-modulation Distortions in a Frequency Mixer

In any RoF system, any extra frequency created as a result of nonlinearity will limit bandwidth therefore these extra frequencies created should be removed in ideal conditions (green colour frequencies) whereas frequencies in blue should be suppressed whenever is possible to enhance dynamic range.

SFDR (Spurious-Free Dynamic Range)

For any system in APL, the main concern distortion product is IMD2 for wider bandwidth and IMD3 for narrow bandwidth as they limit the SFDR. The greater concerns are IMD3 as they are very close to fundamental frequency [29, 30]. Power input of fundamental frequencies is in direct proportion with IMDs which can be measured by third-order Intercepted Point (IP3) [29]. When the power level of IMD3 is equal to the power of fundamental frequencies defines IP3 as shown in Fig.18. Mathematically IP3 can be written as:

$$IP3 = \frac{4V_{\pi}^{2}}{\pi^{2} R_{MZ}} \qquad (26)$$

Where Vπ is half wave voltage.

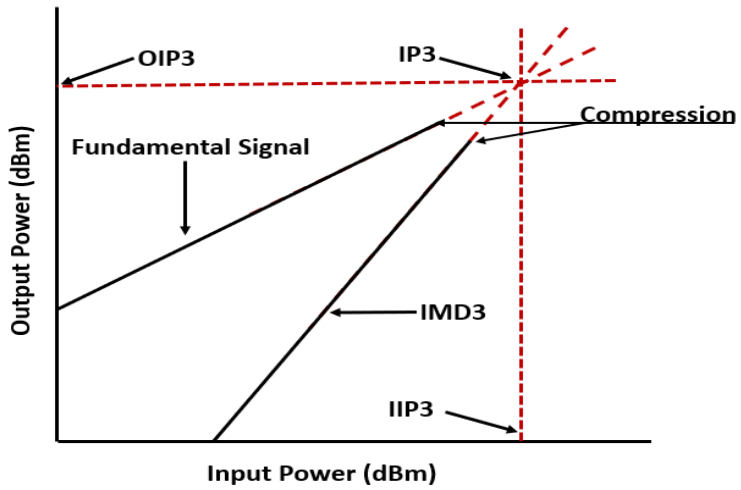

Figure 19: Example of Third Order Intercept point power

In a communication system for signal processing in APL SFDR is very important to be as big as possible [29, 30]. SFDR is a ratio between the highest distortion products and fundamental frequency as shown in Fig.19 [32].

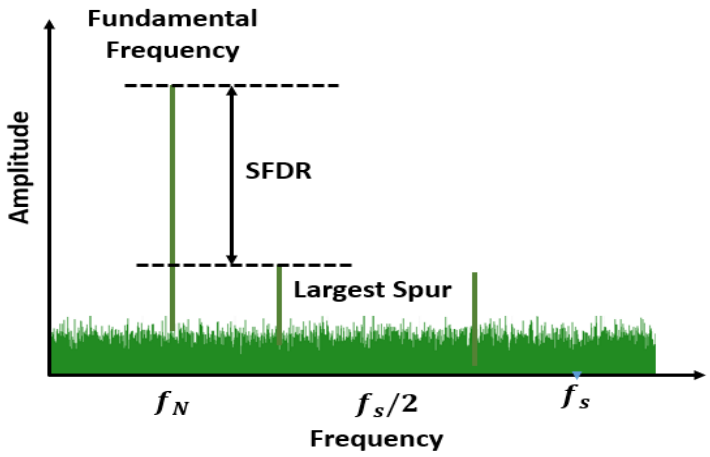

Figure 20: Measurement of SFDR

Signals cannot be measured under noise level which is a noise floor. The ratio between IMD3 and the fundamental signal is also described as SFDR (2f1-f2 and 2f2-f1).

Essential factor to be consider when measuring SFDR are:

- Output System Noise Level (OSNL)
- Input System Noise Level (ISNL)
- Background Noise Level (BNL)
- Noise Figure (NF) which difference of ISNL and BNL

OSNL is output noise power measured in 1 Hz, ISNL is a difference of output noise power from system gain, BNL depends on thermal noise figure which is usually -174dBm/Hz in room temperature. Third-order intercepted point should be considered when measuring SFDR for a high-end bit as shown in eq. 25.

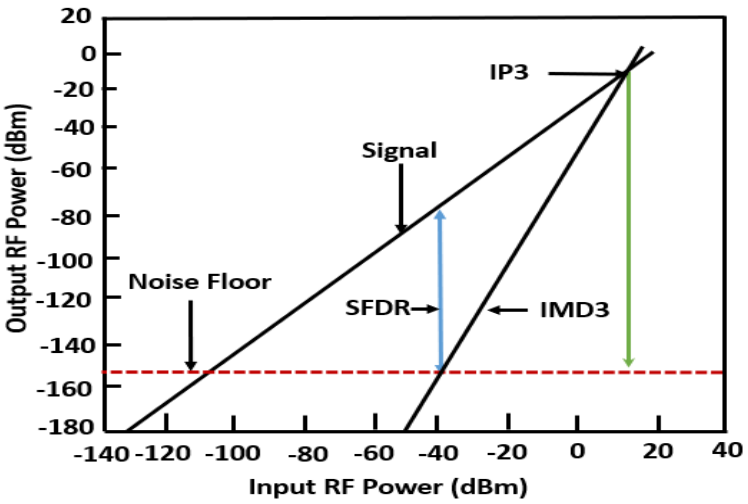

Figure 21: Graph of Spurious-free Dynamic Range

By subtracting BNL and NF in dB from IP3 with bandwidth 1Hz we can measure SFDR as is shown in Fig.20. The minimum power signal detected at receiver to give good output is called MDS. Mathematical representation of SFDR and MDS is:

$$MDS = NF_{dB} + 10\log(BW) + BNL$$

$$SFDR = 2/3\,[IP3 - MDS]$$

$$SFDR = 2/3[-BNL + IP3_{dBm} - NF_{dB} - 10\log(BW)] \qquad (25.1)$$

Self-Phase Modulation

If we consider the non-linear effect of pulse propagation, it means we are assuming for the time being that the dispersion is not playing a role. Choosing a parameter for the pulse in such a way that the dispersion effects are negligible, but the non-linear effects are present. This will happen if the pulse width is large, then the dispersion length is much larger than the physical length of optical fibre. Therefore, the dispersion effects can be neglected but the power in the optical pulse is large enough to have a non-linearity length which is smaller than the optical fibre length. In this instance, the refractive index with the pulse seeds is different at different locations within the pulse, having a refractive index which is a function of the intensity of light.

In the centre of the optical pulse, there is a large refractive index as on either side of the peak of the pulse the refractive index decreases so we have some variation of a refractive index of material inside the pulse itself. Since this pulse is moving inside the optical fibre, this refractive index profile also moves along the pulse inside the optical fibre. But since the refractive index is changing at different locations inside the pulse, the velocity changes and because of that, the phase changes inside the pulse. This change in phases is created because of the pulse itself. Such a phenomenon is called self-phase modulation.

Cross-Phase Modulation

When the other signal is present in optical fibre, changes in refractive index are going to be because of the signal plus itself and contribution coming from another signal which is co-existing along with this signal. The non-linear effect of another signal is twice stronger compared to the signal itself. Refractive index change is going to take place not only because of the signal itself but it is also due to another signal which is propagating. This phenomenon is called cross-phase modulation [14].

Wave Mixing

In the self-phase modulation case phase of a signal gets modified by the neighbouring signal and that phenomenon is called cross-phase modulation. The same phenomenon can also create new frequencies and that is called the four-wave mixing phenomenon. The four-wave mixing phenomena creates cross-talk between the neighbouring channels and its vector can be neglected or reduced by using the fibre, which is having some dispersion so that these signals can keep propagating through with each other. Because of this, the efficiency of non-linear interaction weakens too, so to avoid the cross-phase modulation as well as the four-wave mixing phenomena, we use the fibre that has some dispersion and not a zero dispersion.

Linearized Modulation Techniques

When the non-linear effects are present in the optical fibre, continuous signal propagation is unstable, which means that even if we try and send a continuous signal in the optical fibre, any small perturbation will break this signal into pulses. This means that without taking into consideration the pulse nature of the signal, the non-linear propagation will not be very effective. Microwave photonic links are wildly used in today's communication systems, like antenna remoted, radars and wireless communication. MPL have low loss, wide bandwidth, and low weight. The security data and immunity to electromagnetic interferences compared to coaxial cable [15, 16]. There are two types of modulation techniques to launch signals in optical fibre, direct modulation, and external modulation. Direct modulation uses DFB (Distributed Feedback) laser, external modulation uses intensity modulator, phase modulator or polarization modulator, which are widely used in increasing SFRD and eliminating or suppressing IMD's [17,18]. In Fig.21 a proposed configuration of linearized modulation based on two MZM is shown.

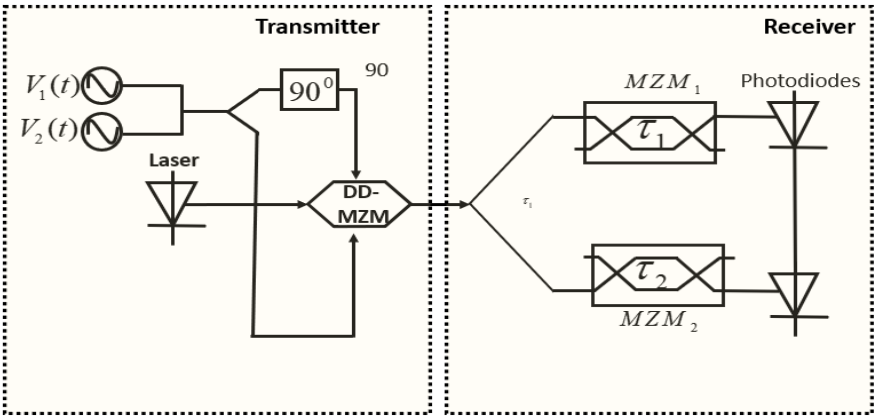

Figure 22: Linearized MPL proposed based on two MZIs

It is already known that second and third-order Intermodulation and Harmonics eliminations are paramount for any analogue communication system. There is much-reported research

papers that have been proposed and investigated various systems, such as a new system configuration of the analogue photonic link is proposed in Ref. [19] where optical polarizer, optic filter and phase modulator are deployed to improve the system performance. In this paper [19], 25.4 dB cancellation of third-order intermodulation distortion has been achieved by adjusting the state of polarization and sending the signal to the phase modulator across the polarizer.

Chapter 3

Linearization and Down-Conversion of Microwave Photonics Signal based on Dual-drive Dual-parallel Mach-Zehnder Modulator with Eliminated Third Order Intermodulation and Second Order Distortions

Introduction

Optical fibre communication systems offer significant benefits for current and future broadband wired and wireless communication systems, due to low losses, high data rate, low electromagnetic interference, and potential high security [20-23]. These communication systems have enormous potential interest for researchers in commercial and defence applications, such as Radio over Fibre (RoF) which is also an important part of optical communication systems, which transmit microwave signals over fibre optics domains. RoF, in particular, is a low cost, a flexible and promising technique for radio access systems [24]. Due to a great demand for high data rate and security in the current transmission systems, and their foreseeable prerequisite in the future, RoF systems have been wildly exploited. Nevertheless, RoF has its limitations, which need to be explored further to handle the significant increase of data capacity demands. These limitations are due to nonlinearity materials, losses due to conversion from electrical to optical, optical to electrical, and other associated signal scatterings. To overcome these limitations, in the literature key performance parameters are explored such as noise figure, gain and dynamic range [25], [26] and [27]. Dual- Electrode Mach-Zehnder Modulator (DE-MZM), which are key devices for such transmission systems, are used for elimination and suppression of IMD3 and suppression of one side to gain a single-sideband. By using DE-MZM, it is possible to increase dynamic range and eliminate or suppress Intermodulation Distortions (IMD's) and higher harmonics, which are essential to improving the signal to noise ratio at the Photo-Detector (PD). However, complex radio-frequency arrangements and synchronizations are required.

It is widely known that the second and third-order IMD's and harmonics eliminations are paramount for any analogue communication system. Many research papers have been written where various systems, such as a new system configuration of analogue photonic link, have been proposed and investigated [8]. Proposals where optical polarizer, optic filter and phase modulator are deployed to improve the system performance. In this report [28], 25.4 dB cancellation of IMD3 has been achieved by adjusting the state of polarization and sending the signal to the phase modulator across the polarizer. In [29], a new system configuration for the analogue photonic link with the digital signal is demonstrated. The proposed structure in Ref. [9] is based on an optical phase modulator and I/Q demodulator where a 30 dB dynamic range has been achieved. Furthermore, in [30], an analogue link with the digital signal is reported based on optical intensity modulator and I/Q demodulator, where a 26.8 dB dynamic range has been achieved. In both papers [29] and [30] reported systems, they require a high coherent part, which is not easy to implement.

An analogue photonic link linearization system is proposed in the paper [31] by setting Mach-Zehnder Modulator (MZM) at the minimum biasing point with a low modulation depth, which decreases nonlinearity without compromising the ratio between Carrier-to-Sideband Ratio (CSR), nonlinearity terms and carrier increases dynamic range. When the modulation depth of RF is higher than the IMD3, is introduced by high order sidebands, which leads to low RF conversion. In Ref. [32] a system configuration of dual parallel Interferometer is proposed using Dual Parallel Mach–Zehnder modulator (DPMZM) based on optical single-sideband modulation technique. Different differential delay is achieved by balancing two parallel interferometers, whereas a result IMD3 is balanced, and limited link response has been limited from fifth-order distortion. However, differential delay and other parameters in the link need to be very accurate, which is a very difficult task to achieve. In [33], an analogue photo link

system is demonstrated based on double sideband suppressed carrier and coherent BPD using D-DPMZM where a 46 dB IMD3 suppression has been achieved. Therefore, an accurate polarization is required for such systems.

A system configuration to achieve a low distortion analogue photo link system is proposed and analysed using DPMZM in paper Ref. [34]. The electrical driver signal ratio in Mach-Zehnder modulator is adjusted for linearization. This configuration enhanced linearization, at the cost of increased power and essential driving voltage. This system first started using DPMZM and contributed a great deal a lot in linearization techniques. In Ref. [35] an RoF system is being demonstrated using single-drive DPMZM. Changing the operating point of the modulator is achieved an opposite phase and equal intensity in sub-MZM. As a result, the Third Order Distortion (TOD) is suppressed. When the modulation depth of the RF signal is high, then the high order optical sideband increases. Hence, the TOD will be introduced.

In [36] a linearized system configuration for analogue photo link based on DPMZM and coherent detection is proposed by simultaneously adjusting ratios between input optical powers split, output optical power split and electrical signal power, whereas a result IMD3 has been theoretically eliminated. A new configuration system for analogue photo link based on DPMZM with electro-optic polymer material is demonstrated [37] by using two MZM in parallel with different lengths and with a phase shifter in one arm. By changing the input and output optical power splitting ratio in the optical field and optimizing modulation depth at the same time. The IMD3 has been suppressed below the noise floor. However, in these two reports [36] and [37], they require combinations of special electric and optical splitting ratios, which are challenging to achieve. In Ref. [38] a photo link for microwave signal is proposed based on symmetric single-sideband modulation using two subs MZM and three electrical

phase shifters. The phase of the electrical signal is controlled by using these three electrical phase shifters where IMD3 is suppressed by 30 dB. However, it is not easy to balance a symmetrical symmetric single-sideband modulation.

An ultra-wideband microwave photonic frequency down converter based on carrier suppressed is reported in [39]. Two radio frequency signals are combined to drive D-DPMZM through the electrical 90° hybrid coupler. The experimental results demonstrate that the proposed frequency downconverter can generate from 2 to 40 GHz. However, mixing spurs are suppressed under the noise floor in the electrical spectrum and if the modulation index increases, mixing spurs would arise, which will not be the case in our current proposed model reported in this study. An analogue photonic link with improved SOD and IMD3 based on two D-DPMZM and BPD is demonstrated [40] where the Spurious-Free Dynamic Range (SFDR) of second and third order with frequency 6 to 40 GHz are 91 dB$Hz^{\frac{2}{3}}$ and 116 dB $Hz^{\frac{2}{3}}$ are achieved. However, the second and third-order IMD's have not been eliminated and if the modulation index increases, the IMD's will appear. Whereas in our proposed model shown below IMD's have been eliminated. In this proposed report I report a high linearized microwave photonic link. The IMD3 and SOD have been cancelled by symmetrically single sideband modulation. Moreover, by controlling the phase of the input signal and driving voltage of D-DPMZM, higher-order harmonics distortion also has been suppressed.

Mathematical model of the proposed system

The schematic diagram of the proposed linearized microwave photonic link and down-conversion using two D-DPMZM and BHD is illustrated in Fig.22. Two D-DPMZM consists of two DPMZM. Each DPMZM consists of two sub MZMs with two-tone microwave frequency used as input RF to the DPMZM1 and DPMZM2 respectively, labelled as ω_1 and ω_2, correspondingly.

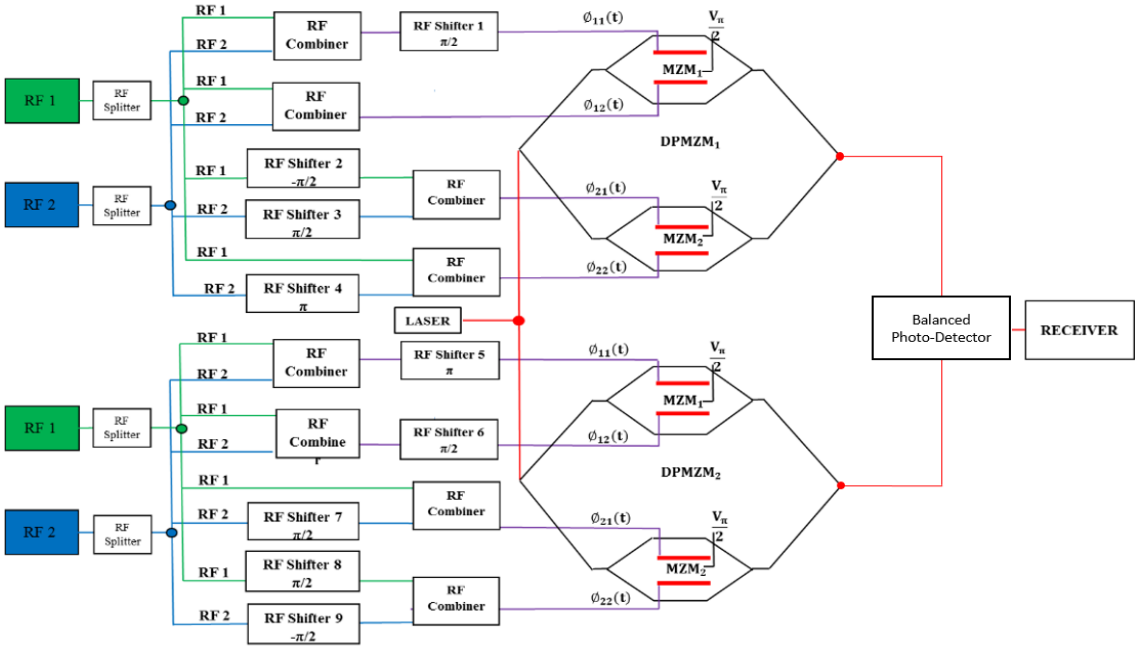

Figure 23: Schematics of proposed D-DPMZM linearized microwave photonic linkwith two input frequencies.

The input RF frequencies of upper and lower sub MZMs of each D-DPMZM are shifted, as shown in Fig.21. External DC bias is applied to adjust the power ratio for system linearization. The recovered signal from BPD shows IMD3 and SOD are cancelled. The other IMD's are suppressed simultaneously. Only fundamental frequencies and high order harmonics are present.

The drive voltage with DC biases of DPMZM1 mathematically can be expressed as [40]:

$$\phi_{11}(t) = V_m \left\{\cos(\omega_1 t + \frac{\pi}{2}) + \cos(\omega_2 t + \frac{\pi}{2})\right\} + \frac{V_\pi}{2} \quad (27)$$

$$\phi_{12}(t) = V_m \left\{\cos(\omega_1 t) + \cos(\omega_2 t)\right\} \quad (28)$$

$$\phi_{21}(t) = V_m \left\{\cos(\omega_1 t - \frac{\pi}{2}) + \cos(\omega_2 t + \frac{\pi}{2})\right\} + \frac{V\pi}{2} \quad (29)$$

$$\phi_{22}(t) = V_m \left\{\cos(\omega_1 t) + \cos(\omega_2 t + \pi)\right\} \quad (30)$$

Where $\emptyset_{11}(t)$ and $\emptyset_{12}(t)$ are drive voltages on two MZM1 (DPMZM1) electrodes; $\emptyset_{21}(t)$ and $\emptyset_{12}(t)$are drive voltages on two MZM2 (DPMZM1) electrodes,V_m is the electrical amplitude of input RF signal. The optical power distributed by laser can be expressed as $E_{in}(t) = E_c e^{j\omega_c t}$, where E_c is the input power and ω_c is angular frequency of the laser. The output optical power driven by RF message signal in MZM1 (DPMZM1) can be expressed as:

$$E_{out1MZM_1}(t) = E_{in}(t)\left\{\exp(j\pi\frac{\phi_{11}(t)}{V_\pi}) + \exp(j\pi\frac{\phi_{12}(t)}{V\pi})\right\} \quad (31)$$

The output optical field driven by RF message signal in MZM_2 ($DPMZM_1$) can be expressed as:

$$E_{out1MZM_2}(t) = E_{in}(t)\left\{\exp(j\pi\frac{\phi_{21}(t)}{V_\pi}) + \exp(j\pi\frac{\phi_{22}(t)}{V_\pi})\right\} \quad (32)$$

If equation 27 and 28 is substituted in to equation 31, then:

$$E_{out1MZM_1}(t) = E_{in}(t)\left\{\begin{array}{l}\exp\left(jm\left\{-\sin(\omega_1 t) - \sin\left(\omega_2 t\right)\right\} + j\frac{\pi}{2}\right)\\ +\exp\left(jm\left\{\cos\left(\omega_1 t\right) + \cos\left(\omega_2 t\right)\right\}\right)\end{array}\right\} \quad (33)$$

Where $m = \frac{\pi V_m}{V_\pi}$;

By applying a Jacobi-Anger Expansion in equation 33 will lead to:

$$E_{out1MZM_1}(t) = E_{in}(t)\sum_{n,m=-\infty}^{\infty} Jn(m)J_m(m)e^{j(n\omega_1 t+\omega_2 t)}\left[(-1)^{n+m}e^{j}\frac{\pi}{4} + \left(j^{n+m}\right)e^{j-\frac{\pi}{4}}\right] \quad (34)$$

Similarly, by substituting equation 29 and 30 in to equation 32 then the output from MZM_1 ($DPMZM_1$) is;

$$E_{out1MZM_2}(t) = E_{in}(t)\begin{Bmatrix}\exp\left(jm\left\{\sin(\omega_1 t)-\sin(\omega_2 t)\right\}+j\frac{\pi}{2}\right)\\+\exp\left(jm\left\{\cos(\omega_1 t)-\cos(\omega_2 t)\right\}\right)\end{Bmatrix} \quad (35)$$

By applying a Jacobi-Anger Expansion in equation 35;

$$E_{out1MZM_2}(t) = E_{in}(t)\sum_{n,}^{\infty} m=-\infty Jn(m)Jm(m)e^{j(n\omega_1 t+\omega_2 t)}\begin{bmatrix}(-1)^m e^{j\frac{\pi}{4}}+\\(-1)^m\left(j^{n+m}\right)e^{j-\frac{\pi}{4}}\end{bmatrix} \quad (36)$$

Biasing the sub MZM_3 to zero-point, the output of $DPMZM_1$ can be expressed as:

$$E_{outDPMZM_1}(t) = \frac{E_{out1MZM_1}(t)+E_{out1MZM_2}(t)}{\sqrt{2}} \quad (37)$$

$$E_{outDPMZM_1}(t) = \frac{E_{in}(t)}{\sqrt{2}}\sum_{n,m=-\infty}^{\infty} J_n(m)J_m(m)\begin{Bmatrix}(-1)^{n+m}e^{j\frac{\pi}{4}}+\left(j^{n+m}\right)e^{j-\frac{\pi}{4}}+\\(-1)^m e^{j\frac{\pi}{4}}+(-1)^m\left(j^{n+m}\right)e^{j-\frac{\pi}{4}}\end{Bmatrix}e^{j(n\omega_1 t+t+\omega_2 t)} \quad (38)$$

The photocurrent I(t) after the photodetector of $DPMZM_1$,mathematically can be obtained by following equation:

$$I_{PD1}(t) = \Re\left|E_{outDPMZM_1}(t)\right|^2 \quad (39)$$

Where $\mathcal{R}$ is responsivity of photodetector. By deploying the Taylor series expansion into the third order in m, the following expression of $I_{PD1}(t)$ can be derived:

$$I_{PD1}(t) = \frac{1}{2}\Re P_{in}\begin{Bmatrix}8+8m\left(\cos(\omega_1 t)+\sin(\omega_2)\right)\\+2m^2\left(-2+\cos(2\omega_1 t)-\cos(2\omega_2)\right)\\-\frac{2}{3}m^3\begin{pmatrix}9\cos(\omega_1 t)-\cos(3\omega_1 t)\\+9\cos(2\omega_2 t)+\sin(3\omega_2)\end{pmatrix}\end{Bmatrix}o(m)^4 \quad (40)$$

Similarly, the drive voltage with DC biases of $DPMZM_2$ can be expressed as:

$$\phi_{11}(t) = V_m \left\{\cos\left(\omega_1 t + \pi\right) + \cos\left(\omega_2 t + \pi\right)\right\} + \frac{V\pi}{2} \tag{41}$$

$$\phi_{12}(t) = V_m \left\{\cos\left(\omega_1 t + \frac{\pi}{2}\right) + \cos\left(\omega_2 t + \frac{\pi}{2}\right)\right\} \tag{42}$$

$$\phi_{21}(t) = V_m \left\{\cos\left(\omega_1 t\right) + \cos\left(\omega_2 t + \frac{\pi}{2}\right)\right\} + \frac{V\pi}{2} \tag{43}$$

$$\phi_{22}\left(t\right) = V_m \left\{\cos\left(\omega_1 t + \frac{\pi}{2}\right) + \cos\left(\omega_2 t - \frac{\pi}{2}\right)\right\} \tag{44}$$

The output optical field driven by RF message signal in MZM1 (DPMZM2) can be expressed as:

$$E_{out2MZM_1}(t) = E_{in}(t)\left\{\exp\left(j\pi\frac{\phi_{11}(t)}{V_\pi}\right) + \exp\left(j\pi\frac{\phi_{12}(t)}{V_\pi}\right)\right\} \tag{45}$$

The output optical field driven by RF message signal in MZM2 (DPMZM2) can be expressed as:

$$E_{out2MZM_2}(t) = E_{in}(t)\left\{\exp\left(j\pi\frac{\phi_{21}(t)}{V_\pi}\right) + \exp\left(j\pi\frac{\phi_{22}(t)}{V_\pi}\right)\right\} \tag{46}$$

If equation 41 and 42 is substituted in to 45 then:

$$E_{out2MZM_1}(t) = E_{in}(t)\begin{Bmatrix}\exp\left(jm\left\{-\cos\left(\omega_1 t\right) - \cos\left(\omega_2 t\right)\right\} + j\frac{\pi}{2}\right)\\ +\exp\left(jm\left\{-\sin\left(\omega_1 t\right) - \sin\left(\omega_2 t\right)\right\}\right)\end{Bmatrix} \tag{47}$$

Where $\mathrm{m} = \frac{\pi \mathrm{V_m}}{\mathrm{V_\pi}}$;

By applying the Jacobi-Anger Expansion in equation 47;

$$E_{out2MZM_1}(t) = \frac{E_{in}(t)}{\sqrt{2}}\sum_{n,m=-\infty}^{\infty} Jn\left(m\right) Jm\left(m\right) e^{j\left(n\omega_1 t + \omega_2 t\right)}\left[\left(-j\right)^{n+m} e^{j\frac{\pi}{4}} + \left(-1\right)^{n+m} e^{j-\frac{\pi}{4}}\right] \tag{48}$$

Similarly, by substituting equation 43 and 45 into the equation 46, the output optical field in MZM2 (DPMZM2) is:

$$E_{out2DPMZM_2}(t) = E_{in}(t)\begin{Bmatrix} \exp\left(jm\left\{\cos(\omega_1 t) - \cos(\omega_2 t)\right\} + j\frac{\pi}{2}\right) \\ +\exp\left(jm\left\{-\sin(\omega_1 t) + \sin(\omega_2 t)\right\}\right) \end{Bmatrix} \quad (49)$$

Also, by applying a Jacobi-Anger Expansion in equation 49;

$$E_{out2DPMZM_2}(t) = E_{in}(t)\sum_{n,m=-\infty}^{\infty} Jn(m)Jm(m)e^{j(n\omega_1 t+\omega_2 t)}\begin{bmatrix} (j)^n(-j)^m e^{j\frac{\pi}{4}} + \\ (-1)^n e^{j-\frac{\pi}{4}} \end{bmatrix} \quad (50)$$

When biasing the sub MZM3 to zero-point, then the output of DPMZM2 can be expressed as:

$$E_{outDPMZM_2}(t) = \frac{E_{out2DPMZM_1}(t) + E_{out2DPMZM_2}(t)}{\sqrt{2}} \quad (51)$$

$$E_{outDPMZM_2}(t) = \frac{E_{in}(t)}{\sqrt{2}}\sum_{n,m=-\infty}^{\infty} Jn(m)Jm(m)\begin{Bmatrix} (-j)^{n+m} e^{j\frac{\pi}{4}} + (-1)^{n+m} e^{j-\frac{\pi}{4}} + \\ (j)^n(-j)^m e^{j\frac{\pi}{4}} + (-1)^n e^{j-\frac{\pi}{4}} \end{Bmatrix} e^{j(n\omega_1 t+\omega_2 t)} \quad (52)$$

The photocurrent I(t) after photodetector of DPMZM2 can be obtained by following equation:

$$I_{PD2}(t) = \Re\left|E_{outDPMZM_2}(t)\right|^2 \quad (53)$$

Where $\mathcal{R}$ is responsivity of photodetector. By using the Taylor series expansion to the third order in m, the following expression can be derived.

$$I_{PD2}(t) = \frac{1}{2}\Re P_{in}\begin{Bmatrix} 8 + 8\left[m\left(\cos(\omega_1 t) + \sin(\omega_2)\right)\right] \\ +2m^2\left(-2 - \cos(2\omega_1 t) + \cos(2\omega_2)\right) \\ \frac{2}{3}m^3\begin{bmatrix} -9\cos(\omega_2 t) + \cos(3\omega_2 t) \\ +9\sin(\omega_1 t) + \sin(3\omega_1) \end{bmatrix} \end{Bmatrix} + o(m)^4 \quad (54)$$

Recovered signal after BPD $I_{PD1}(t) + I_{PD2}(t)$ we will be obtained:

$$I_{PD1+PD2}(t)=\frac{1}{2}\Re P_{in}\left\{\begin{array}{l} 8+8\left[\begin{array}{l} m\left(\cos\left(\omega_2 t\right)-\sin\left(\omega_1\right)\right)+ \\ +m\left(\cos\left(\omega_1 t\right)+\sin\left(\omega_2\right)\right) \end{array}\right] \\ -8m^2 \\ \frac{2}{3}m^3\left[\begin{array}{l} -9\cos\left(\omega_2 t\right)+\cos\left(3\omega_2 t\right) \\ +9\sin\left(\omega_1 t\right)+\sin\left(3\omega_1\right) \\ 9\cos\left(\omega_1 t\right)-\cos\left(3\omega_1 t\right) \\ +9\cos\left(2\omega_2 t\right)+\sin\left(3\omega_2\right) \end{array}\right] \end{array}\right\} o\left(m\right)^4 \qquad (55)$$

Equation 54 illustrates that the microwave photonic link based on two D-DPMZ and BPD can be used to linearize signals, resulting in the elimination of the IMD3 of frequency $2\omega_2-\omega_1$ and $2\omega_1-\omega_2$ and the SOD of frequency $2\omega_2$, $\omega_2-\omega_1$, $\omega_1+\omega_2$ and $2\omega_1$. SOD and IMD3 are the main contribution of the non-linearity. We have used the Taylor series for higher order (up to the ninth order) and the IMD3 and SOD still does not exist, which means that when the modulation index increases, the IMD3 and SOD will not exist in the proposed system configuration.

Simulation results and discussions

In our proposed configurations and developed corresponding mathematical model, we have deployed the VPI commercial software to simulate the system illustrated in Fig.22.

In this structure, we have used two D-DPMZM. A laser with an optical power of 20 dBm is used, two sinusoid signals with frequencies of 17 GHz and 17.5 GHz are also used. The signal is split in equal ratio and modulated in DPMZM1 and DPMZM2

The phase shifting has been performed as follows; In DPMZM1 RF signal ω_1 and ω_2 in MZM1 upper branch have been shifted by $\frac{\pi}{2}$ and in MZM2 signal ω_1 has been shifted by $-\frac{\pi}{2}$; ω_2

signal has been shifted by $\frac{\pi}{2}$ in upper branch whereas in the lower branch the signal ω_2 has been shifted by π. In DPMZM2 signal ω_1 and ω_2 have been shifted by π in upper branch of MZM1, RF signal ω_1 and ω_2 has been shifted by $\frac{\pi}{2}$ in lower branch of MZM1, in MZM2 signal ω_2 has been shifted by π in upper branch as in lower branch of MZM2; ω_1 has been shifted by $\frac{\pi}{2}$ and $\omega_2$has been shifted by $-\frac{\pi}{2}$.

The generated signal from DPMZM1 is transmitted through channel 1 as shown in Fig.23 a, and the generated signal from DPMZM2 is transmitted through channel 2 as shown in Fig.23 b. The recovered signal from BPD is shown in Fig.23 c.

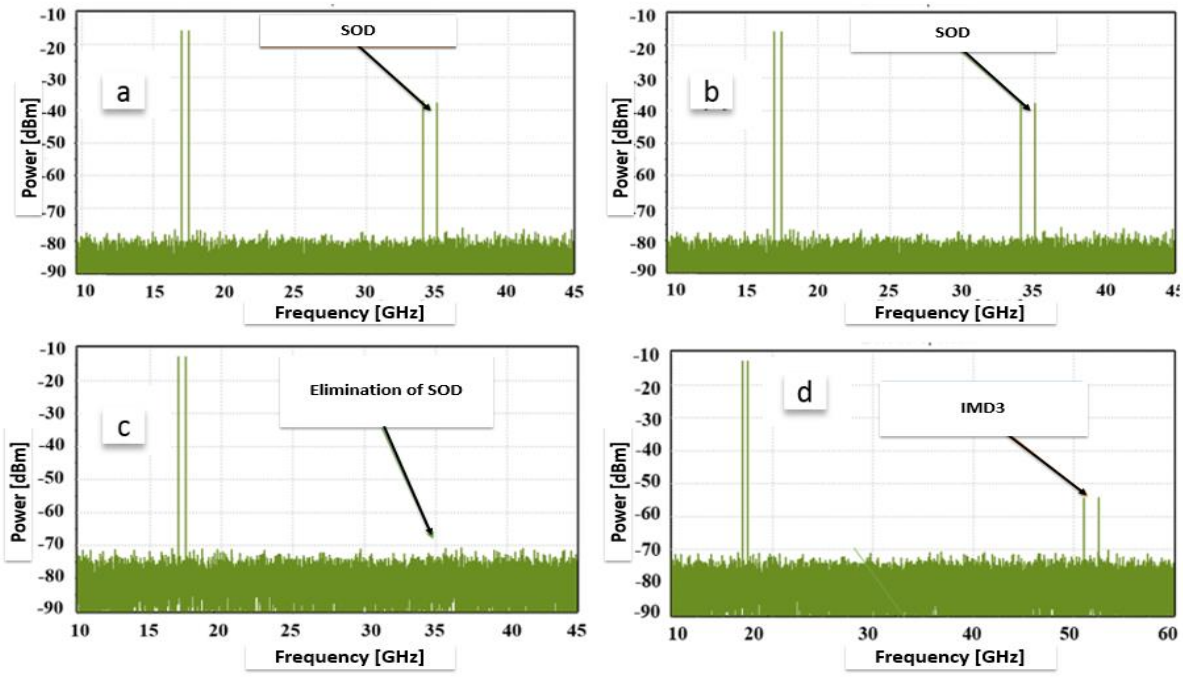

*Figure 24: **A** Output Frequency from $DPMZ_1$; **b** Output Frequency from $DPMZ_2$; **c** Output field after balanced photo-detector; **d** Output field after modification.*

From Fig.23 we can see the elimination of IMD3, whereas the SOH is still present. Similarly, Fig 23 b shows similar behaviour as in Fig. 23 a, however, with opposite SOH fields which enables the elimination of the SOH after BPD. From Fig.23 c it can be observed the SOH has been eliminated. However, higher distortion still exists. We have tested our system purity by changing the parameters of the modulator (Table 3) to match with our lab modulator, where

we obtained the same results as before. Furthermore, by using the same parameters for IMD3 and SOH to be suppressed under the noise floor shifters accuracy should be within four degrees, Fig.24 a. We can only start seeing SOH when shifters accuracy is 5 degrees or more Fig.24 b. By adding a universal fibre optic cable with a length of 1 kilometre for both channels, we find out that the results do not change Fig.24 c. However, if the length of fibre optic cable is not the same, then SOH starts coming up the noise floor. We have used 1 Km fibre optic cable for channel one and 1.2 Km fibre optic cable for channel two and the SOH can barely be seen, Fig.24 d.

	MZM_1	MZM_2	MZM_3	MZM_4
VpiDC /VpiRF	3.5 V	3.5 V	3.5 V	3.5 V
Insertion Loss	6 dB	6 dB	6 dB	6 dB
Extinction Ratio	21.8 dB	18.5 dB	21.8 dB	18.5 dB
dVpiDC_dTemperature	0.005 V/degC	0.005 V/degC	0.005 V/degC	0.005 V/degC
dVpiRF_dTemperature	0.0015 V/degC	0.0015 V/degC	0.0015 V/degC	0.0015 V/degC
OperatingTemperature	25 degC	25 degC	25 degC	25 degC
ReferenceTemperature	25 degC	25 degC	25 degC	25 degC
ElectrodeLengthUpper	23 mm	23 mm	23 mm	23 mm
IndexMismatchUpper	0.05	0.05	0.05	0.05
MicrowaveLossUpper	0.002 dB/m/sqrt(Hz)	0.002 dB/m/sqrt(Hz)	0.002 dB/m/sqrt(Hz)	0.002 dB/m/sqrt(Hz)
ElectrodeLengthLower	23 mm	23 mm	23 mm	23 mm
IndexMismatchLower	0.05	0.05	0.05	0.05
MicrowaveLossLower	0.002 dB/m/sqrt(Hz)	0.002 dB/m/sqrt(Hz)	0.002 dB/m/sqrt(Hz)	0.002 dB/m/sqrt(Hz)

Table 3: MZM_S Parameters used in our simulation

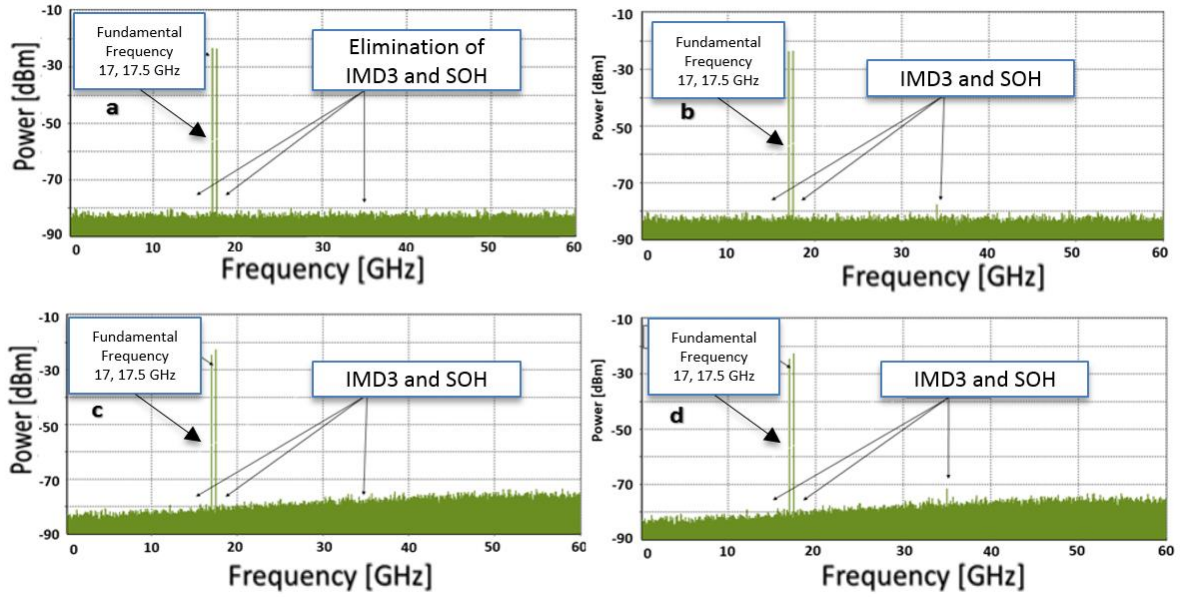

*Figure 25: **a** shifter accuracy within 4 degrees; **b** shifter accuracy 5 or more degrees; **c** output signal spectrum using 1 Km fibre optic cable for both channels; **d** output signal*

spectrum using 1 Km fibre optic cable for channel 1 and 1.2 Km fibre optic cable for channel 2;

Microwave photonic down-conversion using two fibre optic channels

The schematic diagram of the down-conversion linearized microwave photo link deploying two D-DPMZM and two fibre-optic channels is illustrated in Fig.21. We have investigated the down-conversion of the same system configuration. As illustrated in section 3.1.1, we have only modified the operating biased point from quadrature to maximum, where we have achieved a high linearized down-conversion signal. In the same model, as in the above section 3.1.1, we can derive the following mathematic modelling for the down-conversion of the proposed microwave photonic link.

The drive voltage with down-conversion biases of DPMZM1 can be expressed as:

$$\phi_{11}(t) = V_m \left\{ \cos\left(\omega_1 t + \frac{\pi}{2} \right) + \cos\left(\omega_2 t + \frac{\pi}{2} \right) \right\} V_\pi \tag{56}$$

$$\phi_{12}(t) = V_m \left\{ \cos\left(\omega_1 t \right) + \cos\left(\omega_2 t \right) \right\} \tag{57}$$

$$\phi_{21}(t) = V_m \left\{ \cos\left(\omega_1 t - \frac{\pi}{2} \right) + \cos\left(\omega_2 t + \frac{\pi}{2} \right) \right\} + V_\pi \tag{58}$$

$$\phi_{22}(t) = V_m \left\{ \cos\left(\omega_1 t \right) + \cos\left(\omega_2 t + \pi \right) \right\} \tag{59}$$

Where $\emptyset_{11}(t)$ and $\emptyset_{12}(t)$ are drive voltages on two MZM's (DPMZM1) electrodes; $\emptyset_{11}(t)$ and $\emptyset_{12}(t)$ are drive voltages on two MZM's (DPMZM2) electrodes, V_m is the electrical amplitude of RF input signal which is the same for each input signal. The optical power distributed by laser can be expressed as; $E_{in}(t) = E_c e^{jw_c t}$, where E_c is the input power and ω_c is the angular frequency of the laser source. The output optical field driven by RF signal message in MZM1 (DPMZM1) can be expressed as:

$$E_{out1MZM_1}(t) = E_{in}(t)\left\{\exp\left(j\pi\frac{\phi_{11}(t)}{V_\pi}\right)+\exp\left(j\pi\frac{\phi_{12}(t)}{V_\pi}\right)\right\} \quad (60)$$

The output optical field driven by RF signal message in MZM2 (DPMZM1) can be expressed as:

$$E_{out1MZM_2}(t) = E_{in}(t)\left\{\exp\left(j\pi\frac{\phi_{21}(t)}{V_\pi}\right)+\exp\left(j\pi\frac{\phi_{22}(t)}{V_\pi}\right)\right\} \quad (61)$$

Where $\mathrm{m} = \frac{\pi V_m}{V_\pi}$; than by substituting equation 56 and 57 into equation 60 then:

$$E_{out1MZM_1}(t) = E_{in}(t)\begin{Bmatrix}\exp\left(jm\left\{-\sin(\omega_1 t)-\sin(\omega_2 t)\right\}+j\pi\right)\\+\exp\left(jm\left\{\cos(\omega_1 t)+\cos(\omega_2 t)\right\}\right)\end{Bmatrix} \quad (62)$$

By applying a Jacobi-Anger Expansion in equation 62.

$$E_{out1MZM_1}(t) = E_{in}(t)\sum_{n,m=-\infty}^{\infty} Jn(m)Jm(m)e^{j(n\omega_1 t+\omega_2 t)}\left[(-1)^{n+m}e^{j\frac{\pi}{2}}+\left(j^{n+m}\right)e^{j-\frac{\pi}{2}}\right] \quad (63)$$

Similarly, by substituting equation 58 and 59 into equation 61, we can find the output optical field driven by RF signal message in MZM2 (DPMZM1)

$$E_{out1MZM_2}(t) = E_{in}(t)\begin{Bmatrix}\exp\left(jm\left\{\sin(\omega_1 t)-\sin(\omega_2 t)\right\}+j\pi\right)\\+\exp\left(jm\left\{\cos(\omega_1 t)\_\cos(\omega_2 t)\right\}\right)\end{Bmatrix} \quad (64)$$

By applying a Jacobi-Anger Expansion in equation 64;

$$E_{out1MZM_2}(t) = E_{in}(t)\sum\nolimits_{n,m=-\infty}^{\infty} Jn(m)Jm(m)e^{j(n\omega_1 t+\omega_2 t)}\begin{bmatrix}(-1)^m e^{j\frac{\pi}{2}}+\\(-1)^m\left(j^{n+m}\right)e^{j-\frac{\pi}{2}}\end{bmatrix} \quad (65)$$

Optical field from DPMZM1 can be expressed as:

$$E_{outDPMZM_1}(t) = \frac{E_{outMZM_1}(t)+E_{out1MZM_2(t)}}{\sqrt{2}} \quad (66)$$

$$E_{outDPMZM_1}(t) = \frac{E_{in}(t)}{\sqrt{2}}\sum\nolimits_{n,m=-\infty}^{\infty} Jn(m)Jm(m)\begin{Bmatrix}(-1)^{n+m}e^{j\frac{\pi}{2}}+\left(J^{n+m}\right)e^{J-\frac{\pi}{2}}+\\(-1)^m e^{j\frac{\pi}{2}}+(-1)^m\left(j^{n+m}\right)e^{j-\frac{\pi}{2}}\end{Bmatrix}e^{j(n\omega_1 t+\omega_2 t)} \quad (67)$$

The photocurrent I(t) after the photodetector, can be obtained by substituting output fields of

DPMZM1 into the following equation:

$$I_{PD1}(t) = \Re\left|E_{outDPMZM_1}(t)\right|^2 \tag{68}$$

Where $\mathcal{R}$ is responsivity of photodetector. Using Taylor series expansion to the third order in m, the following expression can be derived

$$I_{PD1}(t) = \frac{1}{2}\Re P_{in}\left\{-4m^2 * (J * \cos(\omega_1) + (j * \sin(\omega_2))^2\right\} + o(m)^4 \tag{69}$$

Similarly, the drive voltage of DPMZM2 can be expressed as:

$$\phi_{11}(t) = V_m\left\{\cos(\omega_1 t + \pi) + \cos(\omega_2 t + \pi)\right\} + V_\pi \tag{70}$$

$$\phi_{12}(t) = V_m\left\{\cos\left(\omega_1 t + \frac{\pi}{2}\right) + \cos\left(\omega_2 t + \frac{\pi}{2}\right)\right\} \tag{71}$$

$$\phi_{21}(t) = V_m\left\{\cos(\omega_1 t) + \cos\left(\omega_2 t + \frac{\pi}{2}\right)\right\} + V_\pi \tag{72}$$

$$\phi_{22}(t) = V_m\left\{\cos\left(\omega_1 t + \frac{\pi}{2}\right) + \cos\left(\omega_2 t - \frac{\pi}{2}\right)\right\} \tag{73}$$

Where $\emptyset_{11}(t)$ and $\emptyset_{12}(t)$ are drive voltages on two MZM1 (DPMZM2) electrodes; $\emptyset_{11}(t)$ and $\emptyset_{12}(t)$ are drive voltages on two MZM2 (DPMZM2) electrodes, V_m is the electrical amplitude of input RF signal. The optical power distributed by the laser can be expressed as;$E_{in}(t) = E_c e^{j\omega_c t}$, where E_c is the input power and ω_c is angular frequency of the laser. Then the output optical field driven by RF signal message in MZM1 (DPMZM2) can be expressed as:

$$E_{out2MZM_1}(t) = E_{in}(t)\left\{\exp\left(j\pi\frac{\phi_{11}(t)}{V_\pi}\right) + \exp\left(j\pi\frac{\phi_{12}(t)}{V_\pi}\right)\right\} \tag{74}$$

The output optical field driven by RF signal message in MZM2 (DPMZM2) can be expressed as:

$$E_{out2MZM_2}(t) = E_{in}(t)\left\{\exp\left(j\pi\frac{\phi_{21}(t)}{V_\pi}\right)+\exp\left(j\pi\frac{\phi_{22}(t)}{V_\pi}\right)\right\} \quad (75)$$

Where $m = \frac{\pi V_m}{V_\pi}$; Then by substituting equation 70 and 71 into equation 74;

$$E_{out2MZM_1}(t) = E_{in}(t)\begin{Bmatrix}\exp\left(jm\left\{-\cos(\omega_1 t)-\cos(\omega_2 t)\right\}+j\pi\right)\\+\exp\left(jm\left\{-\sin(\omega_1 t)-\sin(\omega_2 t)\right\}\right)\end{Bmatrix} \quad (76)$$

By applying the Jacobi-Anger Expansion in equation 61;

$$E_{out2MZM_1}(t) = E_{in}(t)\sum_{n,m=-\infty}^{\infty} Jn(m)Jm(m)e^{j(n\omega_1 t+\omega_2 t)}\left[(-j)^{n+m}e^{j\frac{\pi}{2}}+(-1)^{n+m}e^{j-\frac{\pi}{2}}\right] \quad (77)$$

Similarly, by substituting equation 72 and 73 in to equation 75, we can derive the output optical field in MZM2 (DPMZM2);

$$E_{out2MZM_2}(t) = E_{in}(t)\begin{Bmatrix}\exp\left(jm\left\{\cos(\omega_1 t)-\cos(\omega_2 t)\right\}+j\pi\right)\\+\exp\left(jm\left\{-\sin(\omega_1 t)+\sin(\omega_2 t)\right\}\right)\end{Bmatrix} \quad (78)$$

By applying the Jacobi-Anger Expansion in equation 78;

$$E_{out2MZM_2}(t) = E_{in}(t)\sum_{n,m=-\infty}^{\infty} Jn(m)Jm(m)e^{j(n\omega_1 t+\omega_2 t)}\begin{bmatrix}(j)^n(-j)^m e^{j\frac{\pi}{2}}+\\(-1)^n e^{j-\frac{\pi}{2}}\end{bmatrix} \quad (79)$$

Combining output power from two MZMs will represent the optical field of DPMZM2 and it can be expressed as;

$$E_{outDPMZM_2}(t) = \frac{E_{out2MZM_1}(t)+E_{out2MZM_2}(t)}{\sqrt{2}} \quad (80)$$

$$E_{outDPMZM_2}(t) = \frac{E_{in}(t)}{\sqrt{2}}\sum_{n,m=-\infty}^{\infty} Jn(m)Jm(m)\begin{Bmatrix}(-j)^{n+m}e^{j\frac{\pi}{2}}+(-1)^{n+m}e^{j-\frac{\pi}{2}}+\\(j)^n(-j)^m e^{j\frac{\pi}{2}}+(-1)^n e^{j-\frac{\pi}{2}}\end{Bmatrix}e^{j(n\omega_1 t+\omega_2 t)} \quad (81)$$

The photocurrent I(t) after photodetector, can be obtained by substituting the output fields of DPMZM2 into the following equation:

$$I_{PD2}(t) = \Re\left|E_{outDPMZM_2}(t)\right|^2 \tag{82}$$

Where $\mathcal{R}$ is the responsivity of photodetector Using Taylor series expansion into the third order in m, following expression can be shown as:

$$I_{PD2}(t) = \frac{1}{2}\Re P_{in}\left\{-m\hat{}2\left(2j\cos\left(2\omega_1 t\right)+\left(2j\sin\left(\omega_2\right)\right)^2\right)\right\}+o\left(m\right)^4 \tag{83}$$

Combining the output fields of DPMZM1 and DPMZM2 after BPD $\mathrm{I_{PD}(t) = I_{PD1}(t) + I_{PD2}(t)}$ we will obtain:

$$I_{PD}(t) = \frac{1}{2}\Re P_{in}\left\{m^2 * (8-8(\sin(\omega_1-\omega_2))\right\}+o\left(m\right)^4 \tag{84}$$

From equation 84, we can clearly see that the only existing frequency is the sideband Second Order Intermodulation of frequency $\omega_1-\omega_2$. Furthermore, SOH and Second-Order sideband Intermodulation products do not exist. We have used the VPI commercial software to simulate the system configuration, as in section 2.1.1. From Fig.25 we can see that the signal has been Down-converted from high frequency to low frequency. Frequencies used in this configuration are 17 GHz and 17.5 GHz; therefore, the difference between these two frequencies is 0.5 GHz (ω1 − ω2). From the spectrum analyser, we can see that all nonlinear distortions that are close to down-converted signals are eliminated, resulting in a clear and highly linearized signal. In our proposed configuration, we have managed to eliminate IMD3 and SOH simultaneously, and suppress higher order harmonics as illustrated in Fig.25 b. If we expand the electrical spectrum Fig.25 c, we can see that down converted-electrical spectrum is clear up to 65 GHz, which means the SOD, frequency ω1 + ω2 and TOD are eliminated in a very broad spectrum. However, higher order harmonics still exists. In Fig.25 d we have to investigate

systems by using higher frequencies to see how the proposed system behaves and as can be seen in Fig.25 c, results are the same as in the previous case.

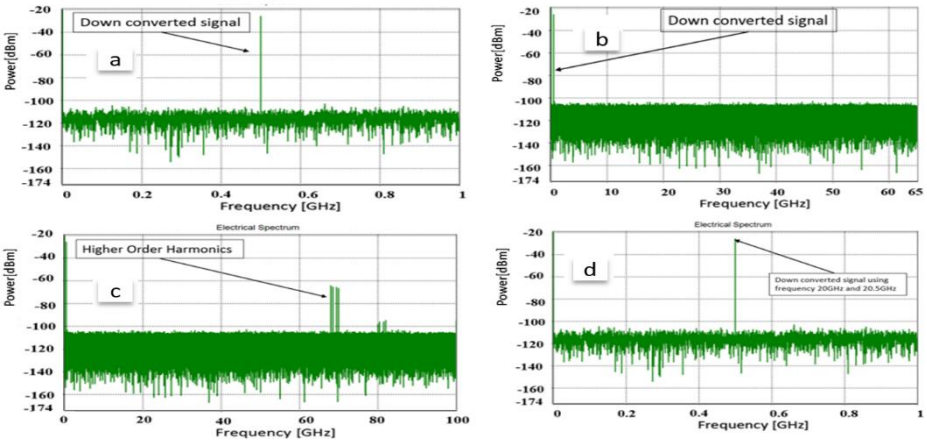

Figure 26: a down-converted frequency 0.5 GHz; b proposed down-conversion spectrum up to 60 GHz; c proposed down-conversion spectrum up to 100 GHz; d down-conversion E.S for higher frequency

In this proposed and developed model for both cases, we have assumed that frequencies are split equally. Due to the 9 phase shifters used, we are aware that there will be losses. However, these minor limitations can be overcome by deploying the RF structure as an integrated circuit and the physical length between RF and the shifters are minimum. The accuracy of shifting should be within one degree to achieve the elimination. Frequencies can be sent in the same fibre in two different channels using a polarizer, this way the signal travels in the same physical length of the fibre, and hence this will lead to eliminating the SOH.

Chapter 4

Elimination of odd and even intermodulation distortions of analogue microwave photonics link based on GaAs MZMs

Introduction

Optical communication systems show great potential for the next generation of wireless communication systems due to the properties of fibre-optic signal propagation, high bandwidth, low propagation loss, low power consumption, and low cost [41–43]. As part of optical communication systems, Radio over Fibre (RoF) has been the centre of intensive research over the last 30 years and is considered a promising technology for various applications, such as defence systems, telecommunications, networking, commercial, and broadcast systems etc. However, RoF systems contain certain limitations as well due to factors like nonlinearity, losses from an electrical to optical signal conversion and vice versa, scattering of light and dispersion of signal [44]. There are a few key system parameters used to overawe some of the stated limitations; like noise figure, gain and dynamic range. One of the most challenging difficulties in such systems is the understanding of the Electro-optic (EO) modulators for suppressing nonlinear distortions, which strongly affects the overall performance of microwave photonic links. Dual-drive Dual-Parallel Mach-Zehnder Modulator (D-DPMZM) is most commonly used to overcome these nonlinear distortions, such as eliminations or suppression of Intermodulation Distortion (IMDs). By using D-DPMZM, it is possible to increase dynamic range, which is defined as the ratio between maximum signal and detectable distortion to the minimum signal. Nonetheless, the required complex radio-frequency arrangement and synchronization cannot be realized [45,46]. In many reported research papers, IMD3 is considered to be the most severe distortion, and therefore, different linearization techniques have been developed to suppress the IMD3 and improve the SFDR [47-60]

An analogue photonic link is proposed and experimentally demonstrated in [47], based on an integrated EO dual-parallel polarization modulator. Theoretical analysis shows that the IMD3 is eliminated, and suppression of the third-order intermodulation has been demonstrated experimentally by 40 dB.

An AMPL with improved SFDR is proposed and experimentally demonstrated in [48]. In this paper, IMD3 is counteracted by optical power and modulation depth relationships between the two wavelengths. The experimental results show that IMD3 is reduced by 28.6 dB. Dynamic-range improvement in Microwave Photonic Link (MPL) based on single sideband phase modulation (PM) is proposed and demonstrated in [49]. Simulations results show that IMD3 is eliminated and SFDR is improved by 22.9 dB. Nevertheless, with phase modulation, high linearity can be achieved. High linearity on the receiver's side is a complicated process and costly [47,48,49]. In [50], a phase-modulated link with IMD3 elimination is proposed and demonstrated. By manipulating the ratios of RF and optical powers, improvements of 25.35 dB in Carrier to Interference Ratio (CIR) and 12.85 dB are reported. However, maintaining the ratio between RF and optical power is not practical. Elimination of IMD3 based on a single-phase modulator is proposed and experimentally demonstrated in [51], where the used technique in this configuration allows suppressing IMD3 in a coherent phase-modulated RF optical link, which requires no external bias or control. The resulting dynamic range is limited by fifth order IMD instead of third-order IMD. However, practical implementation of a coherent phase- modulation is a difficult task.

Intermodulation distortion suppression has been proposed and experimentally demonstrated in [52] based on MZM. SFDR is linearized using mixed polarization. Intermodulation induced power fading and crosstalk via fibre chromatic dispersion for a given RF carrier is reduced compared to using the conventional OSSB MZM and improvements of 13 dB in SDFR has been reported and demonstrated experimentally. An analogue photonic link has been proposed

and experimentally demonstrated in [53] based on a Phase Modulator (PM), a polarizer and an optical filter. Such structure could simultaneously compensate for the chromatic dispersion and the nonlinearity of the modulator. The proposed scheme could also be reconfigured to suppress IMD2 by adjusting the states of polarization. Experimental results show suppressions of the IMD2 and IMD3 by 14-dB and 25.4-dB, respectively. In [54], and MPL using a polarization modulator is proposed and experimentally demonstrated. The proposed approach suppresses the IMD3 and improves the modulation efficiency via partial carrier suppression by producing two channels of intensity-modulated signal. In [55] it has been demonstrated that SFDR is

123.48 dB Hz2/3, from a noise floor of -166 dBm/Hz. An MPL with suppression of IMD3 is proposed and analysed in [55] based on an MZM. Simulation results show a reduction of 40 dB in the IMD3 and an improvement of 21.1 dB in the SFDR. Nevertheless, in [52,53,54] suppressions of IMDs have been reported theoretically, confirming that when the modulation index is increasing, the IMDs will appear, limiting the SDFR.

A linearization technique to improve the dynamic range of an analogue photonic link is proposed and demonstrated in [56] Based on a signal interferometer IMD3 components have been destructively combined in the photodiode, leading to 10.3 dB improvement in dynamic range. These are some of the techniques used to eliminate IMD3. However, in the study above, none of the papers reported elimination of all odd and even IMDs. The need for an advanced interferometer, with a significant number of kilowatts of laser power at the beam splitter, means that it would be difficult to build using existing technology.

The performance analysis of microwave photonic frequency conversion, using double-sideband suppressed-carrier and balance detection, based on DPMZM, has been reported and demonstrated [57]. The Double-sideband technique has been used to suppress high harmonics and high Intermodulation’s distortions and achieved frequency conversion signal. Dual wavelength linearization of analogue photonic link based on PM-IM conversion has been

proposed and demonstrated [58]. A phase modulator, which exhibits different electro-optic modulation indexes, is used. This paper reports and experimentally demonstrate the suppression of IMD3 by 14.54 dB, based on two different channels with opposite fields, permitting a suppression of IMD3. Multi-octave linearised analogue photonic link based on a polarization DPMZM is proposed in [59,60]. An elimination of IMD2 and suppression of IMD3 is reported in this paper, based on integrated polarization-multiplexing D-DPMZM with a free dynamic range of 82 dB. However, in this report, IMD3 is only suppressed theoretically, wherein in our proposed structure all IMDs are experimentally eliminated, and SOH is suppressed under noise floor. A method to realize a highly linear microwave photonics link is proposed based on the dual-drive dual-parallel Mach-Zehnder modulator (MZM). In [61] eliminates IMD3 and suppression of approximately 30 dB is experimentally demonstrated. SFDR improved by 12 dB Hz2/3. However, in this report, IMD2 and higher harmonic distortion have not been considered. Thus, in this research work, we report and experimentally demonstrate suppression under noise floor of all IMDs, TOH and significant suppression of the SOH. In our proposed system, we have used GaAs modulators, as they are known for their thermal stability. The long interferometer used in the Electro-optic (EO) modulator is very sensitive to any imbalance and commercially used lithium niobate (LiNbO3) modulators are particularly prone to bias-point drift due to charge migration. However, this does not occur with GaAs EO modulators, which are highly suitable for harsh environments, such as radiation resistance, the longevity of aerospace, and satellite to ground downlink communication systems [62,63].

Mathematical modelling

The schematic diagram of the proposed Analog Microwave Photonic Link linearization with the suppression under the noise floor of all even and odd IMDs based on two MZMs is shown in Fig.26. In the proposed configuration, two-tone microwave frequencies, RF1 (5 GHz) and RF2 (5.005 GHz) are shifted by 90° and 270° using RF shifters. Such input microwave frequencies (RF1 and RF2) have been reported in [20,21], however with different configurations and much lower system performance.

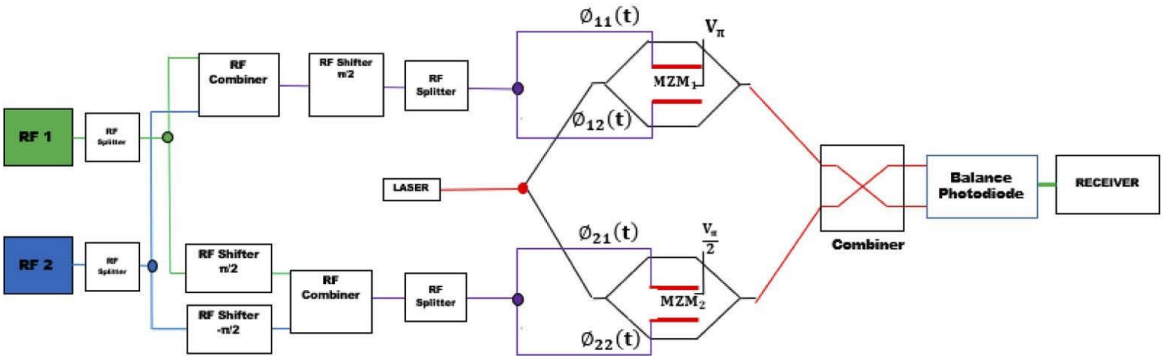

Figure 27: Schematic diagram of the proposed AMPL system configuration using DPMZM with two input frequencies

A microwave signal of two frequencies is combined with an RF combiner and then shifted by 90 degrees for the upper and lower arm of MZM1. Whereas frequency one is shifted by 270 degrees and frequency two is shifted by 90 degrees for the upper and lower arm of MZM2. External DC bias is set to minimum for MZM1 and quadrature for MZM2. Modulated frequencies are combined by the 3dB power combiner and detected by the balanced photodetector. The drive voltage with DC biases of MZMs for the schematic configuration illustrated in Fig.27 can be expressed as:

$$\Phi_{11}(t) = V_m \left\{ \cos\left(\omega_1 t + \frac{\pi}{2} \right) + \cos\left(\omega_2 t + \frac{\pi}{2} \right) \right\} + V_\pi \qquad (85)$$

$$\Phi_{12}(t) = V_m \left\{ \cos\left(\omega_1 t + \frac{\pi}{2} \right) + \cos\left(\omega_2 t + \frac{\pi}{2} \right) \right\} \tag{86}$$

$$\Phi_{21}(t) = V_m \left\{ \cos\left(\omega_1 t + \frac{\pi}{2} \right) + \cos\left(\omega_2 t - \frac{\pi}{2} \right) \right\} + \frac{V_\pi}{2} \tag{87}$$

$$\Phi_{22}(t) = V_m \left\{ \cos\left(\omega_1 t + \frac{\pi}{2} \right) + \cos\left(\omega_2 t - \frac{\pi}{2} \right) \right\} \tag{88}$$

where $\Phi_{11}(t)$ and $\Phi_{12}(t)$ are MZM1 two electrode drive voltages; $\Phi_{21}(\mathrm{t})$ and $\Phi_{22}(\mathrm{t})$ are MZM2 two electrode drive voltages; Vm represents the amplitude of the RF input signals. The laser optical field can be expressed as; $\mathrm{E_{in}(t) = E_c e^{j\omega_c t}}$ where the Ec is the input optical field and ωc is the angular frequency of the laser, consequently, the output optical field in $\mathrm{MZM_1}$ can be expressed as:

$$\mathrm{E_{out1}(t) = E_{in}(t)\left\{ exp\left(j\pi \frac{\Phi_{11}(t)}{V_\pi} \right) + exp\left(-j\pi \frac{\Phi_{12}(t)}{V_\pi} \right) \right\}} \tag{89}$$

Similarly, the output optical field in $\mathrm{MZM_2}$ can be expressed as:

$$\mathrm{E_{out2}(t) = E_{in}(t)\left\{ exp\left(j\pi \frac{\Phi_{21}(t)}{V_\pi} \right) + exp\left(-j\pi \frac{\Phi_{22}(t)}{V_\pi} \right) \right\}} \tag{90}$$

Where $\mathrm{m = \pi V_m / V_\pi}$ is the modulation index of MZM, by substituting 85 and 86 into 89 hence:

$$\mathrm{E_{out1} = E_{in}(t)\left\{ \begin{array}{c} exp\left(-jm\left\{ \sin(\omega_1 t) + \sin(\omega_2 t) \right\} + j\pi \right) \\ +exp\left(jm\left\{ \sin(\omega_1 t) + \sin(\omega_2 t) \right\} \right) \end{array} \right\}} \tag{91}$$

Applying a Jacobi-Anger Expansion in 91 we get:

$$E_{out1}(t) = E_{in}(t) \sum_{p,q=-\infty}^{\infty} J_p(m) J_q(m) e^{j(p\omega_1 t + q\omega_2 t)} \left[(-1)^{p+q} e^{j\pi} + 1 \right] \tag{92}$$

Similarly, by substituting 87 and 88 into 90 we can derive the output optical field in MZM2:

$$E_{out2}(t) = E_{in}(t) \left\{ \begin{array}{c} exp\left(-jm\left\{ \sin(\omega_1 t) - \sin(\omega_2 t) \right\} + j\frac{\pi}{2} \right) \\ +exp\left(jm\left\{ \sin(\omega_1 t) - \sin(\omega_2 t) \right\} \right) \end{array} \right\} \tag{93}$$

Applying a Jacobi-Anger expansion in 93 we obtain:

$$E_{out2}(t) = E_{in}(t) \sum_{p,q=-\infty}^{\infty} J_p(m) J_q(m) e^{j(p\omega_1 t + q\omega_2 t)} \left[\begin{array}{c} (-1)^p e^{j\frac{\pi}{2}} + \\ (-1)^q \end{array} \right] \tag{94}$$

The optical field of the two MZMs after 3 dB optical combiner can be expressed as:

$$E_1(t) = \frac{E_{out1}(t) + E_{out2}(t)}{\sqrt{2}} \tag{95}$$

$$E_2(t) = \frac{E_{out1}(t) - E_{out2}(t)}{\sqrt{2}} \tag{96}$$

The generated photocurrent IPD(t) after the balance-photo detector is:

$$I_{PD}(t) = \Re\left[E_1(t) \cdot E_1(t)^{*} - E_2(t) \cdot E_2(t)^{*} \right] \tag{97}$$

where $\mathcal{R}$ is responsivity of the balance-photo detector. Using Tayler series expansion in "m", the following expression can be derived as;

$$I_{PD1}(t) = -\frac{1}{2}\Re P_{in} \left\{ \begin{array}{l} 8m\left(\cos(\omega_1 t) + \sin(\omega_2)\right) + 4m^2\left(\cos(2\omega_1 t) - \cos(2\omega_2)\right) \\ +4m^3 \left(\begin{array}{c} \sin(3\omega_1 t) + \sin(3\omega_2 t) \\ -\sin(\omega_1 t) - sin(\omega_2) \end{array} \right) \end{array} \right\} + o(m)^4 \tag{98}$$

It should be noted that we have used MATLAB software for Tayler series expansion. From equation 98, it can be observed that the IMD3 of frequency $2\omega_2 - \omega_1$ and $2\omega_1 - \omega_2$ is eliminated mathematically, IMD2 of frequency $\omega_2 - \omega_1$ and $\omega_1 - \omega_2$ and all other IMDs are

eliminated. We have used the Tayler series to higher order and IMDs still do not exist, which confirms that when the modulation index increases, the IMDs will not exist in the proposed model.

Experimental results and analysis

The experimental setup for the proposed AMPL is shown in Fig.27. This experiment is based on the schematic diagram illustrated in Fig.26. The optical carrier operating at a wavelength of 1550nm and a power of 20 dBm is generated from an optical laser (G&H EM650). An optical beam splitter (50/50) is used to equally divide the optical carrier, which is then fed into two MZMs. Two MZMs are driven by two single-tone radio signals (ω1 and ω2) generated from two analogue Radio Frequency signal generators (ROHDE&SCHWARZ, SMF100A), respectively. The optical spectrum is also analysed by using an Optical Spectrum Analyser (OSA) (ID Photonics, ID-OSA-MPD-00). The optical combiner used in the experiment was a Polarization Maintained (PM) with the PM fibre pigtails and all the polarization-maintained links are aligned along the propagation axis of the PM fibre such as fast axis and slow axis. Likewise, the input signal to the combiner is polarization maintained. Therefore, the need for a polarization controller was overcome by using PM fibre. We understand that not maintaining the polarization will make the system vulnerable to environmental conditions like mechanical stress or fibre bend. Moreover, the polarization-maintaining fibre in contrast to polarization controllers, are more robust and reliable.

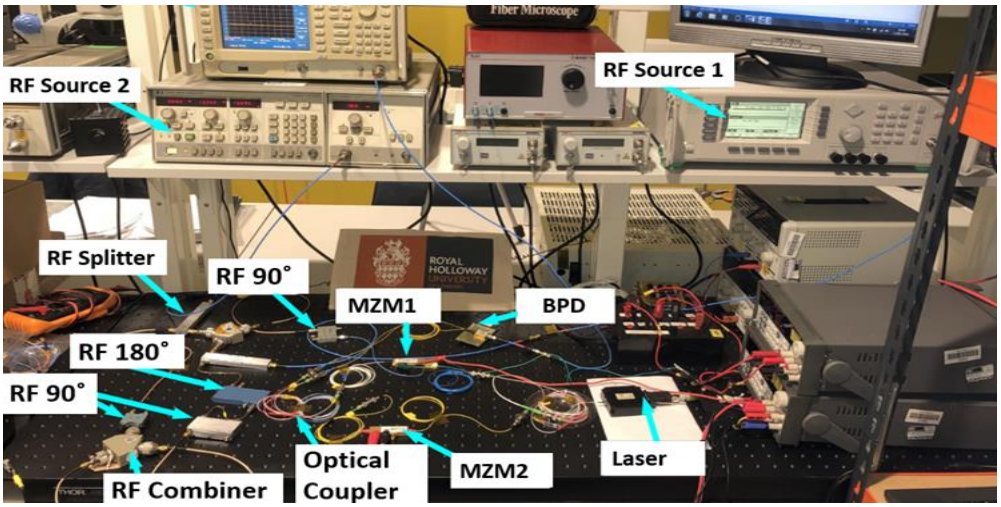

Figure 28: Proposed linearization of AMPL based on two single MZMs. The experiment has been carried out in the Microwave Photonics and Sensors Laboratory at Royal Holloway University London

The upper and lower branches of the MZM1(aXMD2030-GM-FPS) is fed by 5 GHz and 5.005 GHz signals, which are combined by the RF combiner and shifted by a 90-degree RF shifter (QH0226 2-26 5 GHz). The MZM1 is set at the minimum operating point. MZM2 (aXMD2030) is set to a quadrature operating point, and in the upper branch, a single-tone signal ω1 is shifted by the 90-degree shifter (QH0226 2-26 5 GHz) and in a lower branch, single-tone signal ω2 is shifted by 270 degrees.

We have combined one 90-degree and 180-degree shifter to make 270-degree shifting, as shown in Fig.27. The output modulated signal from MZM1 and MZM2 are combined by a 3dB power combiner and then detected at BPD. In our proposed system, we have precisely measured the fibre lengths used in each optical path and also used the polarization maintain fibres to keep the system stability intact. Our system does not in-cooperate long fibre cables, so by using a short patch cable, the system is implemented. We also found that the time delay

is not required to match each optical path length to achieve cancellation of unwanted distortions such as IMD2 and IMD3. The BPD (BPDV2120R) has a bandwidth of 70 GHz and a responsivity of 0.45 A/W. A signal analyser (R&S FSV-18, ESA) is used to measure the electrical spectra. The electrical spectra at the output of the BPD are shown in Fig. 28 a), b), c) and d). As shown in Fig.28 a), the fundamental frequencies are located at 5 GHz and 5.005 GHz with -20dBm and -21dBm power levels, respectively. As revealed in equation (83), we can observe suppression of IMD3 frequencies at 5.01 and 4.995 GHz under the noise floor. Nevertheless, as we increase input power, the IMD3 appears in our experiment due to the RF equipment (combiner, phase shifters) phase imbalance, fibre nonlinearities and BPD. It is worth stating that the RF phase shifter and combiners used in this experiment have a phase variation of 2° to 5°, which have caused some small fluctuations to completely satisfy the equation (14). The measured noise floor from the spectrum analyser is -128.9dBm/Hz. However, in Fig. 30, the noise floor is measured at an RBW of 10 kHz, and the average measured noise floor is -88.9dBm. For the SFDR measurements, an assumed noise floor of -170dBm/Hz is used, which is mainly due to the system being limited to the shot noise.

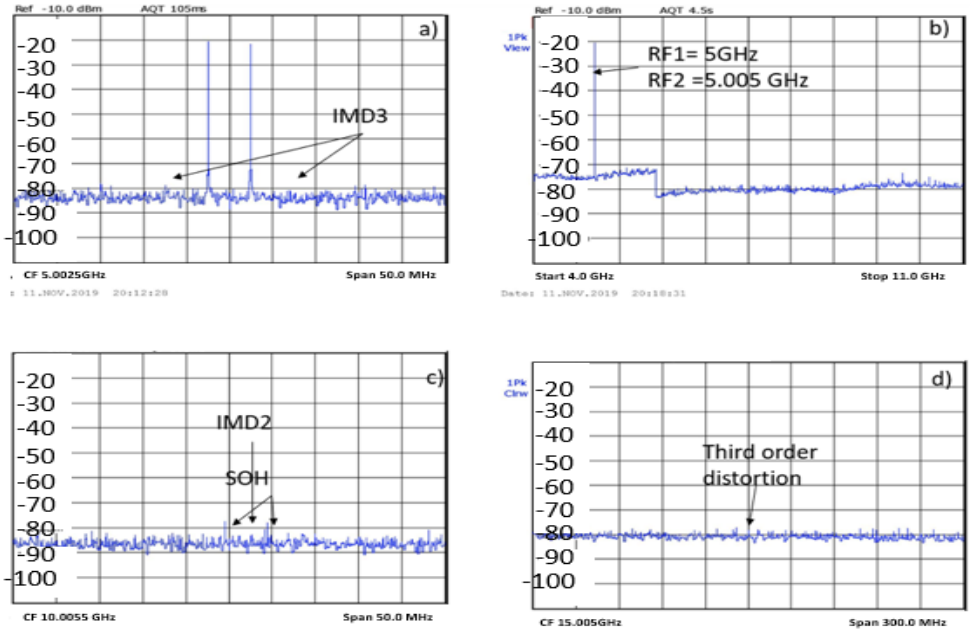

Figure 29: a) Electrical spectrum analyser showing suppression of IMD3. b) Electrical spectrum analyser showing spectrum from 4GHz to 11GHz, c) Electrical spectrum analyser showing suppression of IMD2, d) Electrical spectrum analyser showing suppression of Third order distortion.

In the proposed scheme, we have utilized a balanced photodetector BPD. It is well known that BPD with controlled optical inputs can suppress the laser RIN and ASE noise from EDFA. The common-mode functionality of the BPD removes the RIN noise and doubles the shot noise [44]. With the elimination of RIN and ASE, the system only becomes limited to shot noise [45]. Based on the principle of our developed mathematical model shown in part III, we can verify the claim of the suppression of odd and even IMDs. The SOH is located at 10 and 10.01 GHz frequencies for 5GHz and 5.005GHz input signals, respectively. These SOHs are significantly suppressed to -78dBm, as shown in Fig. 28 c). Furthermore, the IMD2 (10.005GHz and 0.005 GHz) are suppressed under the noise floor for low input power. Nevertheless, they appear, as the input RF power is increased due to the phase variation of the

RF Equipment. Due to nonlinearities in conventional analogue photo links, these two frequencies, described as IMD2, have rather significant power. However, it is suppressed under the noise floor. From Fig.28 d), we can conclude clearly that TOH is suppressed under the noise floor. The obtained experiment measurement results are based and proven by the mathematical modelling shown in equation (83), which confirms the elimination of IMDs, third-order distortion and suppression of SOH. The measured gain and noise figure of the proposed link is -41.6dB and 21.76dB, respectively.

IMD3 and IMD2 will increase as input RF power increases, therefore in Fig.29 a) we have illustrated CIR for IMD3, IMD2 and SOH against the input RF power to find the power threshold. From Fig.29 a), the CIR for IMD3 increases with an increasing RF input power, and then CIR starts to decrease when RF power increases more than 14dBm.

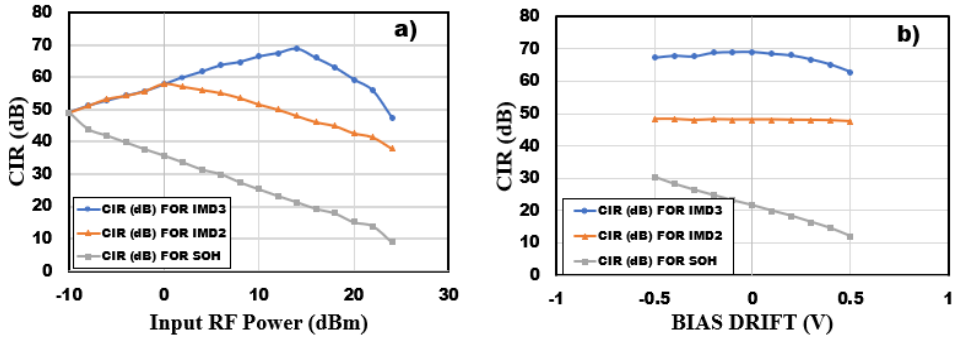

Figure 30: a) Power threshold measurements for proposed configuration, b) System stability analyses.

Therefore, it can be said that the power threshold for IMD3 is around 14dBm as it limits the CIR. Likewise, the CIR for IMD2 increases up to an input RF power of 0 dBm, and beyond this RF power, the CIR starts to deteriorate. Hence the power threshold for the IMD2 is around 0dBm.

To demonstrate the performance of our proposed configuration concerning the bias drift, we have plotted a graph, which shows the CIR for IMD3, IMD2 and SOH Fig.29 b) As it can be

seen from the results, the CIR for IMD3 and IMD2 is almost constant at a bias drift of up to ±0.5V. However, the SOH to the fundamental frequency ratio deteriorates drastically. The results are achieved by manually altering the bias voltages by a step of 0.1V and the impact on the CIR was observed. From Fig.29 b) w can see that the system performance decreases as operating points voltage increases regarding SOH this is due to fact that SOH is present in this system. Based on this analysis we can say our proposed system stability is limited only by SOH regarding bias point drift. Due to fact that IMD3 and IMD2 are significantly suppressed our proposed system performance stay constant as the operating point's voltage changes.

In [66] linearization system has been reported and theoretically demonstrated. This paper was mainly concentrated on IMD3 suppression using a simulation system and backed by mathematic modelling. This paper has been reported an SFDR of 124.4 dB compared to 102dB conventional, However, as before this work was based on theoretical work and even then only IMD3 has been suppressed. Contrarily, in our proposed system we have experimentally demonstrated a 119.5 dB. Hz2/3 SFDR, also we have suppressed all even and odd-order Intermodulation distortion. Furthermore, another linearization technique was reviewed to analyze the elimination of even and odd order IMD. In [67] linearization of photonic link has been proposed and theoretically demonstrated. In this paper OptiSystem software has been used to simulate the proposal structure.

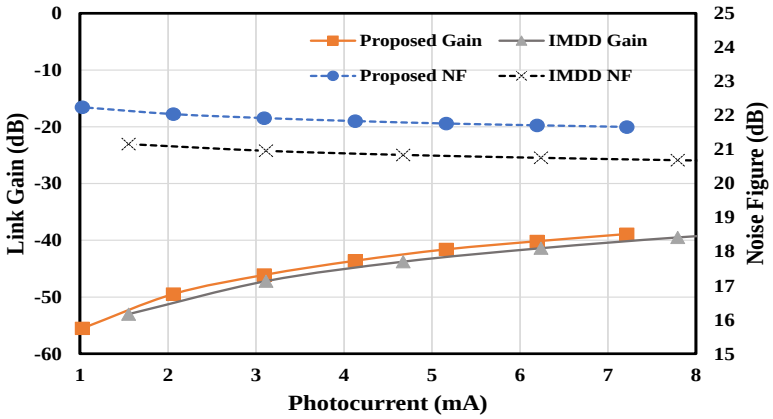

Figure 31: The gain and noise figure of the proposed system is measured.

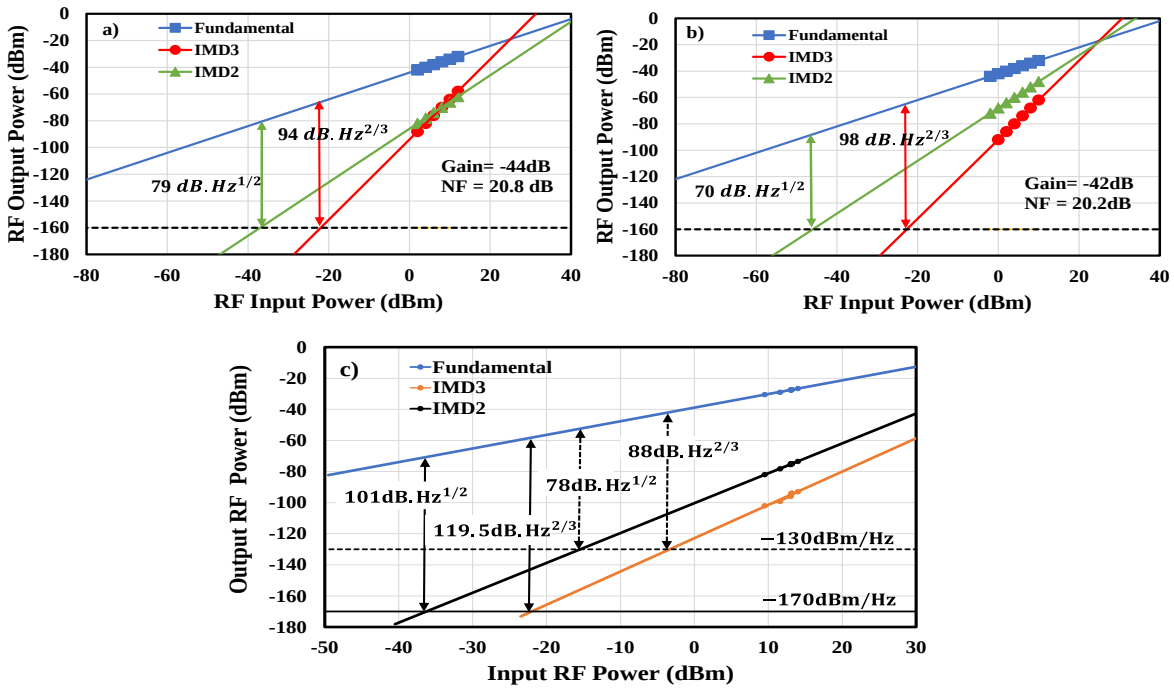

Figure 32: SFDR performance of a) IMDD link with quadrature biasing, b) IMDD link with Low biasing and c) Proposed AMPL with Dual Parallel MZMs.

Where the authors have managed to suppress IMD3 and eliminate even-order products. They also have backed the simulation with mathematic modelling. However, there is no experimental work and there are question marks how this system will behave in real life. Besides, in this proposal, IMD3 has been suppressed theoretically and even-order distortion has been eliminated, whereas in our proposal we have theoretically and experimentally demonstrated the elimination of even- and odd-order intermodulation distortion. Similarly, we develop a full mathematical model for the proposed system.

The proposed link is analysed and compared with the conventional Intensity Modulation Direct Detection (IMDD) link. Therefore, a sheer comparison between them is shown in Fig.30. It is observed from the analysis that the gain and noise figure of our proposed system is measured to be at -41.6dB and 21.76dB, respectively as opposed to that of -39.5dB and 20.68dB for the

IMDD link. The measured results show that the gain of our system is slightly lower as compared to the IMDD system. It can also be observed that the noise figure of the system is higher at a low photocurrent, and it is almost constant at a higher photocurrent. It is also observed that the NF of the conventional IMDD link based on quadrature biasing is slightly less than our proposed NF. It should be stated that the extra cost and slightly low gain of our proposed can be justified from this comparison, as the suppression of IMD in conventional IMDD links is poorer. In the experimental demonstration, an optical carrier signal is generated at a power of 20dBm from a DFB Laser source. The losses that occurred in the proposed configuration were from PM 50:50 optical couplers and insertion loss from the modulators. The laser power of 20dBm is split up into two equal paths incurring a 3dB loss. Therefore, the output power at the optical coupler is measured to be around 16.5dBm, which includes 3dB coupling loss as well as insertion loss. Similarly, the optical output power of each MZM is coupled and a 3dB loss is measured. Furthermore, each MZM device had an insertion loss of 6dB. So, the overall measured optical loss is approximately 18dB. On the other side, the losses from the RF Phase shifters and combiner are accumulated to be around 21dB. However, it is noticed that the losses in the link can be compensated by using a high-power Laser and Erbium-Doped Fibre Amplifier (EDFA). Contrarily, the losses on the conventional IMDD link are measured to be less than the proposed configuration. This is because the link comprises a single standard Intensity modulator, which is operating a quadrature bias point, polarization controller, and a single photodetector. The overall optical and RF losses were around 9dB and 3dB, respectively.

In Fig.31, we present the SFDR performance analysis of our proposed system and a comparison with the conventional IMDD links based on quadrature biasing and low biasing. The analysis of a conventional IMDD link based on quadrature biasing is shown in Fig.31 a). The measured

SFDR2 and SFDR3 for this link are 79dB.Hz1/2 and 94dB. Hz2/3, respectively. For this measurement, the link gain and noise figure are -44dB and 20.8dB, respectively. However, this performance is further enhanced by optimizing the biasing conditions of the MZ modulator to low. The measured SFDR for this configuration is shown in Fig.31 b). Both configurations were identical, but the operation of the modulator was different. One was operated at a quadrature biasing point and the other at a low-biasing point. The comparison shows that at low biasing the SFDR performance was improved by 4dB, and the gain was improved by 2dB. The architecture of both links comprises laser sources, an intensity modulator, a polarization controller, and a single photodetector. The cost of this system was assumed to be around £15000. Contrarily, the cost of our proposed system is £22000, which has been justified by the extreme improvement in the performance of the link. In Fig.31 c), we illustrate the variation of the output power for fundamental signal, IMD3 and IMD2 as a function of the input power. The density of the noise power is measured as -130dBm/Hz from the Electrical Spectrum Analyser. However, the calculated noise floor of -170dBm/Hz for both shot noise and thermal noise is also used to demonstrate the SFDR performance. The SFDR is measured to be 101dB.Hz1/2 for IMD2 and 119dB.Hz2/3 for IMD3. When we compare our measurement results with the benchmark paper in [20], which demonstrates suppression of IMD3 only, we can confirm theoretically and experimentally that our proposed AMPL demonstrates suppression of odd and even IMDs, TOH and SOH at -78dBm.

Chapter 5

Microwave Photonics Analog Link based on two Integrated D-DPMZM Linearized Signals and with Eliminated odd Harmonics and all IMD's

Introduction

Dual-parallel Mach-Zehnder modulator (DMZM) is the most commonly used modulator for elimination or suppression of IMDs and possibly for dynamic increase range which requires complex radio-frequency arrangement and linearization [72, 73]. Whereas Third Intermodulation Distortion (IMD3) is the most rigorous in signal linearization, down to being very close to the transmitted signal and limiting free dynamic range. Conversely, when signals are very close to each other, the Second Intermodulation Distortions (IMD2) along with Second Order Harmonics (SOH) will experience severe distortions, subsequently, many linearization techniques have been developed to suppress IMDs and improving Spurious-Free Dynamic Range (SFDR) [74-80]

In [81] improved linearized Analog Microwave Photonic Link (AMPL) with a double dual-parallel Mach-Zehnder modulator and a differential balanced photodetector is reported. In this paper, polarization maintained (PM) based optical components are used for better system stability. The developed theoretical model of the proposed system illustrates the elimination of even-order distortions and a high suppression to the IMD3 at the BPD. Consequently, the fundamental Signal to Interference ratio (S/I) of 60dB was experimentally achieved. Experimental results, simultaneously, demonstrate a significant increase of Second-order Spurious Free Dynamic Range (SFDR2) and Third-order Spurious-free Dynamic Range (SFDR3) by 19.5dB and 3.1dB, respectively. The performance analysis of microwave photonic frequency conversion has been recorded to use a double-sideband suppressed carrier and

balance based on DPMZM [82]. The double-sideband technique has been used to suppress high harmonics and high Intermodulation's, as well as achieve frequency conversion signals. However, as suggested from the title, in [82], only manage to suppress theoretically IMDs and high harmonics.

Based on the Dual-parallel Mach-Zehnder modulator (DPMZM), a linearization AMPL with IMD3 elimination is proposed and experimentally demonstrated [83]. Using symmetrical sideband modulation, in this paper, the authors have managed to eliminate IMD3, in theory, by using two shifters and 3 dB power combiners. It has also been demonstrated experimentally the 45 dB suppression of the IMD3. Nevertheless, this paper only reports the elimination of IMD3 with all the other Harmonics and IMD's that have been left; consequently, in our paper we have used a similar technique, whereas, we have managed to remove all IMD's. A dual-wavelength linearization of analogue photonic link, based on PM-IM conversion, has been proposed and demonstrated in [84]. Furthermore, a phase modulator that exhibits different electro-optic modulation indexes were used. Primarily, this paper reports and experimentally demonstrate suppression of IMD3 by 14.54 dB based on two different channels with an opposite field which then fabricate a possible suppression of IMD3.

Multi-octave linearized analogue photonic link based on a polarization DPMZM is proposed in [85]. An elimination of IMD2 and suppression of IMD3 is reported in this research which is profoundly based on the integrated polarization-multiplexing DPMZM with a free dynamic range of 82dB. However, in this paper IMD2 has been eliminated whereas IMD3 has only been suppressed, while in our proposed structure all IMD's are eliminated.

In [86] is proposed and demonstrated a high linear analogue photonic link, based on a D-DPMZM with BPD. Moreover, third IMD3 and SOD products have been eliminated. However, our system uses fewer RF shifters, and it is much easier to be implemented in practice as also shown in [19] whereas parts of the system have already been experimentally demonstrated.

Mathematical model of the proposed system

The schematic diagram of the proposed photonic link where all IMDs along with Harmonics Distortions which are based on two D-DPMZM – have been eliminated by using balanced-photo-detectors, shown in Fig.32. In this configuration, we have used a two-tone microwave frequency of 17 GHz and 17.5 GHz using RF shifters by 90 degrees and 270 degrees, respectively. The two D-DPMZM consist of two sub-dual electrode MZMs and two balance photo-detector combined by using a 3dB power combiner.

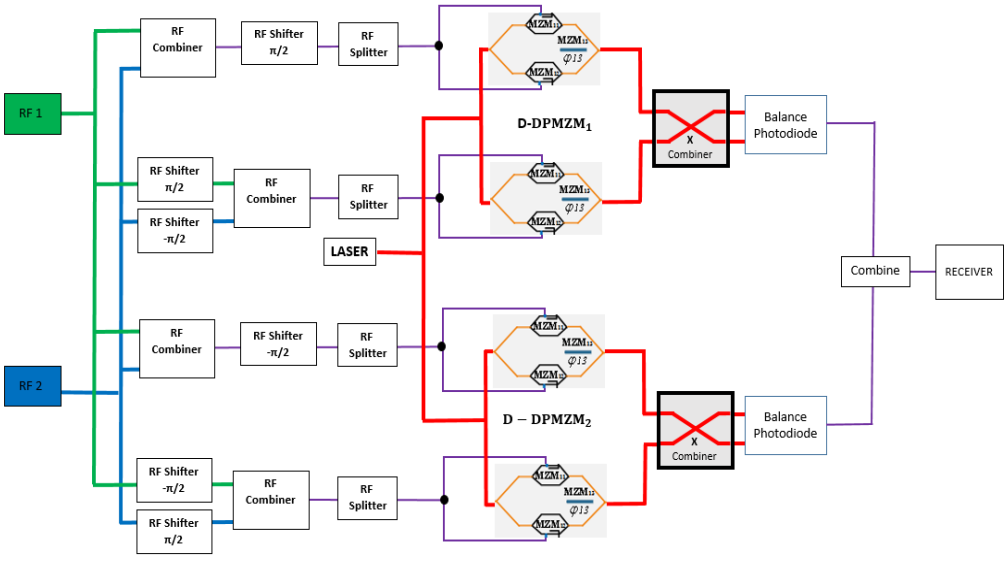

Figure 33: Schematic diagram of the proposed AMPL system configuration using two D-DPMZM with two input frequencies.

Two RF signals are combined by RF combiner and then are shifted by 90 degrees for the upper and lower arm of MZM1 (D-DPMZM1) while frequency one is shifted by 270 degrees whereas frequency two is shifted by 90 degrees for the upper and lower arm of MZM2 (D-DPMZM1). In D-DPMZM2 the RF frequencies are combined and then shifted by 270 degrees for upper and lower arm of MZM1 (D-DPMZM2), frequency one is shifted by 90 degrees and frequency two is shifted by 270 degrees for the upper and lower arm of MZM2 (D-DPMZM2). External DC bias is set to maximum for MZM1 and quadrature for MZM2 for both D-DPMZMs. In addition, frequencies are combined by a 3dB power combiner and detected by a balanced photodetector. Results show that the proposed configuration allows the elimination of all IMDs and all even harmonic distortions. The drive voltage with DC biases of the D-DPMZM1 for the schematic configuration illustrated in Fig.32 can be expressed as:

$$Q_{11}(t) = V_m \left\{ \cos(\omega_1 t + \frac{\pi}{2}) + \cos(\omega_2 t + \frac{\pi}{2}) \right\} + V_\pi \quad (99)$$

$$Q_{12}(t) = V_m \left\{ \cos(\omega_1 t + \frac{\pi}{2}) + \cos(\omega_2 t + \frac{\pi}{2}) \right\} \quad (100)$$

$$Q_{21}(t) = V_m \left\{ \cos(\omega_1 t - \frac{\pi}{2}) + \cos(\omega_2 t + \frac{\pi}{2}) \right\} + \frac{V_\pi}{2} \quad (101)$$

$$Q_{22}(t) = V_m \left\{ \cos(\omega_1 t - \frac{\pi}{2}) + \cos(\omega_2 t + \frac{\pi}{2}) \right\} \quad (102)$$

Where $Q_{11}(t)$ and $Q_{12}(t)$ are drive voltages on two electrodes of MZM1 (D-DPMZM1); $Q_{21}(t)$ and $Q_{12}(t)$ are drive voltages on two electrodes of MZM2 (D-DPMZM1); V_m represent the amplitude of the RF input signals. The laser power is expressed as: $E_{in}(t) = E_c e^{j\omega_c t}$ where the Ec is the input power and ωc is the angular frequency of the laser, consequently the output optical power in MZM1 (D-DPMZM1) can be expressed as:

$$E_{out1D-DPMZ_1}(t) = E_{in}(t)\left\{\exp(j\pi\frac{Q_{11}(t)}{V_\pi}) + \exp(-j\pi\frac{Q_{12}(t)}{V_\pi})\right\} \quad (103)$$

The output optical power in MZM2 (D-DPMZM1) can be expressed as:

$$E_{out2D-DPMZ_1}(t) = E_{in}(t)\left\{\exp(j\pi\frac{Q_{21}(t)}{V_\pi}) + \exp(-j\pi\frac{Q_{22}(t)}{V_\pi})\right\} \quad (104)$$

If $m = \frac{\pi V_m}{V_\pi}$ than by substituting equation 99 and 100 into equation 103 we obtain:

$$E_{out1D-DPMZ_1}(t) = E_{in}(t)\begin{Bmatrix}\exp(jm\{\sin(\omega_1 t) + \sin(\omega_2 t)\} + j\pi) \\ +\exp(-jm\{\sin(\omega_1 t) + \sin(\omega_2 t)\})\end{Bmatrix} \quad (105)$$

Applying a Jacobi-Anger Expansion in equation 105, we obtain:

$$E_{out2D-DPMZM_1}(t) = E_{in}(t)\sum_{n,m=-\infty}^{\infty} J_n(m)J_m(m)e^{j(n\omega_1 t+\omega_2 t)}\left[(-1)^{n+m}e^{j\pi}+1\right] \quad (106)$$

Similarly, by substituting equation 101 and 102 into equation 104, we can derive the output optical power in MZM2 (D-DPMZM1):

$$E_{out2D-DPMZM_1(t)} = E_{in}(t)\begin{Bmatrix}\exp(jm\{\sin(\omega_1 t) - \sin(\omega_2 t)\}) + j\frac{\pi}{2} \\ +\exp(-jm\{\sin(\omega_1 t) - \sin(\omega_2 t)\})\end{Bmatrix} \quad (107)$$

Applying a Jacobi-Anger Expansion in equation 107, we find:

$$E_{out2D-DPMZM_1}(t) = E_{in}(t)\sum_{n,m=-\infty}^{\infty} j_n(m)j_m(m)e^{j(n\omega_1 t+\omega_2 t)}\begin{bmatrix}\{(-1)^m+1\}e^{j\frac{\pi}{2}} \\ +(-1)^n+1\end{bmatrix} \quad (108)$$

Combined power of the two MZMs will represent the optical power for D-DPMZM1. The signal after 3dB power combiner can be expressed as:

$$E_{1D-DPMZM_1}(t) = \frac{E_{out1D-DPMZM_1}(t) + E_{out2D-DPMZM_1}(t)}{\sqrt{2}} \quad (109)$$

$$E_{1D-DPMZM_1}(t) = \frac{E_{out1D-DPMZM_1}(t) - E_{out2D-DPMZM_1}(t)}{\sqrt{2}} \tag{110}$$

The generated photocurrent I(t) after the balance-photodetector is:

$$I_{PDD-DPMZM_1}(t) = R\begin{bmatrix} E_{out1D-DPMZM_1}(t).E_{out1D-DPMZM_1}(t)^* - \\ E_{out2D-DPMZM_1}(t).E_{out2D-DPMZM_1}(t)^* \end{bmatrix} \tag{111}$$

Where $\mathcal{R}$ is responsivity of the photodetector. By deploying Tayler series expansion to the third order in m, the following expression can be derived.

$$I_{PDD-DPMZM_1}(t) = -\frac{1}{2}RP_{in}\left\{\begin{array}{l} 8m(\cos(\omega_1 t)+\sin(\omega_2 t))+ \\ 4m^2(\cos(2\omega_1 t)-\cos(2\omega_2 t)) \\ +4m^3\begin{pmatrix}\sin(3\omega_1 t)+\sin(3\omega_2 t)\\ -\sin(\omega_1 t)-\sin(\omega_2 t)\end{pmatrix} \end{array}\right\} + o(m)^4 \tag{112}$$

Similarly, we can derive equations for D-DPMZM2 as follows:

$$Q_{11}(t) = V_m\left\{\cos(\omega_1 t - \frac{\pi}{2}) + \cos(\omega_2 t - \frac{\pi}{2})\right\} + V_\pi \tag{113}$$

$$Q_{12}(t) = V_m\left\{\cos(\omega_1 t + \frac{\pi}{2}) + \cos(\omega_2 t + \frac{\pi}{2})\right\} \tag{114}$$

$$Q_{21}(t) = V_m\left\{\cos(\omega_1 t + \frac{\pi}{2}) + \cos(\omega_2 t - \frac{\pi}{2})\right\} + \frac{V_\pi}{2} \tag{115}$$

$$Q_{22}(t) = V_m\left\{\cos(\omega_1 t + \frac{\pi}{2}) + \cos(\omega_2 t - \frac{\pi}{2})\right\} \tag{116}$$

Where $Q_{11}(t)$ and $Q_{12}(t)$ are drive voltages on two electrodes of MZM1 (D-DPMZM2); $Q_{21}(\mathrm{t})$ and $Q_{12}(\mathrm{t})$ are drive voltages on two electrodes of MZM2 (D-DPMZM2); V_m represent the amplitude of the RF input signals. The laser power is expressed as: $E_{\mathrm{in}}(t) = E_{\mathrm{c}}\mathrm{e}^{\mathrm{j}\omega_{\mathrm{c}}\mathrm{t}}$ where the Ec is the input power and ωc is the angular frequency of the laser, consequently the output optical in MZM1 (D-DPMZM2) can be expressed as:

$$E_{out1D-DPMZ2}(t) = E_{in}(t)\left\{\exp(j\pi\frac{Q_{11}(t)}{V_\pi}) + \exp(-j\pi\frac{Q_{12}(t)}{V_\pi})\right\} \quad (117)$$

And the output optical power in MZM2 (D-DPMZM2) can be expressed as:

If $m = \frac{\pi V_m}{V_\pi}$ than by substituting equation 113 and 114 into equation 117, we obtain:

$$E_{out1D-DPMZ2}(t) = E_{in}(t)\begin{Bmatrix}\exp(jm\{\sin(\omega_1 t) + \sin(\omega_2 t)\} + j\pi) \\ +\exp(jm\{\sin(\omega_1 t) + \sin(\omega_2 t)\})\end{Bmatrix} \quad (118)$$

Applying a Jacobi-Anger Expansion in equation 118 we get:

$$E_{out1D-DPMZM2}(t) = E_{in}(t)\sum_{n,m=-\infty}^{\infty} J_n(m)J_m(m)e^{j(n\omega_1 t+\omega_2 t)}\left[(-1)^{n+m}e^{j\pi}+1\right] \quad (119)$$

Similarly, by substituting equations 115 and 116 into equation 117, we can derive the output optical power in MZM2 (D-DPMZM2):

$$E_{out2D-DPMZM_2(t)} = E_{in}(t)\begin{Bmatrix}\exp(jm\{-\sin(\omega_1 t) + \sin(\omega_2 t)\}) + j\frac{\pi}{2} \\ +\exp(-jm\{-\sin(\omega_1 t) + \sin(\omega_2 t)\})\end{Bmatrix} \quad (120)$$

Applying a Jacobi-Anger Expansion in equation120, we obtain:

$$E_{out2D-DPMZM2}(t) = E_{in}(t)\sum_{n,m=-\infty}^{\infty} j_n(m)j_m(m)e^{j(n\omega_1 t+\omega_2 t)}\begin{bmatrix}\{(-1)^m+1\}e^{j\frac{\pi}{2}} \\ +(-1)^n+1\end{bmatrix} \quad (121)$$

The combined power of the two MZMs will represent the optical power for D-DPMZM1. The signal after 3dB power combiner can be expressed as:

$$E_{2D-DPMZM_2}(t) = \frac{E_{out1D-DPMZM_2}(t) + E_{out2D-DPMZM2}(t)}{\sqrt{2}} \quad (122)$$

$$E_{2D-DPMZM2}(t) = \frac{E_{out1D-DPMZM2}(t) - E_{out2D-DPMZM_2}(t)}{\sqrt{2}} \quad (123)$$

The generated photocurrent $I_{PD\_D-DPMZM_2}(t)$ after the balance-photodetector is:

$$I_{PDD-DPMZM\,2}(t) = R\begin{bmatrix} E_{out1D-DPMZM_2}(t).E_{out1D-DPMZM_2}(t)^* - \\ E_{out\,2D-DPMZM\,2}(t).E_{out\,2D-DPMZM\,2}(t)^* \end{bmatrix} \quad (124)$$

Where $\mathcal{R}$ is responsivity of photodetector. By using Tayler series expansion to the third order in m, the following expression can be derived:

$$I_{PDD-DPMZM\,2}(t) = -\frac{1}{2}RP_{in}\begin{Bmatrix} 8m(\cos(\omega_1 t)+\sin(\omega_2 t))+ \\ -4m^2(\cos(2\omega_1 t)-\cos(2\omega_2 t)) \\ +4m^3\begin{pmatrix}\sin(3\omega_1 t)+\sin(3\omega_2 t)\\ -\sin(\omega_1 t)-\sin(\omega_2 t)\end{pmatrix} \end{Bmatrix} + o(m)^4 \quad (125)$$

Combining power after two balance-photodetectors

$$I_{PD}(t) = I_{PDD-DPMZM1}(t) + I_{PDD-DPMZM\,2}(t) \quad (126)$$

Then we obtain:

$$I_{PD}(t) = RP_{in}\begin{Bmatrix} 16m(\cos(\omega_1 t)+\sin(\omega_2 t))+ \\ +8m^3\begin{pmatrix}\sin(3\omega_1 t)+\sin(3\omega_2 t)\\ -\sin(\omega_1 t)-\sin(\omega_2 t)\end{pmatrix} \end{Bmatrix} + o(m)^4 \quad (127)$$

From results in equation 127, it can be seen that the third order Intermodulation Distortion of frequency $2\omega_2-\omega_1$ and $2\omega_1-\omega_2$ is eliminated. Second order harmonic and intermodulation of frequency is $\omega_2-\omega_1$, $\omega_1-\omega_2$, and $2\omega_2-2\omega_1$, $2\omega_1-2\omega_2$. We have used the Tayler series to higher order (up to ninth order) and to all intermodulation distortions and even harmonic distortions does not exist which means that the modulation index increases the IMDs and even harmonic distortions will not exist in this model.

Simulation results and discussions

Simulation results are undertaken based on the developed mathematical model representing the novel RF system configuration Fig.32. As stated above, the schematic configuration of the proposed microwave photonic signal linearization includes laser, two-tone microwave frequencies, six shifters four of which are 90-degrees and two 270-degree, 3dB power combiners, two D-DPMZM and two balance-photodetector. Laser optical power of 20dBm are used, and two signals with frequencies of 17 GHz and 17.5 GHz are investigated. The input laser light is split into four equal paths and modulated at four sub-MZMs.

In the D-DPMZM1 lower and upper branch of MZM1, the RF signal ω1 and ω2 are shifted by 90 degrees, while in MZM_2 RF signal ω1 is shifted by $\frac{\pi}{2}$ and ω2 is shifted by -$\frac{\pi}{2}$, frequencies are than combined by RF combiner and modulated in upper and lower branch. Output modulated signal from MZM_1 and MZM_2 are combined by 3dB power combiner than detected by balanced-photodetector. In D-DPMZM2 RF signal are shifted and combined same as in D-DPMZ1 but with opposite phase, output modulated signal from MZM1 and MZM2 are combined and detected by balanced-photodetector two. Electrical signal from both balanced-photodetector is combined, obtained results are shown in Fig. 33.

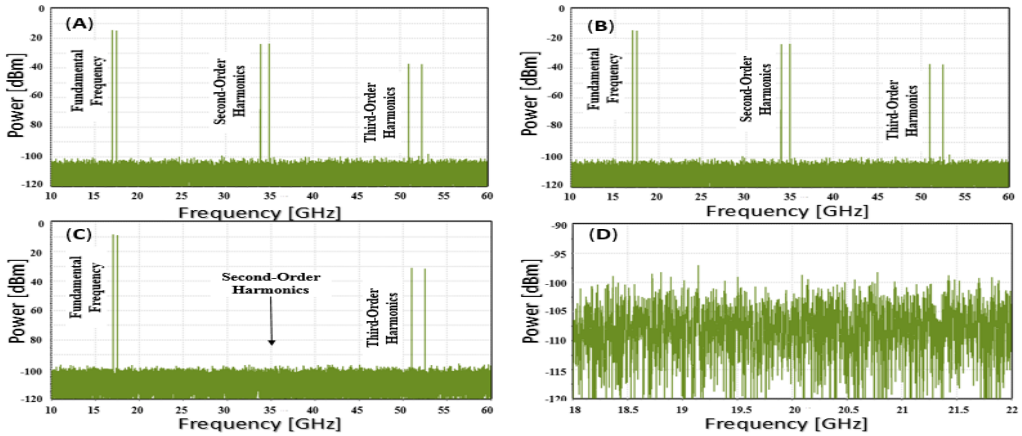

Figure 34: Electrical spectrum of the proposed structure; (A) Two single subcarriers from D-DPMZM1 without any intermodulation distortions, (B) Two single subcarriers from D-

DPMZM2 without any intermodulation distortions, (C) Two single subcarriers after combining without any SOH, (D) shows the non-existence of IMD2 and SOH

Fig.33 (A) shows the signal output from D-DPMZM1, which shows the elimination of IMDs, however, SOH is present as shown in equation (112). Similarly, Fig.33 (B) illustrates the output from D- DMZM2 with the opposite SOH field shown in equation (125) which enables the elimination of SOH. Therefore, SFDR in this system is limited only by Third Order Harmonics (TOH). The TOH are quite far from fundamental signal and can be easily filtered by using low power electrical filter.

By comparing our obtained results with our previous experimental results of similar RF systems publish recently in [85], it can be confirmed that we have managed to improve signal linearization significantly. In the published paper [18], we have demonstrated suppression of IMDs and SOH experimentally and benchmarked by the developed mathematic model, however, in [85] only IMD's and SOH are suppressed, shown in equation (14) section 2 Mathematics Modelling, wherein this proposed RF system configuration, we have eliminated SOH Fig.33 (D) and all other IMD's Fig.33 (C). Obtained simulations shown in Fig.33 (C) have been backed up by the developed mathematical modelling equation (127), showing Tayler series up to fourth-order which confirms that the IMD's and SOH do not exist. To verify simulation results, we have used the Tayler series up to 9th order and still evidence the clear the match.

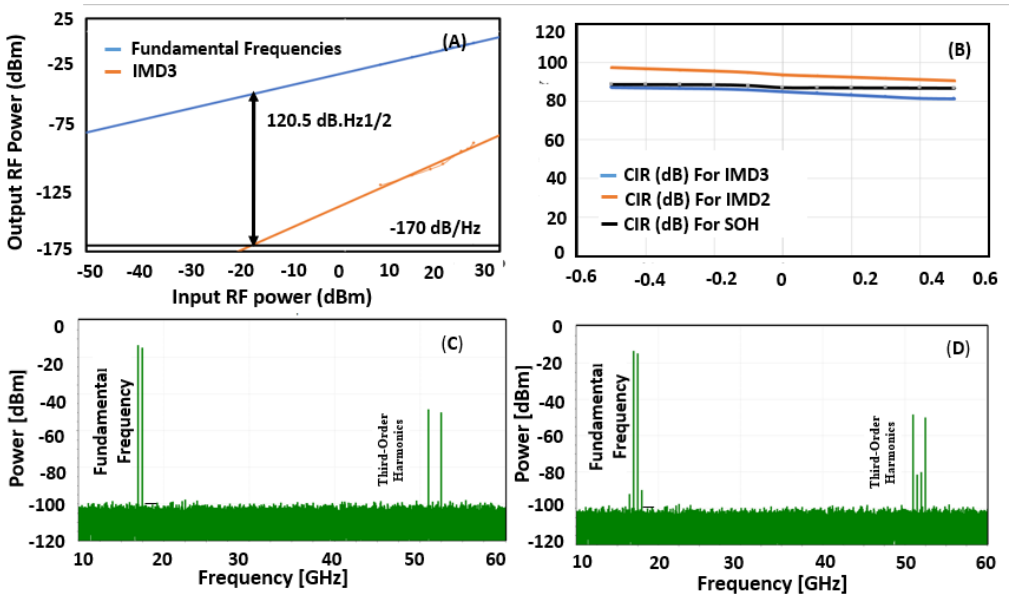

Figure 35: (A) SFDR performance of proposed AMPL with Dual Parallel MZMs, (B) System stability analyses (C). Two single subcarriers after changing RF shifters for 1 degree, (D). Two single subcarriers after changing RF shifters for 1 degree and adding Fibre between BPDs and 3dB power combiner.

	MZM_1	MZM_2	MZM_3	MZM_4
VpiDC /VpiRF	3.5 V	3.5 V	3.5 V	3.5 V
Insertion Loss	6 dB	6 dB	6 dB	6 dB
Extinction Ratio	21.8 dB	18.5 dB	21.8 dB	18.5 dB
dVpiDC_dTemperature	0.005 V/degC	0.005 V/degC	0.005 V/degC	0.005 V/degC
dVpiRF_dTemperature	0.0015 V/degC	0.0015 V/degC	0.0015 V/degC	0.0015 V/degC
OperatingTemperature	25 degC	25 degC	25 degC	25 degC
ReferenceTemperature	25 degC	25 degC	25 degC	25 degC
ElectrodeLengthUpper	23 mm	23 mm	23 mm	23 mm
IndexMismatchUpper	0.05	0.05	0.05	0.05
MicrowaveLossUpper	0.002 dB/m/sqrt(Hz)	0.002 dB/m/sqrt(Hz)	0.002 dB/m/sqrt(Hz)	0.002 dB/m/sqrt(Hz)
ElectrodeLengthLower	23 mm	23 mm	23 mm	23 mm
IndexMismatchLower	0.05	0.05	0.05	0.05
MicrowaveLossLower	0.002 dB/m/sqrt(Hz)	0.002 dB/m/sqrt(Hz)	0.002 dB/m/sqrt(Hz)	0.002 dB/m/sqrt(Hz)

Table 4: MZMS Parameters used in our simulation

In Fig.34 (A), we present the SFDR performance analysis of the proposed system. As we have mathematically presented, the proposed system in an ideal condition, it will not produce any IMD3, IMD2 or SOH, however in real life it is almost impossible to have an ideal condition,

therefore we have changed the modulator parameter to match with our practical laboratory components (shown in Table 4); modulators and RF shifters for 1 degree to measure the SFDR3. Fig.34 (A) shows SFDR3 for the proposed link is 120.5 dB. Hz1/2 from -170 noise floor.

To demonstrate the performance of the proposed RF system configuration concerning the bias drift, we have investigated the following CNR for IMD3, IMD2 and SOH, shown in Fig.34 (B). As it can be seen from the results, the CIR for IMD3, IMD2 and SOH are almost constant at a bias drift of up to ±0.5V, therefore the system is stable. Due to fact that IMDs and SOH are eliminated, the proposed system performance is stable as the operating points voltage changes.

Next, we have tested the system purity by varying the parameters of the modulator (shown in Table. 4) to match with practical modulators and by changing RF shifters for one degree. As can be seen, the obtained results are similar to those in Fig.33 (C). Furthermore, by using the same parameters for modulators and RF shifters, we have tested the system further by adding different fibre lengths between 3dB combiner and BPDs (20-meter fibre between 3dB combiner and BPD1 and 19-meter fibre between 3 dB combiner and BPD2) results are shown in Fig. 34 (D). Simulation from Fig. 34 (D) shows confirms that there is no SOH, however, if the length of fibre optic cable is not the same, then IMD3 starts coming up the noise floor.

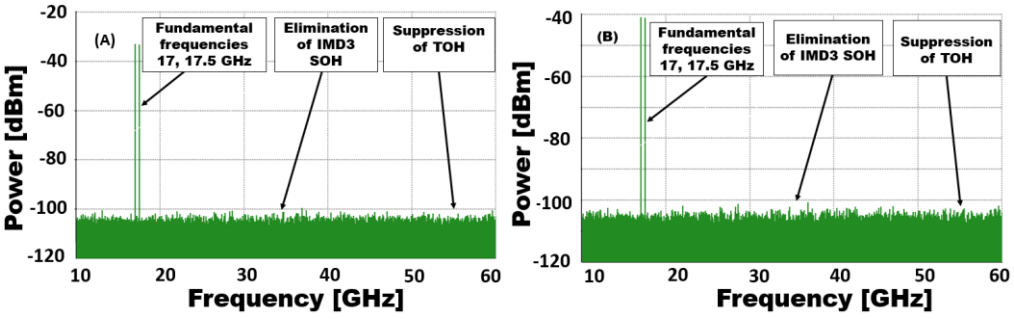

Figure 36: (A) Two single subcarriers after including 42 dB losses, (B) Two single subcarriers after including 42 dB losses and changing the input of laser to 15dB.

The proposed model consists of 6 RF shifters, 4 splitters and 4 combiners, therefore, it is known there will be losses. In this regard, in the simulation model, we have included all potential losses which might occur in practice. Attenuates on each connection have been considered to present the losses for each shifter, splitter, and combiner; obtained results are shown in Fig. 35 (A). Losses added to the system is 42dB, hence the dynamic range is not as shown in an ideal case in Fig.34 (A), however, the obtained results demonstrate that the dynamic range has not been decreased regarding TOH and TOH which have been suppressed under the noise floor. Furthermore, the system performance has been tested by changing the input of the laser to 15 dB, which includes losses as mentioned above to investigate the effects on SFDR, obtained results are shown in Fig. 35 (B).

Chapter 6

Conclusion

In chapter 3, has been developed and demonstrated a high linear analogue photonic link with IMD3, SOH, second-order distortion product eliminated, and with other higher-order distortion products suppressed. It is demonstrated that by deploying two D-DPMZMs and inserting frequencies in two different channels, then by combining the power through the BPD IMD3, SOH, and second-order distortion can be eliminated, and other higher-order harmonics can be suppressed completely. The approach has led to a highly linearized signal with a clean spectrum near the fundamental frequencies. The proposed configuration is suitable for application in short distances and long distances transmission systems. It is also managed to obtain a dynamic range of 58 dB with IMD3, SOHs eliminated, and other harmonics suppressed under the noise floor. To the best of our knowledge, this is the first demonstrated work in literature where IMD3, SOHs and second-order distortion produces have been eliminated. Furthermore, we have also demonstrated that this configuration can be used for a down-conversion only by varying the operating biasing point of the modulator from quadrature to maximum. The optimized linearized proposed configuration, with the above stated high performances, has been used to down-converted signals at a broad spectrum with a high dynamic range of 77.84 dBm. Our developed Mathematical models have been also simulated using commercial software where the obtained results seem to match well.

In chapter 4, we have developed and experimentally demonstrated a high linear analogue photonic link with IMD3, third-order distortion suppressed under noise floor, and significant suppression of SOH. By only using three RF shifters and two single drive MZMs, we

demonstrated a linearized photonic link system with all IMDs, and third-order distortion suppressed under the noise floor. The proposed AMPL configuration consists of only three shifters, two of which are 90 degrees, one 270 degrees, two MZMs, and one BPD. The proposed system configuration is easy to implement in practice and exhibits better performance than already published research papers in literature with comparable configurations. We have developed and demonstrated a full mathematical model for the proposed novel AMPL and confirmed a unique matching between the mathematical model and the experimental measurements. We have demonstrated benchmarking agreement between both theoretical and experimental results, which confirms a high system performance. Furthermore, the proposed AMPL has revealed experimentally an SFDR of 119.5 dB. Hz2/3.

In chapter 5, we have developed and demonstrated a high linear analogue photonic link where all IMDs and SOH have been eliminated, by deploying unique system architecture consisting of 6 RF shifters, 2 D-DPMZMs and 2 balanced photodetectors. The proposed analogue photonic link configuration which exhibits significant performance is easy to implement in practice [85]. We have demonstrated that IMDs and SOH distortion products can be eliminated, which is a challenging task to achieve because if signals are very close to each other, it will be very difficult to filter SOH by using various filtering techniques. We have demonstrated that the system SFDR is only limited by TOH distortions which are far apart from fundamental signals and can easily be filtered by using low electronic filters. We also have benchmarked the developed mathematical model and system simulations, and it has been confirmed that the mathematical model and the simulation results match very well, confirming that the proposed system can be implemented in practice. Additionally, we have also demonstrated the SFDR of 120.5 dB.Hz1/2.

Publications

Published:

Elimination of odd and even intermodulation distortions of analog microwave photonics link based on GaAs MZMs. / Shaqiri, Shemsi; Haxha, Shyqyri; Mirza, Taimur.
In: Optics Express, Vol. 28, No. 12, 27.05.2020, p. 17521-17531.

Linearization and Down-Conversion of Microwave Photonics Signal based on Dual-drive Dual-parallel Mach-Zehnder Modulator with Eliminated 3rd Intermodulation and 2nd Distortions. / Shaqiri, Shemsi; Haxha, Shyqyri.
In: Elsevier Optik , Vol. 204, 164103, 02.2020, p. 1-12.

Microwave Photonics Analog Link based on two Integrated D-DPMZM Linearized Signals and with Eliminated odd Harmonics and all IMD's. / Shaqiri, Shemsi; Haxha, Shyqyri
Ian Flint; Huseyn Ademgil.
In: Springer, DOI: https://doi.org/10.21203/rs.3.rs-419007/v

References:

[1] Chemistry 2e, Openstax "Electromagnetic Spectrum" 11295.

[2] I. Djordjevic, W. Ryan, B. Vasic, "Fundamentals of Optical Communication," In Coding for Optical Channels, Springer US, pp. 25-73, 2010

[3] G.Keiser, optical Fibre communication, Mc Graw Hill, 3rd Edition 2000

[4] Ajoy Ghatak and K. Thyagarajan Department of Physics Indian Institute of Technology New Delhi, India, 1978

[5] C. Yao, "Optical Fibre Dispersion," Fibre Optics for Sale, California, Sep 2010

[6] I. Hong, "Dispersion compensation in Fibre optic communication systems," Master's Thesis, San Jose State University, Paper 2319, 2002

[7] G.P. Agrawal, "Dispersion-Compensating Fibres," in Fibre-Optic communication systems, John Wiley & Sons, pp 345-394, Oct 2010

[8] M.A. Saifi, S.J. Jang, “Triangular-profile single-mode Fibre,” in Optics Letters, Vol. 7, pp.43-45, Jan. 1982

[9] S. J. Mihailov, "Fibre Bragg Grating Sensors for Harsh Environments," in Sensors, 12, no. 2, pp. 1898-1918, 2012.

[10] Qi, LIU Renhao and YU Jian-guo, Journal of Optoelectronics·Laser 25, 1709 (2014). (In Chinese)

[11] Rajani, R. Pal, V. Sharma, “Comparison of Pre-, Post- and Symmetrical-dispersion Compensation Schemes for 10/15 GBPS using Different Modulation Formats at Various Optical Power Levels using Standard and Dispersion Compensated Fibres,” in International Journal of Computer Applications 50(21),pp.6-13, July 2012

[12] M. I. Hayee, A. E. Willner, “Pre- and post-compensation of dispersion and nonlinearities in 10Gb/s WDM systems”, in IEEE Photon. Tech. Lett. 9, pp. 1271, 1997.

[13] O. Arora, A. K. Garg, S. Punia, “Symmetrical dispersion compensation for high-speed optical links,” in International Journal of Computer Science Issues, vol 8(6), No.1, 371–376, 2011

[14] “Tutorial Note 5 – Modulation Schemes”, by SHF communication Technologies AG, Berlin Germany, Availableat: https://www.shf.de/wp-content/uploads/appnotes/shf_tutorial_note_modulation_schemes.pdf (Accessed on 1st December 2019).

[15] S. S. A. Obayya, S. Haxha, B. M. A. Rahman, C. Themistos and K. T. V. Grattan, "Optimisation of the optical properties of a deeply etched semiconductor electrooptic modulator," in Journal of Lightwave Technology, vol. 21, no. 8, pp. 1813-1819, Aug. 2003.

[16] Ebrahim Mortazy, Ke Wu, Microwave and millimeter-wave losses in conventional optoelectronic devices, Optics & Laser Technology, Volume 43, Issue 4, June 2011, Pages 852-857.

[17] “Introduction to iXBlue Mach Zehnder Modulators Bias Controllers”, iXblue S.A.S Photonic Solutions, France.

[18] N. A. Al-Shareefi et al., "A study in OCS millimeter-wave generation using two parallel DD-MZMs," 2013 IEEE 11th Malaysia International Conference on Communications (MICC), Kuala Lumpur, 2013, pp. 418-421.

[19] S. A. Tretter, “Double Sideband Suppressed Carrier Amplitude Modulation and Coherent Detection,” in Communication System design using DSP algorithms, Springer, 2008.

[20] E. Cura, “Experiment 3: Double Sideband Modulation,” in The university of Texas at Dellas, 2012, Accessed online at: http://www.utdallas.edu/~mtacca/courses/EE3150/Spring-2012/Exp3.pdf.

[21] S. A. Tretter, “Single-sideband Modulation and Frequency Translation,” in Communication System design using DSP algorithms, Springer, 2008.

[22] B. Kolner and D. Dolfi, “Intermodulation Distortion and Compression in an Integrated Electrooptic Modulator,” Appl. Optics, vol. 26, no. 17, pp. 3676–3680, Sep 1987. 73.

[23] M. S. Islam, T. B. Chau, and M. C. Wu, “Distributed balanced photodetectors for high-performance RF photonic links," in IEEE Photonics Technology Letters, vol. 11, no. 4, pp. 457-459, April 1999.

[24] Di Peng, Zhiyao Zhang, Yangxue Ma, Yali Zhang, Shangjian Zhang, and Yong Liu, "Broadband linearization in photonic time-stretch analog-to-digital converters employing an asymmetrical dual-parallel Mach-Zehnder modulator and a balanced detector," in Optics Express, vol. 24, pp. 11546-11557, 2016.

[25] M. Saiful h, T. Chau, S. Mathai, T. Itoh, M. Wu, D. Sivco, and A. Cho, “Distributed balanced photodetectors for broad-band noise suppression,” IEEE Trans.Microw. Theory Tech., vol. 47, no. 7, pp. 1282–1288, Jul 1999.

[26] X Xie, Y. Dai, Y. Ji, K. Xu, Y.Li, J. Wu and J. Lin, "Broadband Photonic Radio-Frequency Channelization Based on a 39-GHz Optical Frequency Comb," in IEEE Photonics Technology Letters, 24 (8), 661-663 (2012).

[27] S. Shaqiri, and S. Haxha," Linearisation and Down-Conversion of Microwave Photonics Signal based on Dual-drive Dual-parallel Mach-Zehnder Modulator with Eliminated 3rd Intermodulation and 2nd Distortions," in Optik, 164103, (2019).

[28] D. A. Hall, "Understanding Intermodulation distortion Measurements," in Engineering Essentials-Electronics design, October 2013.

[29] X. Meng, "Designing high dynamic range microwave photonic links for radio applications," in Fibre and Integrated Optics, vol.23, pp1–56, 2004.

[30] C. Henn, "Intermodulation Distortion (IMD)," in Application Bulletin, Burr-Brown, USA, April 1994.

[31] G. Gonzalez, "Microwave Transistor Amplifier: Analysis and Design," 2nd edition, City: Prentice Hall, 1997.

[32] J. Garcia, S. G. LaJeunesse, D. Bartow, "Measuring Spurious free dynamic range in a D/A converter," Technical Brief, Intersil, January 1995.

[33] N. Kikuchi, K. Sekine, and S. Saski, “Analysis of XPM effect on WDM transmission performance,” in Electronic Letter, Vol. 33, 653– 654, 1997.

[34] C. H. Cox, “Analog Optical Links: Theory and Practice,” Cambridge University press, 2004

[35] ZHU Zi-hang, ZHAO Shang-hong, LI Yong-jun, CHU Xing-chun, ZHANG Hui, WANG Xiang and ZHAO Gu-hao, Journal of Optoelectronics•Laser 24, 500 (2013). (in Chinese)

[36] ZHOU Wei, ZOU Xi-hua, PAN Wei, YAN Lian-shan, LUO Bin and LU Bing, Journal of Optoelectronics·Laser 24, 2332 (2013). (in Chinese)

[37] WANG Zhao, MA Jian-xin, ZHANG Rui-jiao, LI Yan-jie, ZHANG Qi-qi, ZHANG Qi, LIU Renhao and YU Jian-guo, Journal of Optoelectronics·Laser 25, 1709 (2014). (in Chinese)

[38] C. Lim, A. Nirmalathas, K. Lee, D. Novak, and R. Waterhouse, “Inter-modulation distortion improvement for Fibre-radio applications incorporating OSSBþC modulation in an optical integrated-access environment,” J. Lightw. Technol., vol. 25, no. 6, pp. 1602–1612, Jun. 2007.

[39] J. Yao, Microwave photonics, J. Lightw. Tcchnol. Vol. 27, No. 3, (2009), pp. 225-314.

[40] C. Cox, Analog Optical Links, Theory and Practice, Cambridge University, (2004).

[41] X. Zou, B. Lu, W. Pan, L. Yan, A. Stohr, J. Yao, Photonics for microwave measurements, Laser Photonics Rev. 10, No. 5, (2016), pp.711-734.

[42] F. Pail; S. Haxha, T. N. Mirza, M. S. Alom: Microwave Photonic Downconversion With Improved Conversion Efficiency and SFDR, IEEE Access, (2018), No. 6.

[43] A.J. Cooper, Electron. Lett. Vol.26, No. 24, (1990), pp.2054.

[44] J-M. Merolla, Y. Mazurenko, J-P. Goedgebuer, H. Porte, W. T. Rhodes: Phase modulation transmission system for quantum cryptography, Optics Letters, vol. 24, No. 2, (1999), pp. 104.

[45] L. Duraffourg, J-M. Merolla, J-P, Goedgebuer, Y. Mazurenko, W. T. Rhodes: Compact transmission system using single-sideband modulation of light for quantum cryptography, Optics Letters, vol. 26, No. 18, Sept.(2001), pp, 1427.

[46] Zhiyu Chen,1 Lianshan Yan, Wei Pan,1 Bin Luo, Xihua Zou, Yinghui Guo, Hengyun Jiang, and Tao Zhou: SFDR enhancement in analogue photonic links by simultaneous compensation for dispersion and nonlinearity, Opt. Exp., vol. 21, No. 18, Sep.(2013), pp. 20 999–21 009.

[47] T. R. Clark, S. R. O'Connor, and M. L. Dennis: A phase-modulation I/Q-demodulation microwave-to-digital photonic link, IEEE Trans. Microw. Theory Tech., vol. 58, No. 11, Nov. (2010), pp. 3039–3058.

[48] Y. Cui et al.: Enhanced spurious free dynamic range in intensity modulated analogue photonic link using digital post processing, IEEE Photon. J., vol. 6, No. 2, Apr. (2014), Art. ID. 7900608.

[49] C. Lim, A. Nirmalathas, K. Lee, D. Novak, and R. Waterhouse: Inter-modulation distortion improvement for Fibre-radio applications incorporating OSSBþC modulation in an optical integrated-access environment, J. Lightw. Technol., vol. 25, No. 6, Jun. (2007), pp. 1602–1612.

[50] Z. H. Zhu, S. H. Zhao, Q. G. Tan, and W. Jiang: A linearized optical single-sideband modulation analogue microwave photonic link using dual-parallel interferometers, IEEE Photon. J., vol. 5, No. 5, Oct. (2013), Art. ID. 5501712.

[51] X. Li, Z. H. Zhu, and S. H. Zhao: An intensity modulation and coherent balanced detection intersatellite microwave photonic link using polarization direction control, Opt. Laser Technol., vol. 56, Mar. (2014), pp. 362–366.

[52] S. K. Korotky and R. M. Ridder: Dual parallel modulation schemes for low-distortion analogue optical transmission, IEEE J. Sel. Areas Commun., vol. 8, No. 7, Sep. (1990), pp. 1377–1381.

[53] S. Li, X. Zheng, H. Zhang, and B. Zhou: Highly linear radio-over-Fibre system incorporating a single-drive dual-parallel Mach–Zehnder modulator, IEEE Photon. Technol. Lett., vol. 22, No. 24, Dec. (2010), pp. 1775–1777.

[54] G. H. Zhu, W. Liu, and H. R. Fetterman: A broadband linearized coherent analogue Fibre-optic link employing dual parallel Mach–Zehnder modulator," IEEE Photon. Technol. Lett., vol. 21, No. 21, Nov. (2009), pp. 1627–1629.

[55] S. K. Kim, W. Liu, Q. Pei, L. R. Dalton, and H. R. Fetterman: Nonlinear intermodulation distortion suppression in coherent analogue Fibre optic link using electro-optic polymeric dual parallel Mach–Zehnder modulator, Opt. Exp., vol. 19, No. 8, Apr. (2011), pp. 7865–7871.

[56] J. Li et al.: Third-order intermodulation distortion elimination of microwave photonics link based on integrated dual-drive dual-parallel Mach–Zehnder modulator, Opt. Exp., vol. 38, No. 21, Nov. (2013), pp. 4285–4287.

[57] Y. Wang, Jingnan Li, Dayong Wang, Tao Zhou: Ultra-wideband microwave photonic frequency downconverter based on carrier-suppressed single-sideband modulation, Optics Communications Vol. 1, March (2018), pp. 799-804.

[58] Q. Tan, Yongsheng GAO, Yangyu Fan, You He: Multi-octave analog photonic link with improved second and third-order SFDRs, Optics Communications Vol. 410, March (2018), pp. 685-689.

[59] J Li, YC Zhang, S Yu, T Jiang, Q Xie, W Gu: Third-order intermodulation distortion elimination of microwave photonics link based on integrated dual-drive dual-parallel Mach–Zehnder modulator, Optics letters, (2013), osapublishing.org Vol. 38, Issue 21, pp. 4285-4287.

[60] J.Yao, ‘‘Microwave Photonics’’ Journal of Light Technology, 23(3) 314-335 (2009).

[61] C. Cox, Analog Optical Links Theory and Practice, (Cambridge University, 2004).

[62] X. Zou, B. Lu, W. Pan, L. Yan, A. Stöh, J. Yao, ‘‘Photonics for microwave measurements’’, Laser Photonics, 10(5), 699-854 (2016).

[63] A. Zadok, A. Eyal, and M. Tur, "Extended delay of broadband signals in stimulated Brillouin scattering slow light using synthesized pump chirp," Opt. Express, 14(19), 8498-8505 (2006).

[64] X. Chen, W. Li, J. Yao, ‘‘Dynamic-Range Enhancement for a Microwave Photonic Link Based on a Polarization Modulator’’. IEEE, 63(7), 2384-2389 (2015).

[65] F. Pail; S. Haxha, T. N. Mirza, M. S. Alom, ‘‘Microwave Photonic Downconversion with Improved Conversion Efficiency and SFDR’’, IEEE Access, 6, 8089-8097 (2018).

[66] M. Huang, J. Fu, S. Pan, ‘‘Linearized Analog Photonic Links Based on a Dual-Parallel Polarization Modulator’’, Opt. Lett., 37(11), 1823-1825 (2013).

[67] T. Jiang, R. Wu, S. Yu, D. Wang, W. Gu, ‘‘A novel high-linearity microwave photonic link based on the strategy of adding a compensation path using a bidirectional phase modulator’’, IEEE Photonics, 8(5), (2016).

[68] E. Xu, M. Zhang, P. Li, Z. Zhang, ‘‘Dynamic-range enhancement in microwave photonic link based on single-sideband phase modulation’’, in Asia Communications and Photonics Conference, (ACP, 2016), pp. 2-5.

[69] Z. Xie, S. Yu, S. Cai, W. Gu, ‘‘Linearized phase-modulated analog photonic link with large spurious-free dynamic range’’, Optical Society of America., (APC, 2016), pp.AF3H.7.

[70] B.M Haas, T.E Murphy, ‘‘A Simple, Linearized, Phase-Modulated Analog Optical Transmission System’’ IEEE Photonics, 19(10), 729-731 (2007).

[71] M. Biagio, B. Hraimel, X. Zhang, ‘‘Enhanced Spurious-Free Dynamic Range Using Mixed Polarization in Optical Single Sideband Mach–Zehnder Modulator’’, IEEE, 27(15), 3034-3041 (2009).

[72] Z Chen, L. Yan, W. Pan B. Luo X. Zou Y. Guo H. Jiang, T. Zhou, ‘‘SFDR Enhancement in Analog Links by Simultaneous Compensation for Dispersion and Nonlinearity’’, Optics Express, 21(18) 20999-21009 (2013).

[73] X. Chen, W. Li, J. Yao, ‘‘Dynamic-range enhancement for a microwave photonic link based on a polarization modulator’’, IEEE Explore, 63(7), 2384-2389 (2015).

[74] S. Wang, Y. Gao, A. Wen, L. Liu, ‘‘A microwave photonic link with high spurious-free dynamic range based on a parallel structure’’, SpringerLink, 11, 137-140 (2015).

[75] W. Zhu, M. Zhao, F. Fan, J. Hu, Y. Gu, ‘‘Sagnac interferometer-assisted microwave photonic link with improved dynamic range’’, IEEE Photonics, 9(2), 550909 (2017).

[76] W. Qin, W. Jiang, ‘‘The performance analysis of microwave photonic frequency conversion using double-sideband suppressed-carrier and balance detection", in IEEE International Conference on Communication Problem-Solving, (IEE, 2015), pp. 582-585.

[77] W. Zhang, A. Wen, A. Xu, W. Zhai, K.Wei, Konkan; H. Zhang, ‘‘Dual-wavelength linearization of analog photonic link based on PM–IM conversion’’, Optics Communications, 420, 174-178 (2018).

[78] D. Zhu, J. Chen, S. Pan, ‘‘multi-octave linearized analog photonic link based on a polarization-multiplexing dual-parallel Mach-Zehnder modulator", Optics Express, 24(10), 11009-11016 (2016).

[79] W. Jiang, Q. Tan, W. Qin, D. Liang, X. Li, H. Ma, Z. Zhu, ‘‘A Linearization Analog Photonic Link with High Third-Order Intermodulation Distortion Suppression Based on Dual-Parallel Mach-Zehnder Modulator’’, IEEE Photonics Journal, 7(3), 1-8 (2015).

[80] J Li, YC Zhang, S Yu, T Jiang, Q. Xie, W. Gu’’Third-order intermodulation distortion elimination of microwave photonics link based on integrated dual-drive dual-parallel Mach–Zehnder modulator’’ Optics letters, 38(21), 4285-4287 (2013).

[81] R.G. Walker, N. Cameron, Y. Zhou, and S. Clements, “Electro-Optic modulators for space using Gallium Arsenide” in Proc. SPIE 10562, (International Conference on Space Optics-ICSO, 2016), paper 105621A.

[82] R.G. Walker, I Bennion and A C Carter; “Low voltage, 50Ω GaAs/AlGaAs travelling-wave electro-optic modulator with bandwidth exceeding 25GHz”, Electron. Lett., 25(23), 1549–1550 (1989).

[83] Q. Tan, Y. Gao, Y. Fan, and Y. He, “Multi-octave analog photonic link with improved second- and third-order SFDRs,” Optic Express, 24(10), 11009–11016, (2016).

[84] M. S. Islam et al., "Distributed balanced photodetectors for high performance RF photonic links," in International Topical Meeting on Microwave Photonics. Technical Digest (High Speed Photonics Components Workshop, 1998), pp. 177-180.

[85] Z. Zhu, Sh. Zhao, X. Li, K. Qu, T. Lin, B. Lin, " Dynamic Range Improvement for an Analog Photonic Link Using an Integrated Electro-Optic Dual-Polarization Modulator" IEEE Photonics, 8(2), (2016).

[86] Z. Zhu, Y. LI, X. Li, K. Qu, T. Lin, J. Ma “Broadband linearized analog intersatellite microwave photonic link using a polarization modulator in a Sagnac loop" Applied optics, 55(5), (20

[87] J. Yao, Microwave photonics, J. Lightw. Tcchnol. 27 (3) 225-314, (2009).

[88] C. Cox, Analog Optical Links, Theory and Practice, Cambridge University, (2004).

[89] X. Zou, B. Lu, W. Pan, L. Yan, A. Stohr, J. Yao, Photonics for microwave measurements, Laser Photonics Rev. 10 (5) (2016) 711-734.

[90] A.J. Cooper, Electron. Lett. 26 (24) (1990) 2054.

[91] Jean-Marc Mérolla, Yuri Mazurenko, Jean-Pierre Goedgebuer, Henri Porte, and William T. Rhodes, "Phase-modulation transmission system for quantum cryptography," Opt. Lett. 24, 104-106 (1999)

[92] Menghao Huang, Jianbin Fu, and Shilong Pan, "Linearized analog photonic links based on a dual-parallel polarization modulator," Opt. Lett. 37, 1823-1825 (2012)

[93] T. Jiang, R. Wu, S. Yu, D. Wang and W. Gu, "A Novel High-Linearity Microwave Photonic Link Based on the Strategy of Adding a Compensation Path Using a Bidirectional Phase Modulator," in IEEE Photonics Journal, vol. 8, no. 5, pp. 1-7 (2016).

[94] E. Xu, M. Zhang, P. Li, and Z. Zhang, "Dynamic-Range Enhancement in Microwave Photonic Link Based on Single-Sideband Phase Modulation," in Asia Communications and

Photonics Conference 2016, OSA Technical Digest (online) (Optical Society of America, 2016), paper AF2A.16.

[95] Z. Xie, S. Yu, S. Cai and W. Gu, "Linearized Phase-Modulated Analog Photonic Link with Large Spurious-Free Dynamic Range," Asia Communications and Photonics Conference (ACP), Wuhan, China, pp. 1-3 (2016).

[96] B. M. Haas and T. E. Murphy, "A Simple, Linearized, Phase-Modulated Analog Optical Transmission System," in IEEE Photonics Technology Letters, vol. 19, no. 10, pp. 729-731 (2007).

[97] B. Masella, B. Hraimel and X. Zhang, "Enhanced Spurious-Free Dynamic Range Using Mixed Polarization in Optical Single Sideband Mach–Zehnder Modulator," in Journal of Lightwave Technology, vol. 27, no. 15, pp. 3034-3041 (2009).

[98] F. Pail; S. Haxha, T. N. Mirza, M. S. Alom, ‘‘Microwave Photonic Downconversion with Improved Conversion Efficiency and SFDR’’, IEEE Access, 6, 8089-8097 (2018).

[99] T. N. Mirza, S. Haxha and I. Dayoub “A Linearized Analog Microwave Photonic Link with an Eliminated Even-Order Distortions," in IEEE Systems Journal (DOI: 10.1109/JSYST.2021.3051394), pp.1-9 (2021).

[100] Weize Qin and Wei Jiang, "The performance analysis of microwave photonic frequency conversion using double-sideband suppressed-carrier and balance detection," 2015 IEEE International Conference on Communication Problem-Solving (ICCP), Guilin, pp. 582-585 (2015).

[101] W. Jiang et al., "A Linearization Analog Photonic Link with High Third-Order Intermodulation Distortion Suppression Based on Dual-Parallel Mach–Zehnder Modulator," in IEEE Photonics J., vol. 7, no. 3, pp. 1-8, (2015).

[102] Wu Zhang, Aijun Wen, Xinyao Xu, Weile Zhai, Kongkun Wei, Huixing Zhang, ‘‘Dual-wavelength linearization of analog photonic link based on PM–IM conversion’’, Optics Communications, Vol. 4, pp.20174-178 (2018).

[103] Dan Zhu, Jian Chen, and Shilong Pan, "Multi-octave linearized analog photonic link based on a polarization-multiplexing dual-parallel Mach-Zehnder modulator," Opt. Express 24, 11009-11016 (2016).

[104] Shemsi Shaqiri, Shyqyri Haxha. Linearization and down-conversion of microwave photonics Signal based on dual-drive dual-parallel mach-zehnder modulator with eliminated 3rd intermodulation and 2nd distortions’’, Elsevir, Vol.204, pp. 164103 (2020).

[105] Shemsi Shaqiri, Shyqyri Haxha, and Taimur N. Mirza, "Elimination of odd and even intermodulation distortions of analog microwave photonics link based on GaAs MZMs," Opt. Express 28, 17521-17531 (2020).

[106] Y. A. Shpolyanskiy, S. A. Kozlov and V. G. Bespalov, "Stimulated Raman scattering and four waves mixing with self-phase and cross-phase modulation of intense fs laser pulses," *Quantum Electronics and Laser Science Conference,* Baltimore, USA, 128-, 1999.

[107] A. B. Ruffin, "Stimulated Brillouin scattering: an overview of measurements, system impairments, and applications," *Optical Fibre Measurements, 2004. Technical Digest: Symposium on*, Boulder, CO, USA, pp. 23-28, 2004.